FLUID MIXING STUDIES IN A HEXAGONAL 37-PIN, WIRE WRAP ROD BUNDLE

by

King-Wo Thomas Chiu

B.S., University of Lowell
1977

SUBMITTED IN PARTIAL FULFILLMENT
OF THE REQUIREMENTS FOR THE DEGREE OF
MASTER OF SCIENCE IN NUCLEAR ENGINEERING
at the
MASSACHUSETTS INSTITUTE OF
TECHNOLOGY

September 1979
~~February~~

Signature of Author.....
Department of Nuclear Engineering

Certified by.....
Professor Neil E. Todreas
Thesis Supervisor

Accepted by.....
Chairman, Departmental
Committee on Graduate Students

ABSTRACT

FLUID MIXING STUDIES IN A HEXAGONAL

37-PIN, WIRE WRAP

ROD BUNDLES

by

King-Wo Thomas Chiu

Submitted to the Department of Nuclear Engineering on Sept. 13th 1979, in partial fulfillment of the requirement for the degree of Master of Science in Nuclear Engineering.

The design and construction of a test-section for the 37-pin bundle is presented. Only the flow split experiment and the pressure drop experiment have been done. A modified interior subchannel flow collector is used to sample interior subchannel flow rates. The pressure drop data is collected using the injection rod.

The flow split data shows that the flow split parameters X_1 and X_2 agree very well with Chiu's prediction It also indicates predictable flow rate patterns for edge and interior subchannel.

From the subchannel pressure data, local subchannel friction factors (for edge and interior subchannel) and the bundle average friction factor are derived. Theoretical predictions of the bundle average friction factor lie within the range of experimental error.

Thesis Supervisor: Neil E. Todreas
Title: Professor of Nuclear Engineering

TABLE OF CONTENTS

ACKNOWLEDGMENTS

The author would like to express his gratitude to Professor Neil E. Todreas for his assistance and advice throughout the course of this project. Professor Todreas has continually provided encouragement as supervisor of this thesis.

Technical advice and assistance from Mr. J.A. Caloggero of the Mechanical Engineering Department Engineering Project Laboratory and Mr. Raymond Johnson of the Mechanical Engineering Machine Shop are greatly appreciated.

Thanks are given to Mr. Jim Hawley, Mr. Song-Feng Wang, Mr. Paul Symolon and Mr. Chong Chiu for their advice and discussion during the course of this work. Proof-reading by Mr. Symolon is deeply appreciated.

A special, final acknowledgment goes to my wife, Lucia, for her understanding and patience throughout the course of this thesis. She also painstakingly typed this thesis.

NOMENCLATURE

A_b	=	Bundle flow area in^2
A_1	=	Interior subchannel flow area in^2
A_2	=	Edge subchannel flow area in^2
A_3	=	Corner subchannel flow area in^2
A_i	=	Flow area for subchannel i in^2
C_1	=	Swirl flow parameter (ref. 7)
C_{1L}	=	Local swirl flow parameter (ref. 7)
D	=	Pin diameter, inch
De_1	=	Interior subchannel hydraulic diameter, inch
De_2	=	Edge subchannel hydraulic diameter, inch
De_3	=	Corner subchannel hydraulic diameter, inch
De_b	=	Bundle subchannel hydraulic diameter, inch
De_i	=	Hydraulic diameter for subchannel i, inch
ε_1^*	=	Fffective eddy diffusivity (ref. 7)
ε_{1L}^*	=	Effective enhanced eddy diffusivity (ref. 7)
F	=	Looseness factor (ref. 8)
f	=	Constant in equation (1.2.3)
f_1	=	Interior subchannel friction factor
f_2	=	Edge subchannel friction factor
f_3	=	Corner subchannel friction factor
f_b	=	Averge bundle friction factor
f_i	=	Local friction factor for subchannel i
g_c	=	Constant, 32,174 $\frac{lbm\ ft}{lb\,f\ sec^2}$

H	=	Lead length, inch
i, K	=	Index : i=1 for interior subchannel i=2 for edge subchannel i=3 for corner subchannel
L	=	Distance over which pressure drop is measured (equation 4.3.1)
M_b	=	Expected bundle flow rate (equation 3.1.2), gpm
M_{loop}	=	Bundle flow rate read from flow meter, gpm
$\bar{m}_1$	=	Average interior subchannel flow rate, gpm
$\bar{m}_2$	=	Average edge subchannel flow rate, gpm
$\bar{m}_i$	=	Average subchannel flow rate from subchannel i
$\overline{m_{K,L}}$	=	Average K type subchannel flow rate over one lead length for any particular K type subchannel, gpm
$m_{K,i}$	=	K subchannel flow rate at the bundle exit plane for K type subchannel i
N_1	=	Number of interior subchannels
N_2	=	Number of edge subchannels
N_3	=	Number of corner subchannels
N_K	=	Number of K type subchannels
N_R	=	Number of rings of pin in the test-section
P	=	Pitch, inch
P	=	Pressure, psi (or inch of water)
Re	=	Reynolds number
Re_i	=	Reynolds number in i type subchannel
$\bar{V}_b$	=	Average bundle axial velocity, ft/sec

$\bar{V}_1$	=	Average interior subchannel axial velocity, ft/sec
$\bar{V}_2$	=	Average edge subchannel axial velocity, ft/sec
$\bar{V}_3$	=	Average corner subchannel axial velocity, ft/sec
V_i	=	Average subchannel axial velocity in i type subchannel, ft/sec
X_1	=	Interior subchannel flow split parameter
X_2	=	Edge subchannel flow split parameter
X_3	=	Corner subchannel flow split parameter
ρ	=	Density lbm/ft^3
ΔP_b	=	Average bundle pressure drop, psia
ΔP_1	=	Interior subchannel pressure drop, psia
ΔP_2	=	Edge subchannel pressure drop, psia
ΔP_3	=	Corner subchannel pressure drop, psia
ΔP_i	=	Pressure drop in i type subchannel, psia

CHAPTER 1

INTRODUCTION

In the core of a reactor, which is made of rod bundles, the knowledge of temperature distribution is of paramount importance to the core designer. The temperature field affects the mechanical and physical behavior of the reactor material such as fuel and clad, as well as the neutronics of the core. Thus, the temperature field directly or indirectly imposes a limit on the thermal power production of a reactor. This is particularly true in a Liquid Metal Fast Breeder Reactor (LMFBR) because the core in a LMFBR is subjected to high power density and a fast neutron spectrum environment. Knowledge of the temperature field enables the core designer to determine cladding hot spots, assembly housing bowing and deformation. Bowing and deformation are also enhanced by swelling of stainless steel cladding under fast neutron environment, and the pressure field in the case of nature and/or mixed convection. Knowledge of the temperature field is important to the prediction of the location of incipient boiling and subsequent voiding in core.

In current LMFBR core design, fuel rods are packed into a hexagonal array with uniform spacing provided by wire wraps. The use of wire wraps increases the pressure drop across the core and thus the required pumping power. However it enhances flow mixing in the bundle and thereby reduces the temperature gradient.

1.1 The need for Mixing and Flow Split Data

A series of computer codes of the ENERGY family (Ref. 1,2,3,4) using a lumped subchannel energy equation have been developed to predict the temperature field in LMFBR core. In the original version of SUPERENERGY (Ref. 5) the required inputs are C_1 and ε_1^*. However, these two parameters were found to be functions of the bundle size (Ref. 6). In SUPERENERGY, the latest version of the ENERGY family, these parameters were then changed to $\overset{*}{}_{1L}$ and C_{1L} (Ref. 7) which depend only on local fluid characteristics. These parameters are defined as:

$$\varepsilon_{1L}^* = \frac{\varepsilon_1^*}{X_1} \qquad (1.1.1)$$

$$C_{1L} = \frac{C_1}{X_2} \qquad (1.1.2)$$

This implies the necessity for determination of the flow split parameters, X_1 and X_2. Moreover, a sensitivity study on the relative importance of these parameters (Ref. 8) to the determination of an accurate temperature field by the SUPEERENERGY code showed that the accuracy of subchannel flow (therefore flow-split) is of major importance. Also in evaluation of the subchannl friction factor from pressure drop data, the knowledge of subchannel flow velocity is required. Hence the result of flow split experiments also serves as an input to the calculation of

the friction factor. The relation between these three parameters is illustrated in Fig.(1.1).

The above parameters could be evaluated experimentally by performing flow split and mixing experiments or by an analytical and physical model. Actually both have been done to check the validity of the developed model for these parameters.

1.2 Current Analytical Method

The recent analytical methods used to derive the flow split parameters X_1, X_2 and X_3 are developed by Novendstern (Ref. 9) and Chiu (Ref. 10). The Novendstern method is based on the assumption that same pressure drops are experienced by all three types of subchannel. Therefore, we can write:

$$f_1 \frac{L}{De_1} \frac{\rho V_1^2}{2g_c} = f_2 \frac{L}{De_2} \frac{\rho V_2^2}{2g_c} = f_3 \frac{L}{De_3} \frac{\rho V_3^2}{2g_c} \qquad (1.2.1)$$

and the continuity equation

$$M_b = V_1 A_1 N_1 + V_2 A_2 N_2 + V_3 A_3 N_3 \qquad (1.2.2)$$

From the above equations, the ratios

$$X_1 = \frac{V_1}{V_b} \quad , \quad X_2 = \frac{V_2}{V_b} \quad , \quad X_3 = \frac{V_3}{V_b}$$

can be determined if the friction factors f_1, f_2 , f_3 are

known. Novendstern writes the friction factors by using the smooth tube friction factor for each subchannel. Therefore:

$$f = \frac{C}{Re^{0.25}} \qquad (1.2.3)$$

By using this method, the turbulent flow-split parameters X_1, X_2 & X_3 can be evaluated for the bundle under consideration as a function of the looseness factor F (Ref. 8). The results are tabulated in Table(1.1). It is noted that this method assumes the friction factor to be independent of the wire wrapped lead length. This leads to the conclusion that the flow split parameters derived will also be independent of wire wrapped lead length.

In the latest model developed by C. Chiu (Ref. 10) equations (1.2.1) and (1.2.2) are also used. However a detail analysis of the nature of the pressure drop of each subchannel is made. In Chiu's model, two components of pressure drop are assummed. One component is the form drag pressure loss caused by the wire and the other component is the skin friction pressure loss due to flow over the rod surface. In the edge subchannel, the swirl flow is expected to follows the wire. mostly. Hence the pressure loss by the form drag component may be neglected. However in the interior, the wire does not produce a steady sweeping flow that always follows the wire. As a result, the form drag pressure loss is dominant in the interior subchannel.

From these condiserations, the friction factors derived are different from each other and dependent on wire lead length. The predicted flow split values are also listed in Table (1.2).

1.3 Objective

The objective of this thesis is to measure the interior subchannel average flow split parameter X_1, the edge subchannel average flow split parameter X_2, the interior subchannel pressure drop and the edge subchannel pressure drop on the bundle with geometric characteristics of P/D = 1.15 and H/D - 21. The results from subchannel pressure drop and flow split measurements are used to determine the subchannel friction factors and the bundle average friction factor.

A mixing experiment was also planned for this bundle. However the break down of the data acquisition computer system has postponed the timing of this measurement.

No corner subchannel data has been taken in this experiment because the subchannel area size is too small to insert instrumentation probes. Since no data is available for the corner subchannels, calculation of flow split parameter X_1, X_2 and of the mass balance are made by assuming $X_3 = X_2$ as suggested in (Ref. 11). This assumption will not introduce large errors in the values of X_1 & X_2 since the number of corner subchannels is small and the mass flow rate in corner subchannels is relatively low when compared to that of interior and edge subchannels.

The choice of this particular geometry is based on the

fact that no flow split experimental results have been published with P/D = 1.15 .

CHAPTER 2

EQUIPMENT DESIGN AND FABRICATION

2.1 Test Section Design

2.1.1 Test Section Housing Design and Fabrication

The design of the 37 pin bundle test section is essentially identical to a previous 61 pin bundle design (Ref. 12) with some necessary modifications. In the original design of the test section, two plates of plexiglass are screwed on the ½ inch thick stainless steel plates which are then secured by ½ inch thick aluminum pieces (Fig. 2.1.1). Since a different number of pins and a different P/D ratio (P/D = 1.15) are required, the necessary adjustment from the previous bundle is the reduction of the previous 61 pin bundle flow area to the desired bundle flow area for the 37 pin bundle with desired tolerence. The reduction in area is accomplished in two ways. In the lateral dimension, the metal parts are moved inward. In the vertical dimension, two wedge shaped strips made of plexiglass are inserted between the pins and the plexiglass plates. The modified configuration is depicted in Fig.(2.1.2). Therefore, the metal pieces are basically retained while the two new plexiglass plates and inserts have to be machined. On the metal pieces, holes for the support pins had to be drilled.

The test section fabrication was done in the Nuclear Engineering Machine shop located in Building NW 13. However some difficulties were confronted during fabrication. When all the

necessary parts (the plexiglass plates and inserts) were machined and ready to be put together, we could not come up with a tight and uniform dimension in the bundle flow area along the axial length of the bundle. The defect is primarily due to deformations of the stainless steel part of the bundle. Two kinds of deformation were quite apparent when a dial indicator was pushed steadily along the axial direction of the metal part. We observed that the two metal pieces were bent approximately at the mid-plane. The two metal pieces were also twisted slightly around the axes. Both kinds of deformation may possibly be due to non-uniform distribution of stresses from the tightened cap screws and mis-alignment of the plexiglass plates and metal pieces during previous fabrication of the 61 pin bundle.

Since both time and money were limited, we went ahead and put the bundle together (with wire wrapped pins) as best as we could. Before the wire wrapped pins were placed inside the housing, cross flat dimensions were measured on six faces with the housing tighened. It was found that the flow duct does not have a regular hexagonal shape. However, the geometry is constant over the top 2 feet of the bundle, the portion of the bundle adjacent to the exit measuring plane. The as-built cross flat dimension before wire wrapped pins were placed inside the housing is illustrated in Fig. (2.1.3). With the "hollow" housing tighened, three alignment pins were machined into each side of the two faces of the plexiglass plates. This is to insure that same dimension will result when the wire wrapped pins are placed into the housing. When the whole

test section was put together the cross flat dimensions were measured at the exit of the test section. It was found that there was only a slight change in the irregular dimensions. Thus it can be assummed that the irregular cross flat dimensions will be constant at least 2 feet along the axial length from the exit plane. The as-built cross flat dimensions at the exit plane are also illustrated in Fig.(2.1.3).

2.1.2 Fuel Pin Fabrication

The same kind of stainless steel pins S.S. 306, 60 inches long are used as mock-up fuel pin in this bundle as were used previously. Therefore 40 pins with the closest diameters were chosen from the previous set of pins. Due to some soldering and sanding on the pins, the diameter of the pin does not remain uniform along the length. Measurement of the diameter was done on both ends and the middle of each pin. It is the average diameter of the pin that was used to choose the group of pins used in this experiment.

Since a different lead length is used, some modifications of the wire wrap machine was necessary. The wire wrap machine was designed by B. Bosy in 1975. Details of the construction of the machine and the procedures for wire wrapping can be obtained from Ref. (13). The machine was designed primarily for the fabrication of the fuel pins of the 61 pin bundle. However, the only adjustment needed was to calculate what gears are needed, and to construct a different gear box. The calculation and the design are presented in Appendix B.

As mention before, a new hole to accomodate the support pins had to be drilled dead center on each pin. This was done before the wire was wrapped.

2.1.3 Bundle Fabrication

After the housing and mock up pins were constructed, the complete test section was put together. The locations of each pin put into the housing was recorded. The map is shown in Fig. (2.1.4). The location of the wire at the exit plane is illustrated in Fig. (2.1.5). Attempts were made to measure the actual area of each subchannel. However due to the looseness of pin locations, exact measurement cannot be made. Measurement of the distances between edge rods and duct at the exit plane has been performed to evaluate the average F-factor for this bundle. The results show that the gap has the average dimension of 0.0787 inch with a variation of ± 0.005 inch on the non-symmetrical side. This leads to an F-factor of 0.66 which means that the pins are slightly packed towards center because the nominal value of the F-factor is 0.72 for this bundle. The subchannel geometric parameters, based on F = 0.66 are calculated according to the formula suggested in Ref.(8) The results are listed in Table (2.1).

2.2 Equipment for the Mixing Experiment

2.2.1 Conductivity Probe and Support Structure Design

The same type of conductivity probes used in the previous 61 pin bundle is used in this experiment. They had to be cleaned up, replantinized and repaired as necessary. The

procedures on replantinization and construction of new probes are listed in Ref.(14).

As contrasted to the previous 61 pin bundle mixing experiment, a flow separator to house the conductivity probes is not needed in this bundle. This is due to the fact that larger wires are used in this bundle. Hence the actual flow area of each type of subchannel (therefore interior, edge and corner) is large enough so that the platinum wire of the probe can be inserted into the subchannel without touching either the pin or the wire. Therefore, a support structure similar to the one used in Hanson's bundle (Ref. 15) is designed.

The support structure is illustrated in Fig.(2.2.1) Three ¼ inch thick plexiglass plates and a 1/8 inch thick rubber gasket are used. They are cut in a hexagonal shape with a 4 inches cross flat dimension. All holes needed to be drilled are identical in location in these three plexiglass plates and the rubber gasket. Since locations of holes are required to be quite precise, in particular the holes for the conductivity probes, use of a numerical controlled drill press located in the Material Processing Laboratory in Building 35 is desirable. That particular drill press can provide accuracy up to 0.001 of an inch. After the locations of holes are calculated, a paper tape which codes the information is made. At actual drilling, the tape is fed into the machine and all holes are drilled automatically. However a test drilling has to be done in order to make sure the information on the paper tape is correct. The plexiglass plates were all

drilled at the same time with proper set up. The rubber gasket was drilled separately due to its softness.

All the plates are supported by 4 threaded brass rods located on 4 corners of the hexagon at the exit plane of the bundle. Holes for the support pins are drilled with tight dimension (¼ inch). While holes for the conductivity probes are drilled slightly larger than the diameter of the probes, the securtiy of the probes is provided by the rubber gasket in two ways. The actual diameter of the holes for probes in the rubber gasket are slightly smaller than the diameter of the probes. Therefore the probes would not slip through but an easy passage of the probe is provided without scratching the platinum deposit on the wire when the probes are inserted through the gasket. When all the probes are in place, tightening of the upper pair of plexiglass plates at four corners will provide further security of the probes.

2.2.2 Probes Mounting Procedures

The numbering scheme of the probes which is similar to that of the preceding 61 pin bundle experiment is shown in Fig.(2.2.2). Before the probes are mounted, the support structure is put up. The following are the procedures for setting up the structure and the probes:

1) The four brass rods are inserted into the mock-up pin at the corners of a square at the exit plane.
2) The lower plexiglass support plate is slid down to and leveled at about 1 inch above the exit plane

of the bundle.

3) All pointed support pins are inserted through the hole of the lower plates to the mock up pins.

4) Brass nuts are screwed down the threads of the brass rods.

5) Then the "sandwich" is put through the holes at the corner and another set of brass nuts are screwed down on top of the "sandwich".

6) A carpenter leveler is used to make sure the sandwich is leveled. Careful adjustments on the brass nuts are made.

7) The probes are inserted according to the numbering scheme starting from 1 to 128. Note that all platinum wires at the tip of the probes are actually inserted below the exit plane.

8) Then brass nuts are tightened to secure the probes in place.

2.2.3 Data Acquisition System

Basically, the same data acquisition used in the previous experiment will be used in the mixing experiment. Details of the structures of the system and procedures in collecting data are given in Ref.(16). In preceeding experiments, all salt mixing data were stored onto a floppy disk. The disk is then taken to the Joint Computer Facility (JCF) for processing. However, during the month of January, the JCF had updated its computer system so that no floppy disk unit was used as an

input peripheral. This presents a problem in processing the salt mixing data.

Two solutions are proposed to solve the problem. One solution is to use a telephone line to transmit the salt mixing data directly to the computer in JCF. This solution has two drawbacks. One drawback is due to the lower speed of data transmission through the telephone line. The other drawback is that modification of existing software is necessary because different interfacing units are used. Since the people who wrote the original software are not available, significant time would be consummed to do the modification. The other solution to the problem is to installed the suitable interfacing unit between a floppy disk unit and the new JCF computer system. This also involves significant modification in both software and hardware. Still another solution which is very unlikely due to financial difficulties was to increase the memory capacity of the minicomputer (blue box) which would eliminate the processing of data in JCF. However, this involves a large amount of money. It was decided that installation of the interfacing unit was the most practical solution for both our long term and short term needs.

2.3 Flow Split Measurement Equipment

Isokinetic flow measuring technique is used in this experiment (Ref. **8**). The basic principle behind this technique is to measure the flow rate of the subject subchannel without disturbing the flow field at the exit plane by the

measuring instrument. This criterion is met when the static pressure at the exit of the subject subchannel is equal to the static pressure of the surroundings. Thus a flow collector capable of collecting flow, measuring and adjusting the inside and outside static pressure is desirable. A basic collector design was used in the previous experiment by Chong Chiu at MIT (Ref. 8). This collector design consists of a tube with the walls on the boundary of the subject subchannel (i.e. rectangular for edge subchannel and triangular for interior subchannel). Two static pressure pitot tubes, one on the wall and the other through the wall, are welded on the collector. These two pitot tubes are connected with plastic tubes leading to outside of the upper plenum to monitor the relative water level (i.e. relative static pressure) from the two pitot tubes. The collector itself is connected with a fitted siphon tube to lead the subchannel flow to a scaled container outside the upper plenum. To measure the flow rate from a subject subchannel, a C-clamp is screwed on the siphon tube to adjust the subchannel flow so that the water levels leading from both pitot tubes are equal. Then the flow collected with the scale container during the measurement time period can be used to calculate the subchannel flow rate under the isokinetic condition.

In Chong Chiu's design for interior flow collector, only one outside pitot tube is used. Therefore this set up only measures part of the surrounding static pressure. Later in his 61 pin shaved wire bundle experiment, Song-Feng Wang of MIT modified the design by putting pitot tubes on each

side of the collector. By joining these three pitot tubes to a hollow ring which has a tube connected to it to measure the static pressure , this modified design is capable of measuring the average surrounding static pressure. Hence the modified interior collector is used in this experiment. The edge subchannel collector is basically the same as Chiu's design. Both collectors are illustrated in Figs.(2.3.1) and (2.3.2).

2.4 Pressure Drop Experiment

During the fabrication and machining of the test section, one of the metal walls was accidentally flipped around and machined. Since readjustment would result in shortening of both metal pieces and the metal pins, any attempt to do so was abandoned. This mistake resulted in destroying the symmetry of pressure wall taps originally machined on both metal pieces. Redrilling those pressure tap holes involves a tremendous amount of machine shop work and possible further damage on the already slightly deformed test section. Therefore, the idea of measuring bundle pressure drop data by using wall tap holes was abandoned.

However, bundle pressure drop data can be deduced from interior and edge pressure drop data (Ref. 17). Subchannel pressure measurement is done with a specially designed intrumentation rod (Ref. 12). The instrument consists of a hollow tubes with consecutive holes drilled along the axis and an injector which is capable of sliding inside the hollow

tube. When the end holes of the injector is aligned with the hole in the hollow tube, static pressure will be transmitted through the injector to a pressure gauge. The design is shown on Fig.(2.4.1).

Due to substantial use of the injector during previous experiment, the injector is badly deformed. A new injector stem was made. It is cut into two lengths. During experiment, the lower length of the injector is inserted into the hollow tube first. Then using a connecting rod, the upper part is screwed on. By this way of inserting the injector, bending and therefore permanent deformation can be avoided.

2.5 Flow Loop Instrumentation

The flow loop set up for this experiment is illustrated in Fig.(2.5.1). As the flow loop is set up, there are two flow lines leading to the test section. The bigger line is intended to accomodate larger flow rates ranging from 50 GPM to 200 GPM. The smaller line which has two flowmeters in parallel is intended to accomodated small flow rate ranging from 0 GPM to 56 GPM. Due to the limitation on diameter in the smaller line, no filter could be installed. Also due to the fact that larger wire is wrapped onto the mock-up fuel pins leading to larger subchannel area, the test section is vulnerable to deposition of larger particles inside the test section. This indeed happened in the earlier period of the experiment. We were forced to take apart the bundle to get

rid of the dirt. As a result, a copper wire mesh was installed underneath the test section to avoid further deposition.

On the bigger flow line, due to the long period of usage, apparently, dirt is deposited on the flow meter which gives erroneous reading on the total flow rate through the test section. The error in reading was proved when a standard method of using a weight tank tc measure the flow rate was used. However, only the lower range of the flow rate can be measured because of the limitation of the weight tank capacity.

The flow meter which is manufactured by Fisher & Porter is composed of two parts: a squared edge orifice plate with flanged tap and a variable area flow meter. It works on the principle that flow rate is a function of pressure drop across the orifice plate. Apparently, dirt is deposited on the range orifice inside the variable area flow meter. Knowledge of where the range orifice is requires disassembly of the whole flow meter which has been integrated into the flow line. This involves a large amount of time and possible risk of alteration of the configuration of the parts inside the flow meter. An alternate method of measuring flow rate was used. A differential pressure gauge is installed across the orifice plate. Since flow rate is a function of pressure drop across the orifice plate, reading from the differential pressure gauge determines uniquely the flow rate by a suitable correlation. The appropiate correlation and theory are shown in Appendix A.

CHAPTER 3

EXPERIMENTAL RESULTS

3.1 Flow Split

The subchannel flow rate for each subchannel is measured at the bundle exit plane at different Reynold numbers using the flow collector described in Chapter 2. Note that the corner subchannel flow rate has not been measured due to space limitations. The corner flow split value is assumed to be equal to the edge flow split value (Ref. 11). The average subchannel flow rate (over one lead length) for each type of subchannel can be obtained by simply dividing the total flow rate at the bundle exit plane in that type of subchannels by the corresponding number of subchannels in the bundle. Therefore, we have from Ref.(8):

$$\overline{m_{K,L}} = \frac{\sum_{}^{N_K} m_{K,i}}{N_K} \qquad (3.1.1)$$

K=1 for interior subchannel
K=2 for edge subchannel
K=3 for corner subchannel

where $\overline{m_{K,L}}$ = average K type subchannel flow rate over one lead length for any particular K type subchannel

$m_{K,i}$ = K subchannel flow rate at the bundle exit plane for K type subchannel i

N_K = total number of K type subchannels

It is noted that the right hand side of equation (3.1.1) also represents the average flow rate of subchannel type K.

The interior subchannels lying along three cross flat traverses, instead of a whole full map, were sampled at each Reynolds number. This procedure has an advantage of reducing the necessary experimental time by 2/3 without the need to take a full map. This is true because the collector in this method goes through different kind of interior subchannels with respect to the wire configuration. At several Reynold numbers the average interior subchannel flow rates from cross flat traverse measurements were checked against those from a full map result and they differ only by 1% randomly. So all the measurements of interior subchannel flow rate are done by the cross flat method.

The numbering scheme for the flow split measurement is shown on Fig.(3.1.1). The wire location at bundle exit plane is illustrated in Fig.(2.1.5). The experimental results are presented in a form of normalized subchannel flow rate (i.e., subchannel flow rate di vided by the total expected bundle flow rate) as illustrated in Fig.(3.1.12) to Fig.(3.1.23).

The total expected bundle flow rate is evaluated as:

$$M_b = \left(\sum_{i=\text{interior sub.}}^{N_1} m_i + \sum_{j=\text{edge sub.}}^{N_2} m_j\right)/0.955 \qquad (3.1.2)$$

$$\overline{m_1} = \frac{\sum_{i}^{N_1} m_i}{N_1} \qquad \overline{m_2} = \frac{\sum_{j}^{N_2} m_j}{N_2} \qquad (3.1.3)$$

$$\therefore \quad M_b = (N_1\overline{m_1} + N_2\overline{m_2})/0.955$$

where $\overline{m_1}$ = average interior subchannel flow rate (gpm)

$\overline{m_2}$ = average edge subchannel flow rate (gpm)

M_b = expected bundle flow rate (gpm)

and 0.955 is a factor to take into account the total corner subchannel flow rate proveded:

$$X_3 = X_2 = 1.034$$

Flow rate mass balance error is included in these figures to illustrate the validity of the isokinetic technique used in this experiment. The mass balance error is defined as:

$$\text{Mass balance error} = \frac{M_b}{M_{loop}} - 1.0$$

where M_b is defined in Equation (3.1.3)

and M_{loop} is the flow rate indicated by the differential pressure gauge using the correlation from Appendix A.

The Reynold number range covered in this experiment runs from 3000 to 14000. It would be desirable to extend the range on both ends. However it could not be done due to limitations of the instrumentation. The size of the upper plenum limits the achievement of higher bundle mass flow rates. The highest mass flow rate obtained is around 120 GPM. Higher flow rate would cause water to overflow from the upper plenum. Extension on the lower end is limited by high water temperature (therefore lower Reynold number) and possibily the measurement technique. The lowest flow rate that can be obtained without interruption of flow from the flow collector is 27 GPM. Measurements at lower bundle flow rate were taken. However flow from

the collector could not be sustained with inside and outside static pressures in equilibrium, i.e. our isokinetic condition.

3.2 Pressure Drop

For both interior subchannel and edge subchannels, the static pressure is taken with the instrumentation rod described in Chapter 2. The static pressure readings are taken at two different axial levels a distance of about 2 lead length (20.5 inches) apart. A seperation exactly 2 lead lengths could not be obtained because of the location of the static pressure tap holes along the axial length of the instrumention tube (see Fig. 2.4.1). Therefore measurements are taken at 15.5 inches and 36 inches below the exit plane of the bundle. The results are illustrated in Figs.(3.2.1) and (3.2.2). The raw data for the two figures are shown in Appendix C .

The pressure drop data, as a function of the Reynold number, can be calculated for the interior and edge subchannels. They are illustrated in Figs.(3.2.3) and (3.2.4). Using these data, bundle average pressure can also be determined.

CHAPTER 4

DISCUSSION OF RESULTS

Two aspects of the flow split experimental results will be discussed. The flow pattern of the edge subchannel flow rate with respect to the wire wrap configuration and the flow pattern of the interior subchannel flow rate will be discussed in Section (4.1). The characteristics of the flow split parameters X_1 and X_2, calculated from experimental results presented in Chapter 3, will be discussed in Section (4.2). Finally, discussion of the results of pressure drop will be presented in Section (4.3).

4.1 Edge and Interior Flow Pattern

As the results of Chapter 3 indicated, the edge subchannel flow pattern is observed to be independent on bundle Reynolds number. A typical edge subchannel flow rate pattern is depicted in Fig.(4.1.1). A solid line is plotted in this figure to illustrate the possible trend of the edge subchannel flow rate with respect to the wire wrap configuration. This figure shows that most of the edge subchannel flow rate data falls within ±10% of the line. The scattering of the edge subchannel flow rate data (±9%) may be due to the large variation of the edge subchannel flow areas.* However the line drawn takes the shape of a 3 cycle sinusoidal wave. Also it is noticed that the amplitutde of the wave is relatively small. This means the influence of the wire configuration on the edge subchannel flow rate is not bery

* Possible edge subchannel area variable is illustrated in Fig. (2.1.3)

strong. This can be explained by the large H/D ratio of this bundle. Large H/D ratio implies larger axial velocity of the fluid which in turns implies the fluid would not follow the direction of the wire wrap very closely.

For the interior subchannel, the cross flat flow rate pattern is illustrated in Fig.(4.1.2). It is observed that the interior subchannel flow rates are relatively constant in magnitude with respect to the edge subchannel flow rate. The amount of scattering is about ± 16%. This may seems large. However, it can be observed that there are two kinds of interior subchannel configurations. One configuration is that the base of the triangular shape facing up and the other facing down as illustrated in Fig.(4.1.3). The interior subchannel with base facing up has the wire end right inside the subchannel while the other does not. Obviously, existence of the wire reduces the flow area and therefore the mass flow rate. As the flow collector goes from flat to flat,it encounters alternate kinds of interior subchannels. Thus relatively large scattering is expected.

A plot of normalized interior subchannel flow rate against the wire position is illustrated in Figs.(4.1.4) and (4.1.3). As observed, the data shows a 3 cycle sinusoidal wave with respect to the wire position.

The uniform magnitutde of the interior subchannel flow rate indicates that the edge subchannel flow rate does not affect the interior subchannel flow rate. Hence using the

average interior subchannel flow rate to calculate the interior flow split parameters is valid .

4.2 Flow Split Parameters

The average subchannel mass flow rates calculated from the previous Chapter are used to obtain the flow split parameters according to the relation :

$$X_i = \frac{\bar{m}_i}{M_b} \frac{A_b}{A_i} \qquad i = 1.2 \qquad (4.2.1)$$

where M_b is the expected bundle flow rate defined in Equation (3.1.2)

The experimental results of flow split parameters X_1 and X_2 are illustrated in Figs.(4.2.1) and (4.2.2) respectively. The analytic predictions of Novendstern (Ref. 9) and Chiu (Ref. 11) are also illustrated in these figures. Two aspects of the flow split parameters in these figures will be discussed. One aspects is the trend of the flow split parameter with respect to the flow regime and the other is the agreement of these parameters with the analytical prediction.

Due to the limitation of the equipment and possibly the experimental technique discussed in Chapter 3, the range of the Reynolds number in this experiment lies mainly in the turbulent regime. Two solid lines are drawn through both flow

split parameters. These solid lines are the values predicted by hiu's analytical method (Ref. 11). Despite the scattering of the parameters around these lines within ± 1.3% the flow split parameters remain quite constant at the values predicted by Chiu's Correlation.

The total error involve in determining the flow split parameters is calculated according to the following relation derived from Equation (4.2.1).

$$\left|\frac{\Delta X_i}{X_i}\right| = \left|\frac{\Delta m_i}{m_i}\right| + \left|\frac{\Delta M_b}{M_b}\right| + \left|\frac{\Delta A_b}{A_b}\right| + \left|\frac{\Delta A_i}{A_i}\right| \qquad i=1.2 \qquad (4.2.2)$$

The expected bundle flow rate is a calculated value. Therefore no error should be involved. The subchannel flow area is determined solely by the area of the flow collector. The area of the flow collector can be adjusted to the desired value to within 1%. Thus the expected error contributed by the subchannel flow area could be estimated as ± 1%. Due to the irregularity of the flow duct shape and its reluctance to adjustment, average cross flat distance is used to calculate the bundle flow area. Error involved in the bundle flow area is estimated to be about ± 2%. Errors contributed by these two factors are systematic errors while the average subchannel mass flow rate is a randomly distributed experimental error. The average subchannel mass flow rate error can be calculated from the result of repeating the same experiment with same set up. It is found

that they are ranging within ± 3%. Hence the total error is estimated to be ± 6%.

With this range of error involved in the flow split value, we may conclude that prediction by Chiu's method is within ± 1.5% while the prediction by Novendstern is still within experimental error.

4.3 Pressure Drop Experiment

The main purpose of the pressure drop experiment is to determine the bundle average friction factor, interior subchannel and edge subchannel friction factors. The bundle average friction factor will be discussed in Section (4.3.1) and the results for subchannel friction factor will be discussed in Section (4.3.2).

4.3.1 Bundle Average Friction Factor

The average bundle friction factor can be calculated according to the following relation:

$$\Delta P_b = f_b \frac{L}{De_b} \frac{\rho \bar{V}_b^2}{2g_c} \qquad (4.3.1)$$

provided that ΔP_b is known.

By considering the force balance in the bundle, we may write:

$$\Delta P_b = \frac{\Delta P_1 N_1 A_1 + \Delta P_2 A_2 N_2 + \Delta P_3 A_3 N_3}{N_1 A_1 + N_2 A_2 + N_3 A_3} \qquad (4.3.2)$$

assumming that all types of subchannel have the same pressure drop.

Because of the small number of corner subchannel and assuming the same order of magnitude in the values of ΔP, Equation (4.3.2) can be simplified as:

$$\Delta P_b = \frac{\Delta P_1 N_1 A_1 + \Delta P_2 A_2 N_2}{N_1 A_1 + N_2 A_2} \qquad (4.3.2)$$

Also it is observed that in Figs.(3.2.3) and (3.2.4), the pressure drop of edge and interior subchannels are within 3%. Thus the assumption of the same constant pressure drop would not introduce a large error.

Using the data presented in Chapter, the bundle average friction factors are calculated and plotted in Fig.(4.3.1) against bundle Reynolds number. In this figure, Rehme's correlation (Ref. 8) and Novendstern's correlation (Ref. 9) are also illustrated for comparision.

It can be concluded from this figure that:

1) In the highly turbulent regime. therefore $Re > 4000$ the bundle average friction factor is proportional to $Re^{-0.5}$ and may be characterized by the following relation:

$$f_b = \frac{.31}{Re^{0.25}} \quad Re > 4000 \qquad (4.3.3)$$

2) In the laminar regime .. $Re < 700$, the bundle average friction factor is inversely proportional

to Re and may be characterized by the following relation:

$$f_b = \frac{85}{Re} \qquad Re < 700 \qquad (4.3.4)$$

3) In the transition region, the friction factor is observed to be proportional to Re^{-n} where n varies between 0.25 and 1.0 .

4) Novendstern's correlation predicts the bundle friction factor higher than the experimental result. The defect may be due to the fact that the rod diameter used in this experiment falls outside the applicable range of Novendstern's correlation.

5) The prediction by Rehme's correlation agrees very closely to the experimental result from the laminar region up to the end of the transition region. In the turbulent range, the friction factor is proportional to Re^{-n} where $1>n>0.25$. However it still falls within the error range of the experiment for the Reynolds number range tested.

4.3.2 Local Friction Factor of Interior and Edge Subchannel

The local friction can be calculated by the following relation:

$$\Delta P_i = f_i \frac{L}{De_i} \frac{\rho \overline{V}_i^2}{2g_c} \qquad i = 1,2 \qquad (4.3.5)$$

The parameter ΔP_s is from the experimental result presented in Chapter 3 and the parameter $\bar{V}_i$ is calculated by the relation:

$$V_b X_i = \bar{V}_i \qquad (4.3.6)$$

where X_i is the result from the flow split experiment

Using Equation (4.3.5), the local friction factors for both interior and edge subchannel are calculated and plotted in Figs.(4.3.2) and (4.3.3) respectively against the local Reynolds number Re_i which is based on $\bar{V}_i$ as:

$$Re_i = \frac{\bar{V}_i De_i}{\mu} \qquad i=1,2 \quad (4.3.7)$$

From these two figures, it may be concluded that both interior and edge local friction factors,in the highly turbulent range $\therefore$ Re $>$ 4000, both values vary in proportion to $Re^{-0.25}$ and can be characterized by the relations:

$$f_1 = \frac{.294}{Re_1^{0.25}} \qquad (4.3.8)$$

$$Re_i > 4000 \quad i=1,2$$

$$f_2 = \frac{0.35}{Re_2^{0.25}} \qquad (4.3.9)$$

It can be verified that the values of f_1,f_2 and f_b are consistent with each other according to Equation (4.3.2).

A pressure drop experiment has been done in Italy with the test section of the same geometric characteristic (P/D = 1.15, H/D = 21.0) except that the Italian test section is made up of 19 pins. The Italian pressure drop experiment is composed

of two parts: Edge subchannel axial pressure drop and edge subchannel radial pressure drop experiments (Ref. 19).

Fig.(4.3.4) illustrates the results of the edge subchannel pressure drop of this experiment and the Italian experiment in the form of plotting ΔP_2 in mm H_2O against the axial velocity (m/sec). However, meaningful conclusions cannot be drawn due to two reasons. One reason is that the axial distance over which the pressure loss is recorded is not reported. The other reason is that the complete geometry of the test section is not reported.

TABLES

TABLE 1.1

Flow Split Parameters Predicted by

Novenstern's Method at Different F-factor Values

Flow Regime	= Turbulent
Cross Flat Distance	= 3.664 inches
Cross Flat Tolerence	= 0.0219 inch
Rod Diameter	= 0.5007 inch
Wire Diameter	= 0.075 inch
No. of Rods	= 37
Lead Length	= 10.5 inches
P/D Ratio	= 1.155

F-factor	X_1	X_2	X_3
0.72	.951	1.096	.767
0.00	.923	1.132	.845
0.10	.927	1.127	.834
0.20	.932	1.123	.824
0.30	.936	1.118	.812
0.40	.939	1.114	.801
0.50	.943	1.110	.790
0.60	.946	1.106	.778
0.70	.950	1.102	.765
0.80	.954	1.098	.753
0.90	.957	1.093	.741
1.00	.960	1.089	.729

TABLE 1.2

Flow Split Parameters Predicted by

Chiu's Correlation at Different F-factor values

Flow Regime	= Turbulent
Cross Flat Distance	= 3.664 inches
Cross Flat Tolerence	= 0.0219 inch
Rod Diameter	= 0.5007 inch
Wire Diameter	= 0.075 inch
No. of Rods	= 37
Lead Length	= 10.5 inches
P/D Ratio	= 1.155

F-factor	X_1	X_2	X_3
0.72	.976	1.033	1.033
0.00	.951	1.061	1.061
0.10	.955	1.057	1.057
0.20	.958	1.053	1.053
0.30	.962	1.049	1.049
0.40	.965	1.046	1.046
0.50	.968	1.042	1.042
0.60	.971	1.039	1.039
0.70	.975	1.034	1.034
0.80	.978	1.030	1.030
0.90	.981	1.026	1.026
1.00	.984	1.022	1.022

TABLE 2.1

As Built Geometric Parameters for Subchannels

Cross Flat Distance * = 3.664 inches
Rod Diameter = 0.5007 inch
Pitch = 0.5783 inch
Wire Diameter = 0.075 inch
Lead Length = 10.5 inches
Bundle F-factor ** = 0.66

Interior Subchannel (Number:54)	Area	0.0442 $inch^2$
	Wetted Perimeter	0.9043 inch
	Hydraulic Diameter	0.1955 inch
Edge Subchannel (Number:18)	Area	0.0894 $inch^2$
	Wetted Perimeter	1.4826 inches
	Hydraulic Diameter	0.2412 inch
Corner Subchannel (Number:6)	Area	0.0303 $inch^2$
	Wetted Perimeter	0.6819 inch
	Hydraulic Diameter	0.1777 inch
Total Bundle Area	4.1776 $inch^2$	
Total Wetted Perimeter	79.6112 inches	
Bundle Average Hydraulic Diameter	0.2099 inch	

* Average
** Nominal F-factor = 0.722 (see ref. 8)

FIGURES

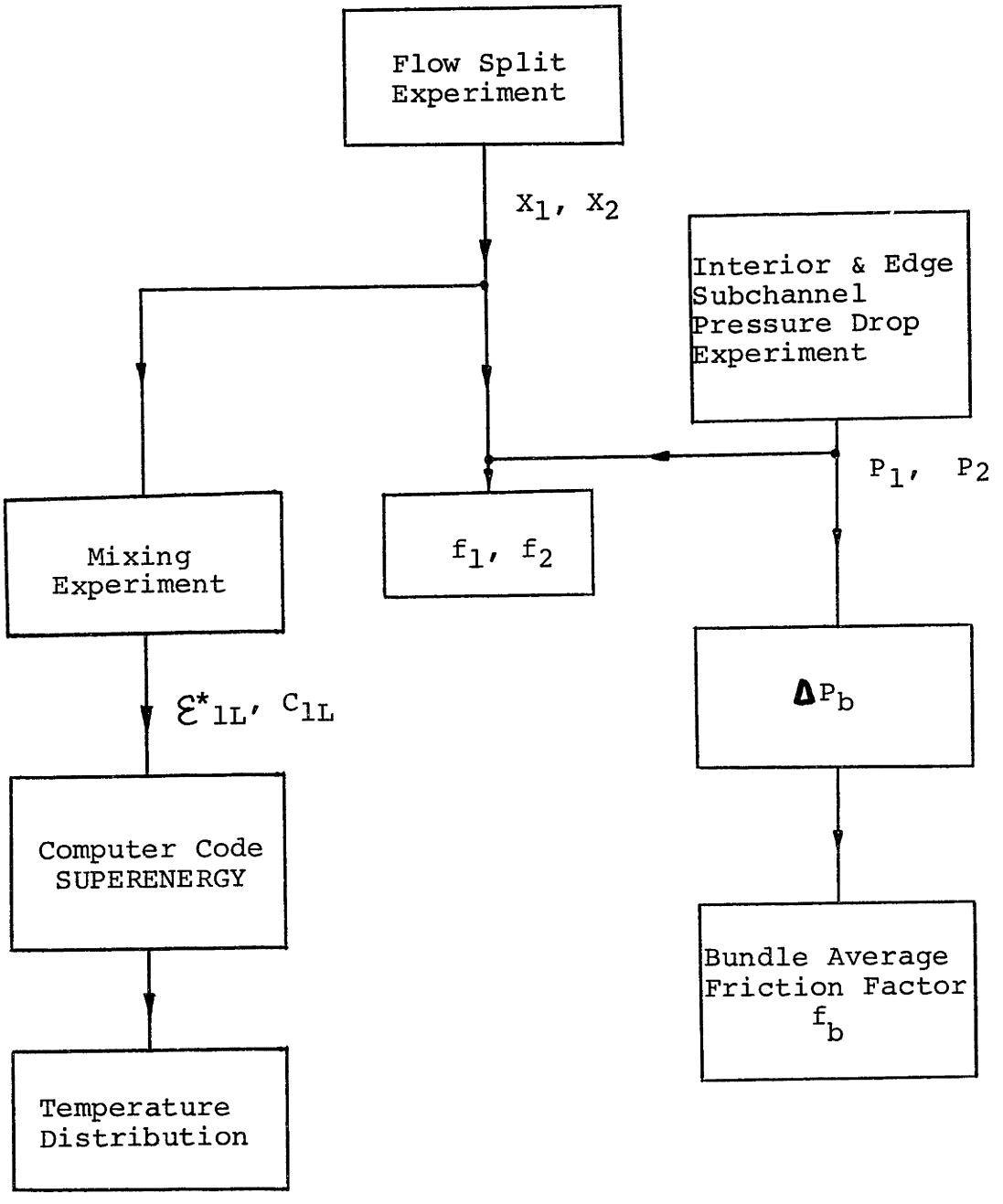

FIGURE 1.1 Relations between Flow Split Experiment, Mixing Experiment and Pressure Drop Experiment

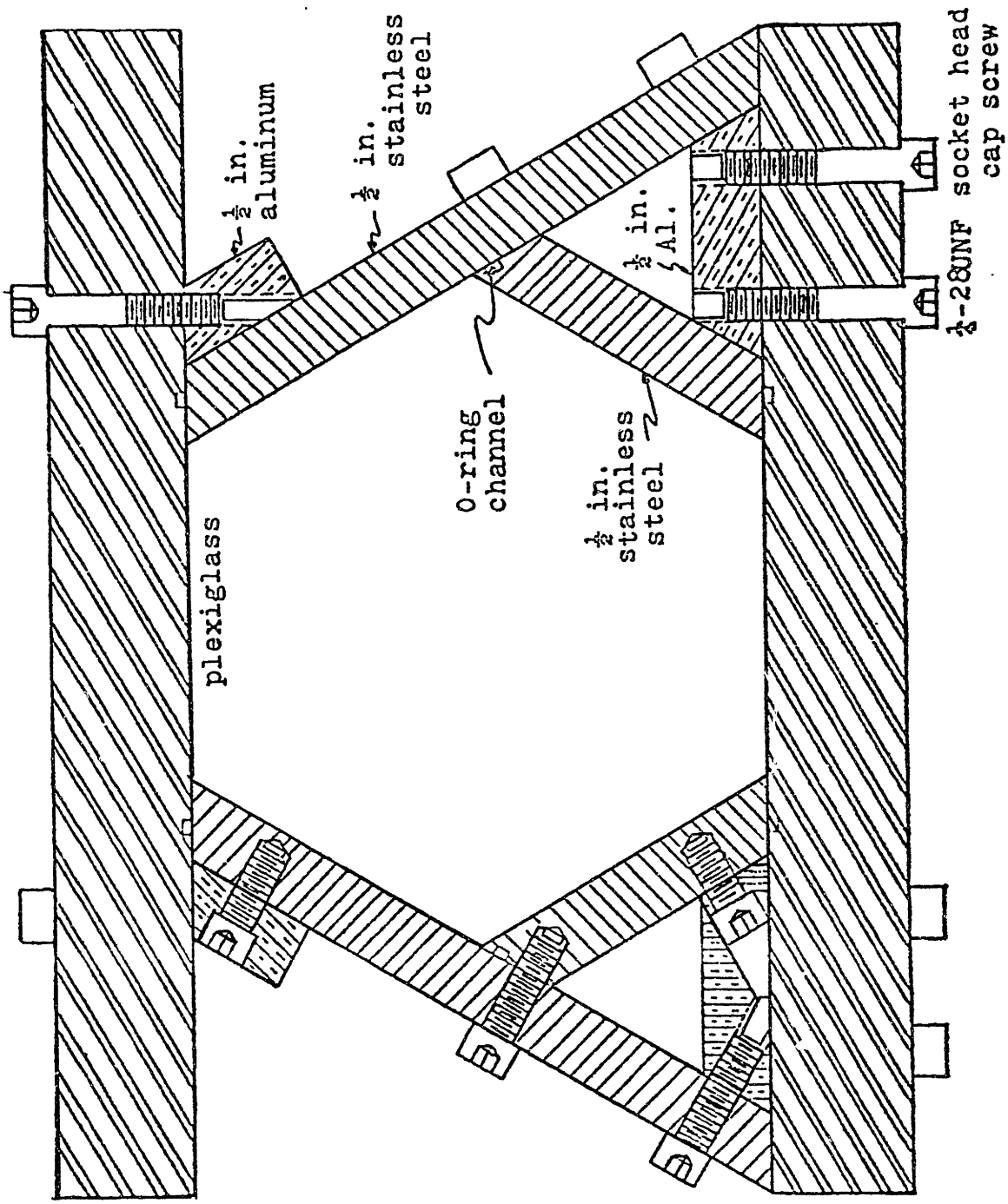

FIGURE 2.1.1 Previous Flow Housing Design

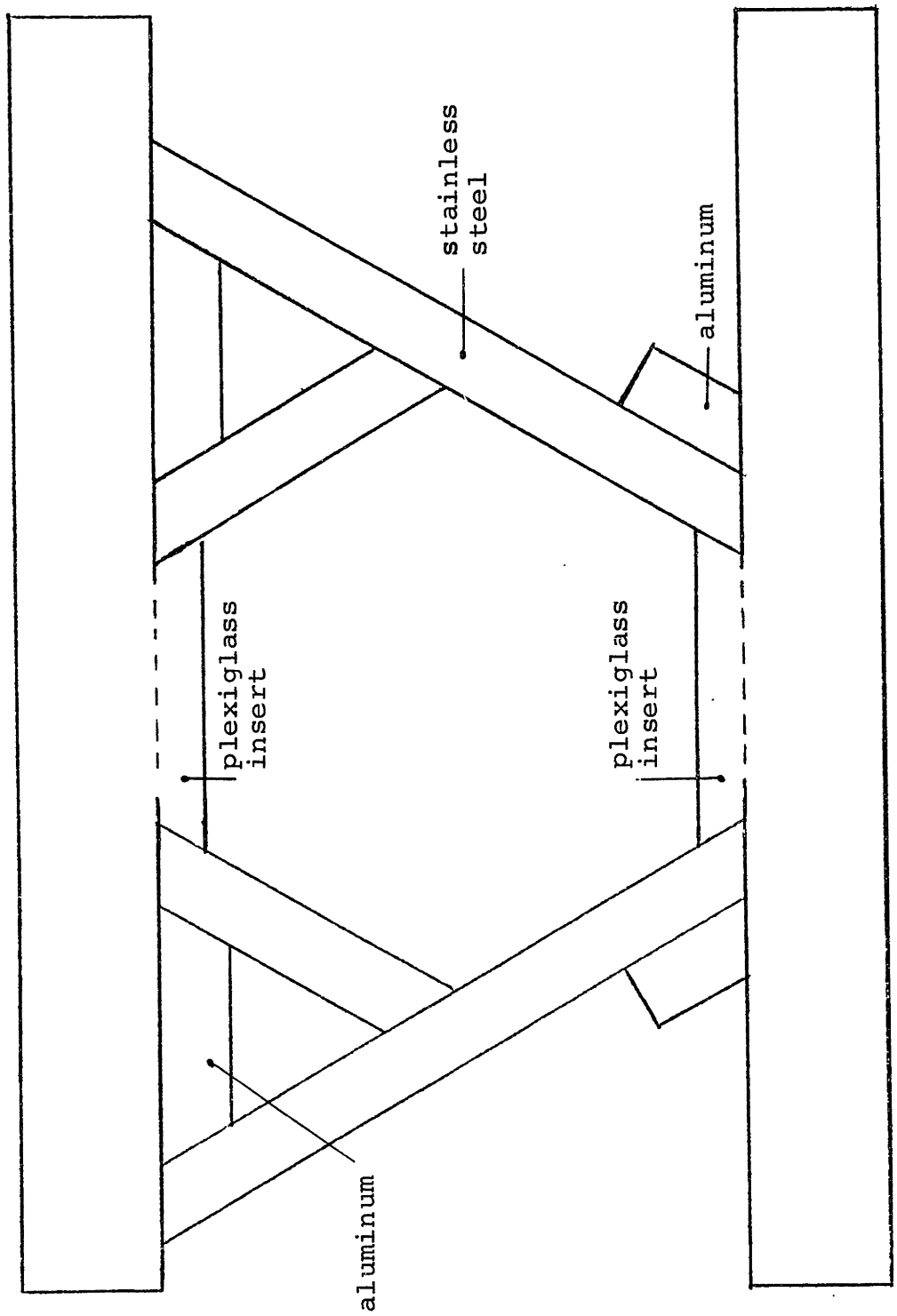

FIGURE 2.1.2 Flow Housing Design Configuration for the 37 Pin Bundle

Faces Measured	Housing Assembled without Pins (in)			Housing Assembled with Pins (in)
	exit plane	1' down	2' down	exit plane
1	3.664	2.664	3.664	3.665
2	3.662	3.664	3.664	3.665
3a	3.656	3.653	3.653	3.655
3b	3.668	3.669	3.670	3.670

Possible Edge Subchannel Area Variation

Faces		F-factor	Area A_2 in^2	$\frac{(A_2)_{nom} - (A_2)}{A_2}$ %
3a	With Wire in	1.00	0.0874	- 2.23
	Without Wire in		0.0918	2.68
3b	With Wire in	0.42	0.0910	2.00
	Without Wire in		0.0960	7.38

$(A_2)_{nom}$=0.0894 along on faces (1) & (2)

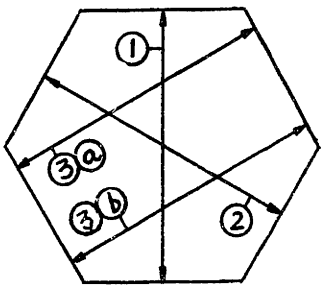

Faces Identification

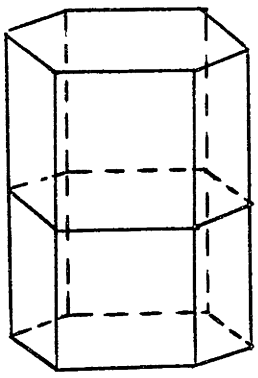

FIGURE 2.1.3 As-Built Cross Flat Dimensions of the Flow Housing and Possible Edge Subchannel Area Variation

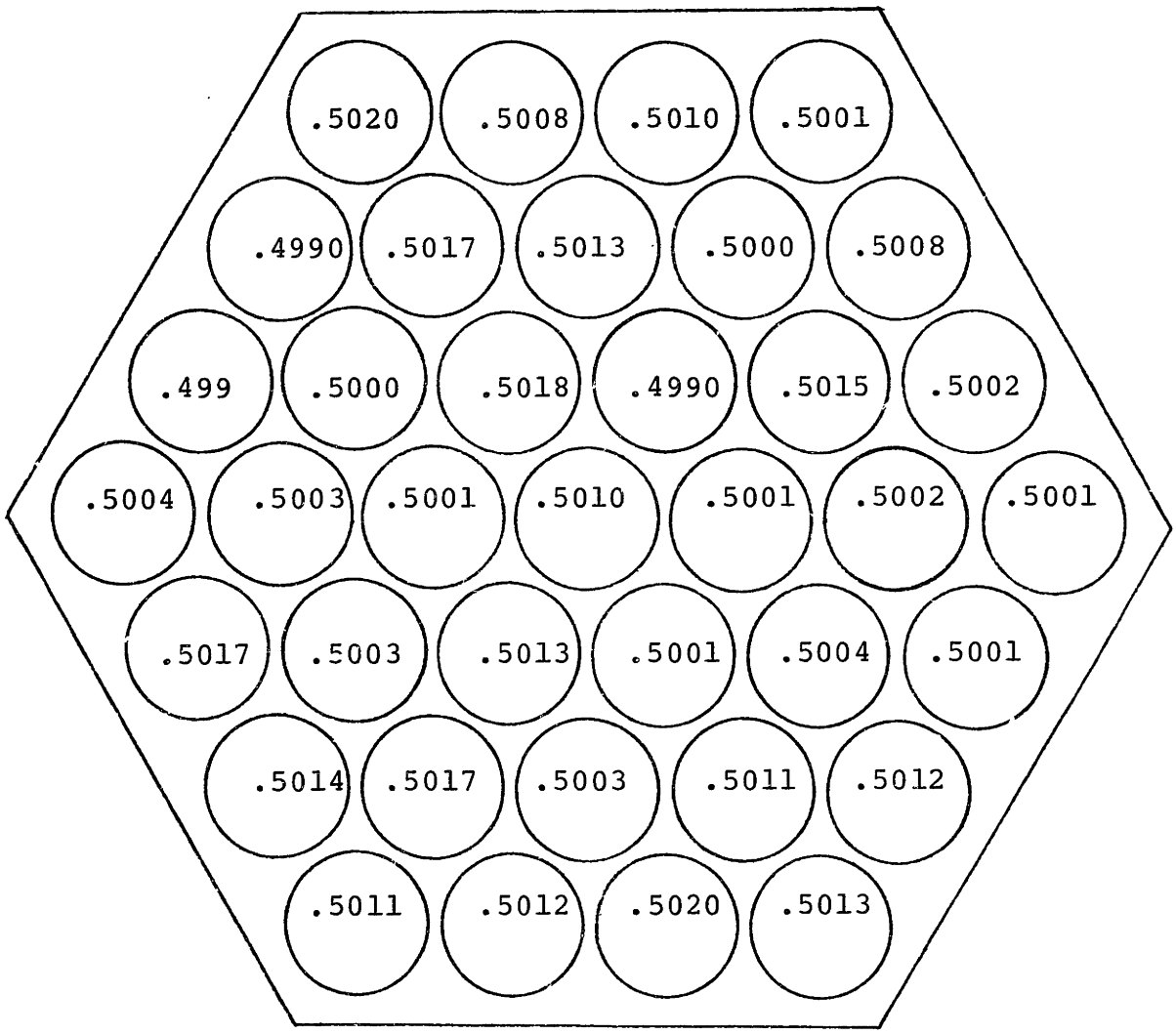

FIGURE 2.1.4 As-Built Pin Diameter Map

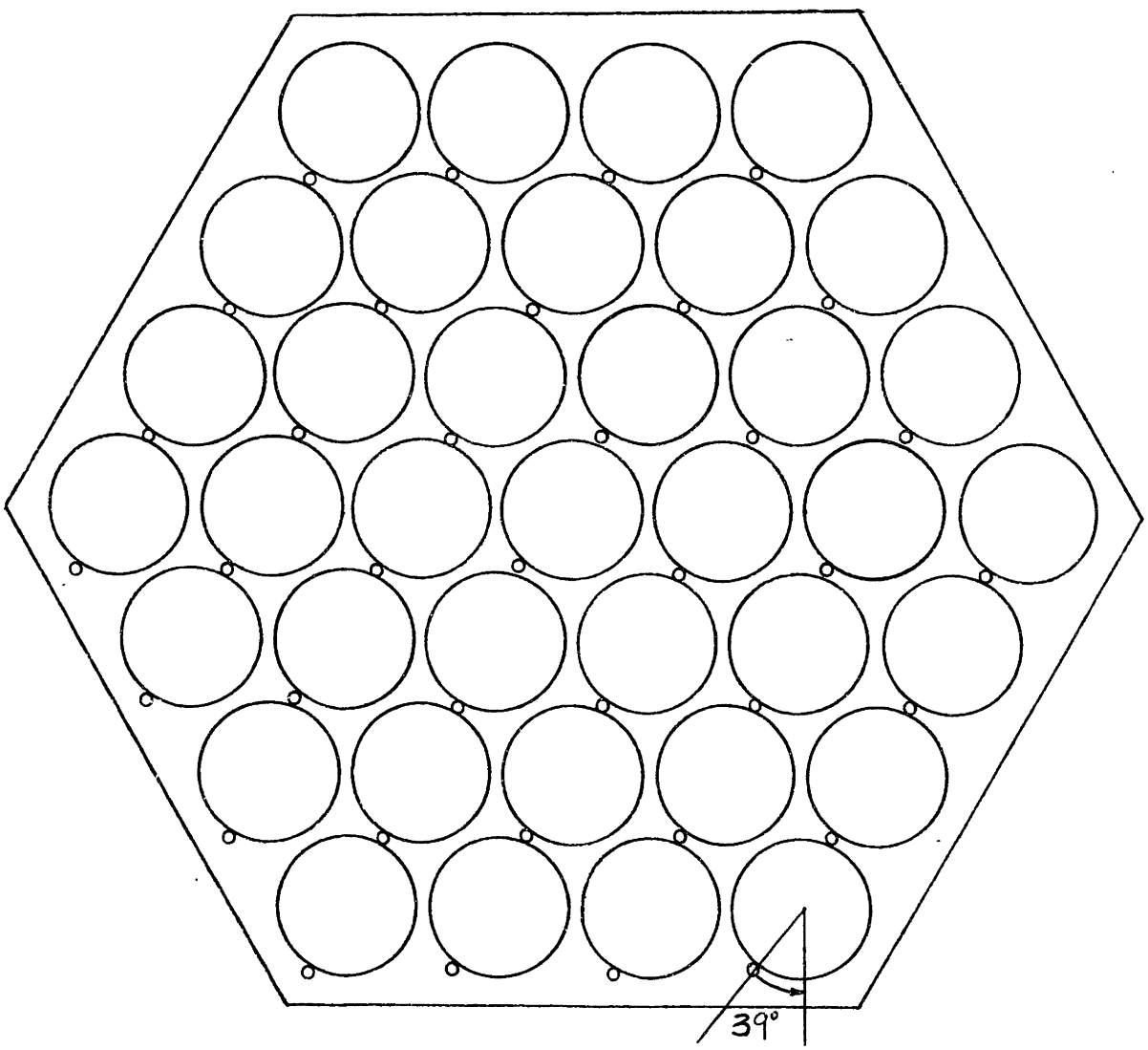

FIGURE 2.1.5 As-Built Wire Location at Exit Plane

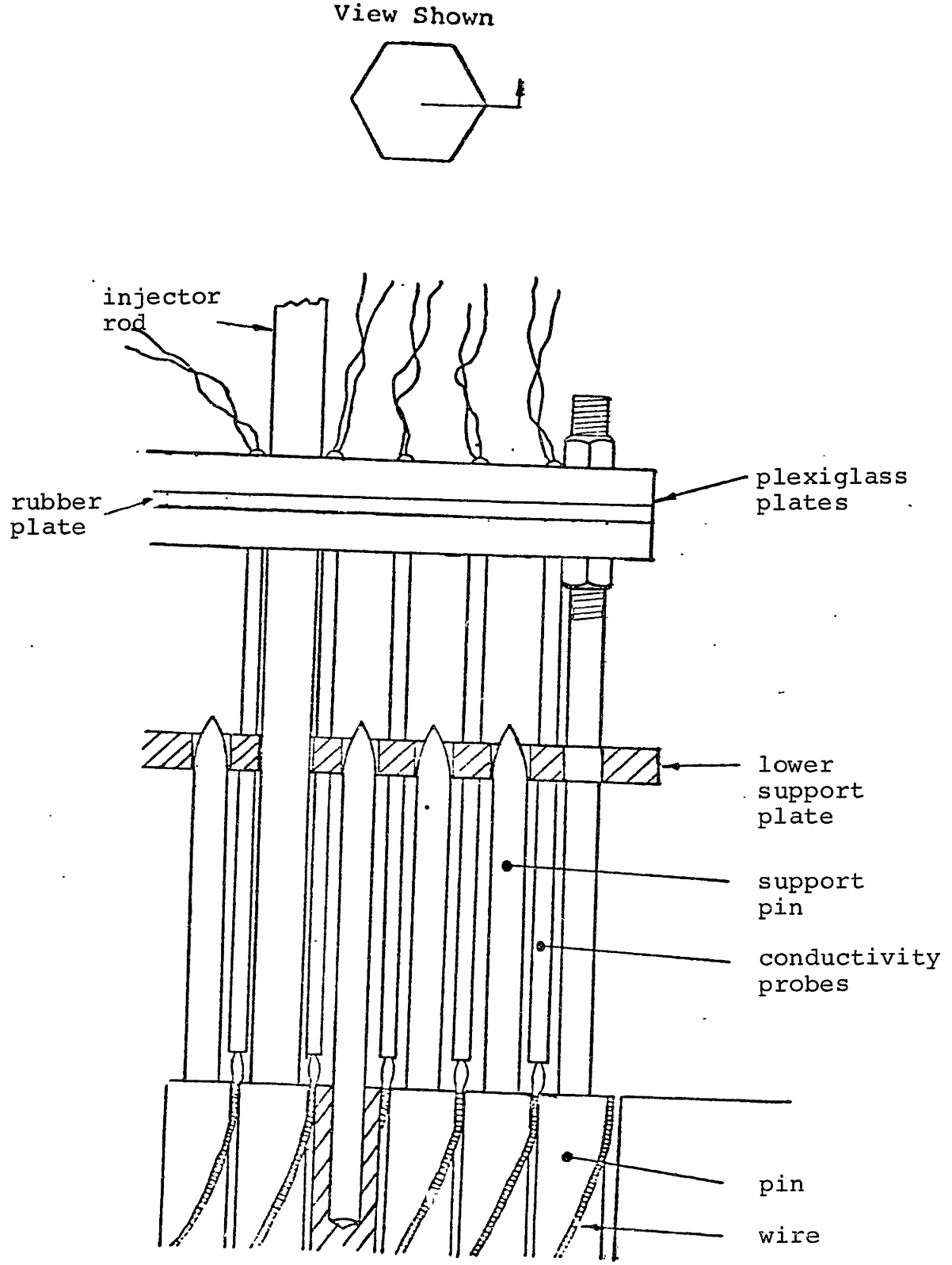

FIGURE 2.2.1 Probe Support Structure in Mixing Experiment

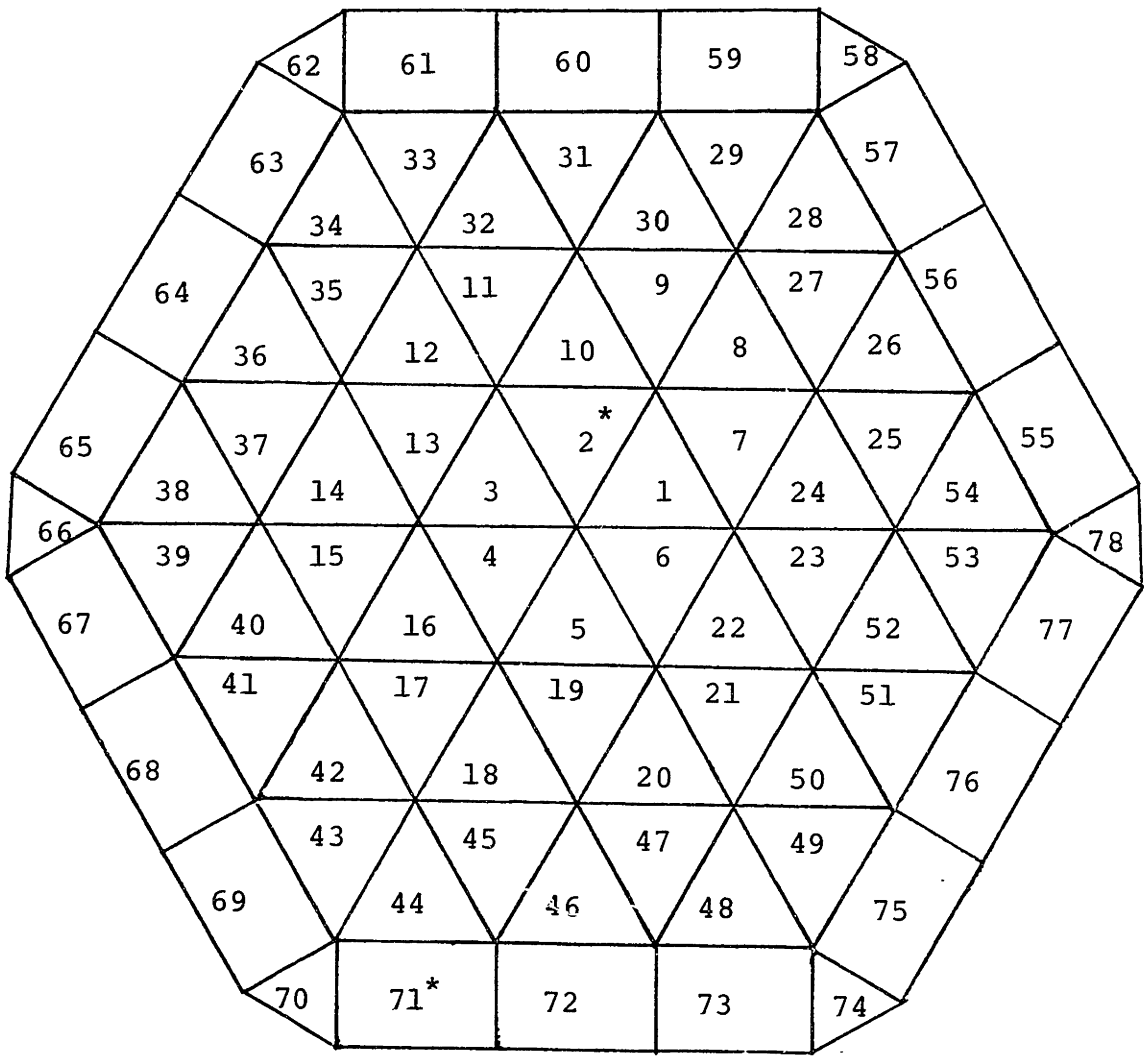

* salt injection subchannel

FIGURE 2.2.2 Subchannel Numbering Scheme for Mixing Experiment

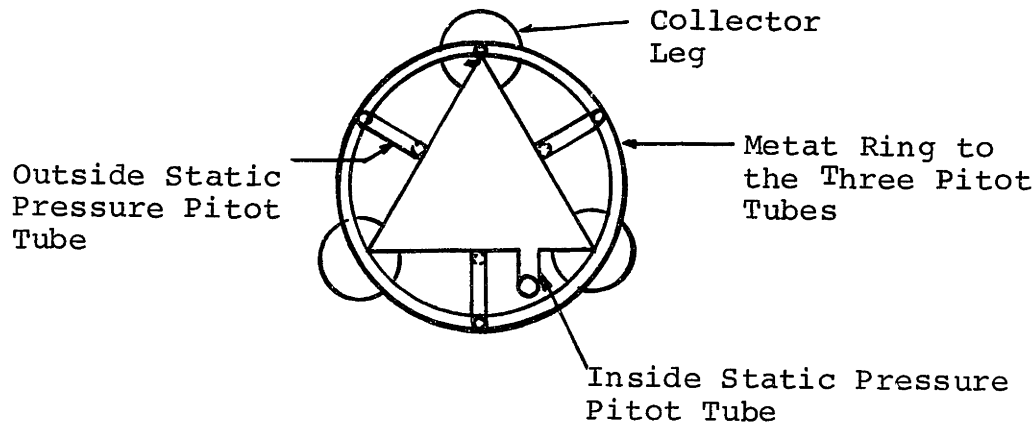

TOP VIEW

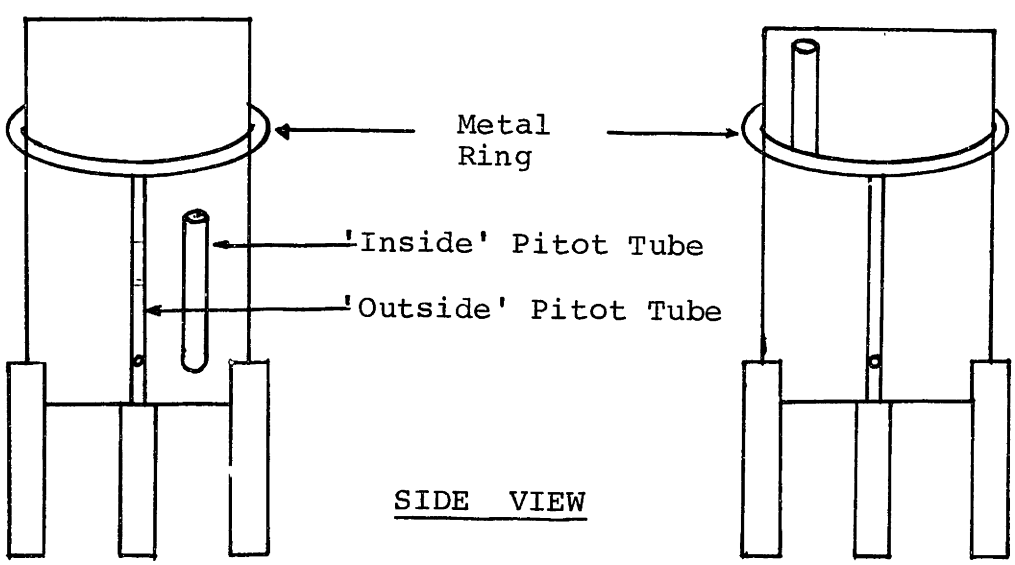

SIDE VIEW

FIGURE 2.3.1 Design Scheme of Sampler for Interior Subchannel

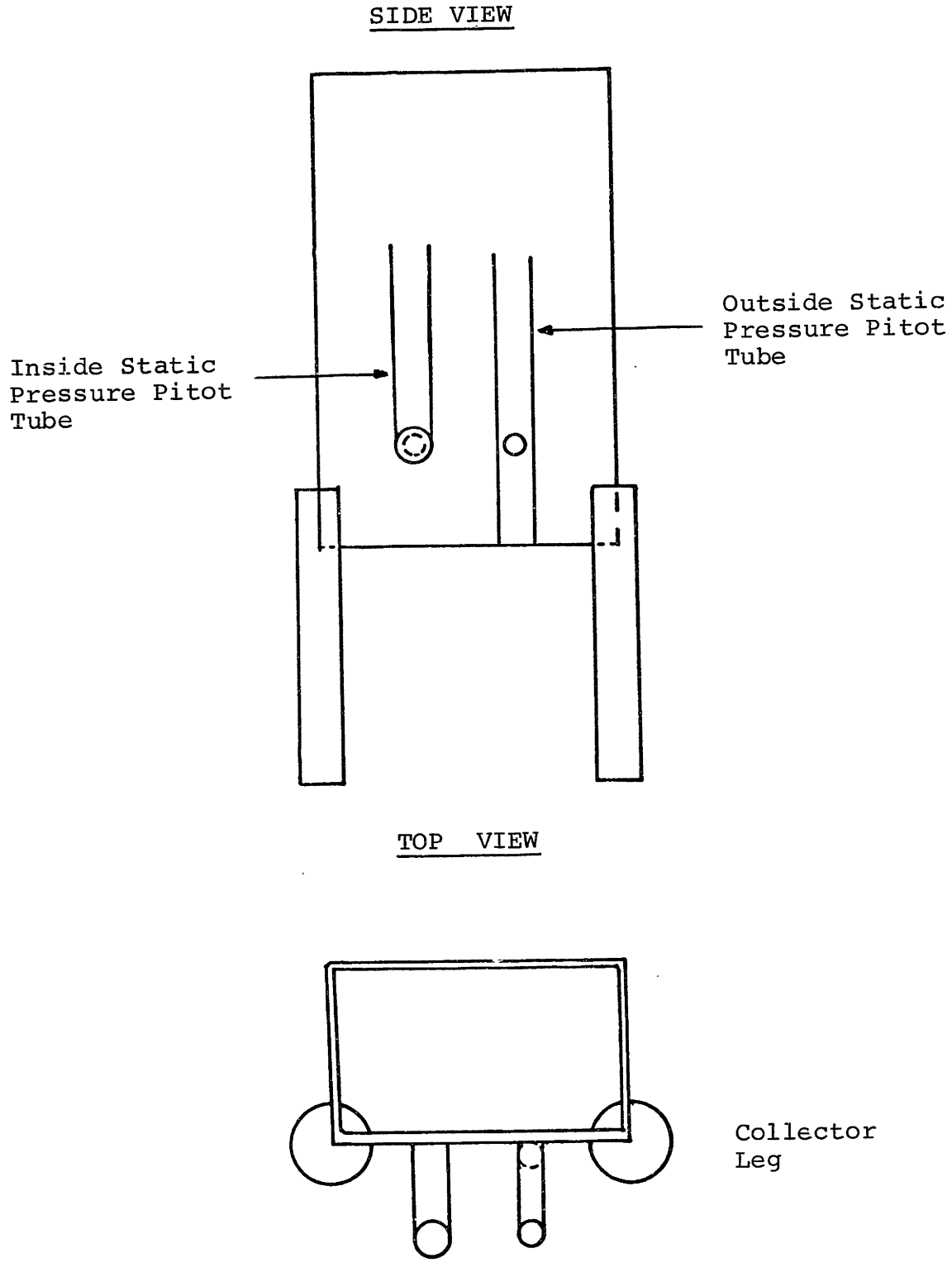

FIGURE 2.3.2 Design Scheme of Sampler for Edge Subchannel

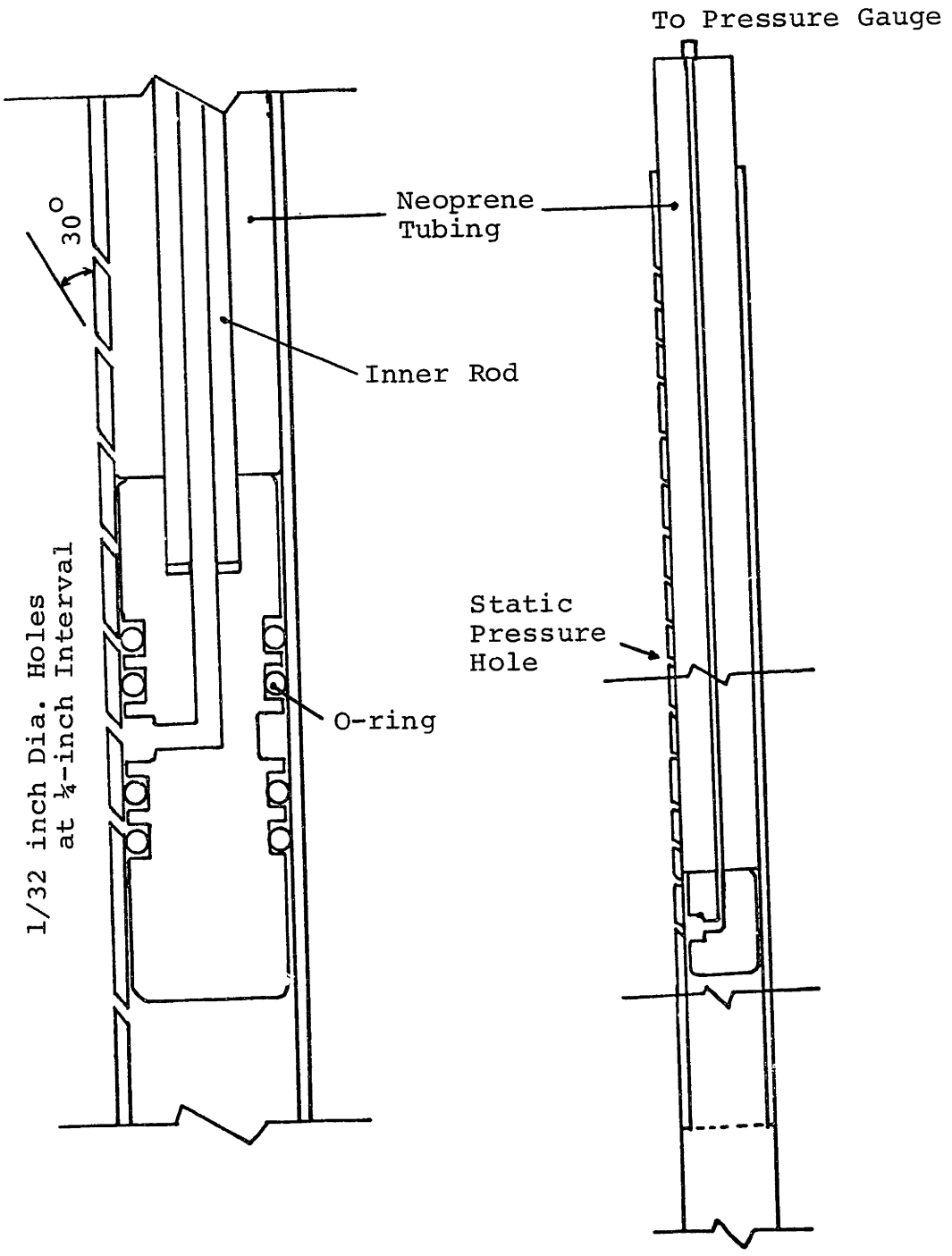

FIGURE 2.4.1 Design Configuration of Instrumentation Rod

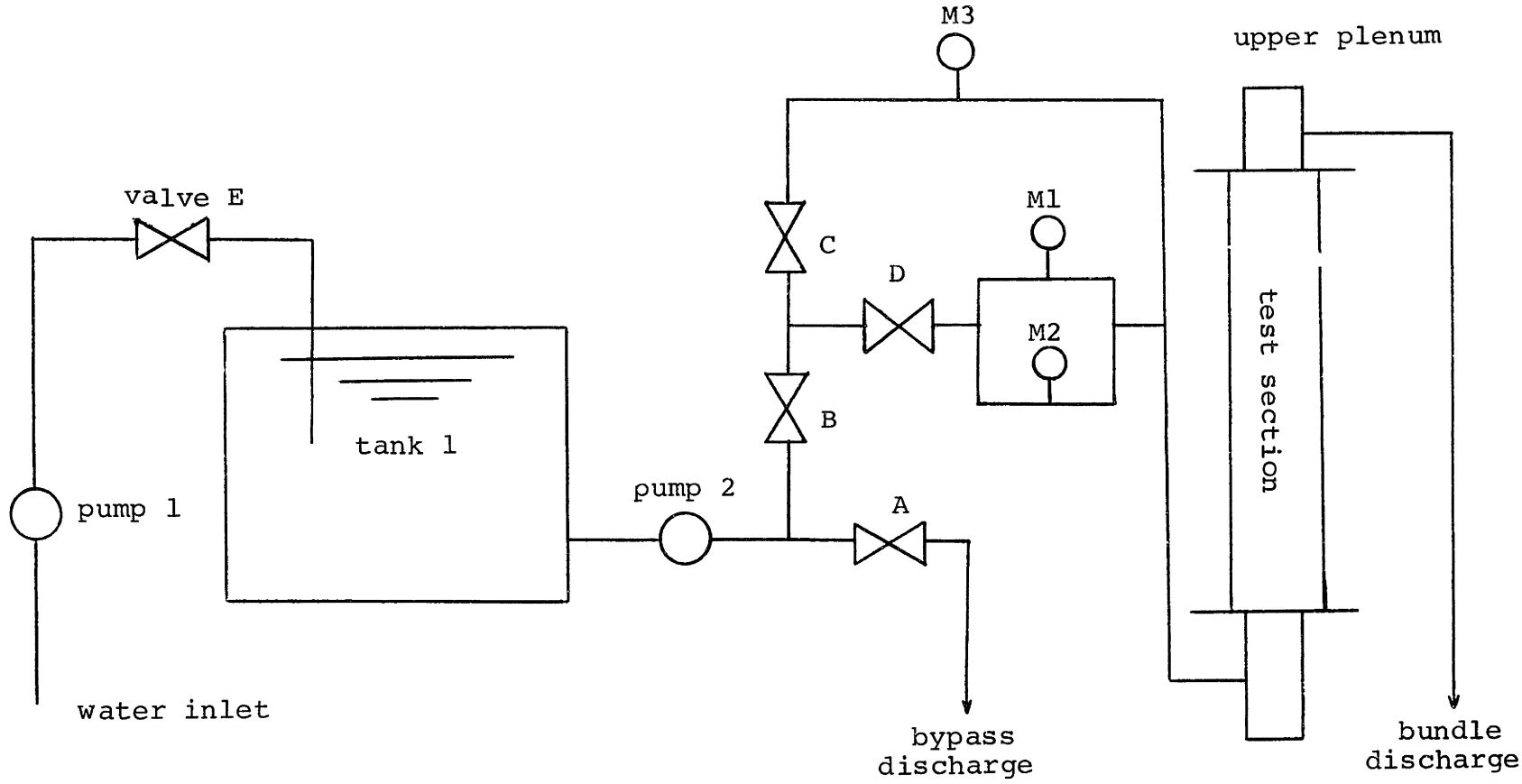

FIGURE 2.5.1 Layout of the Test Section Flow Loop

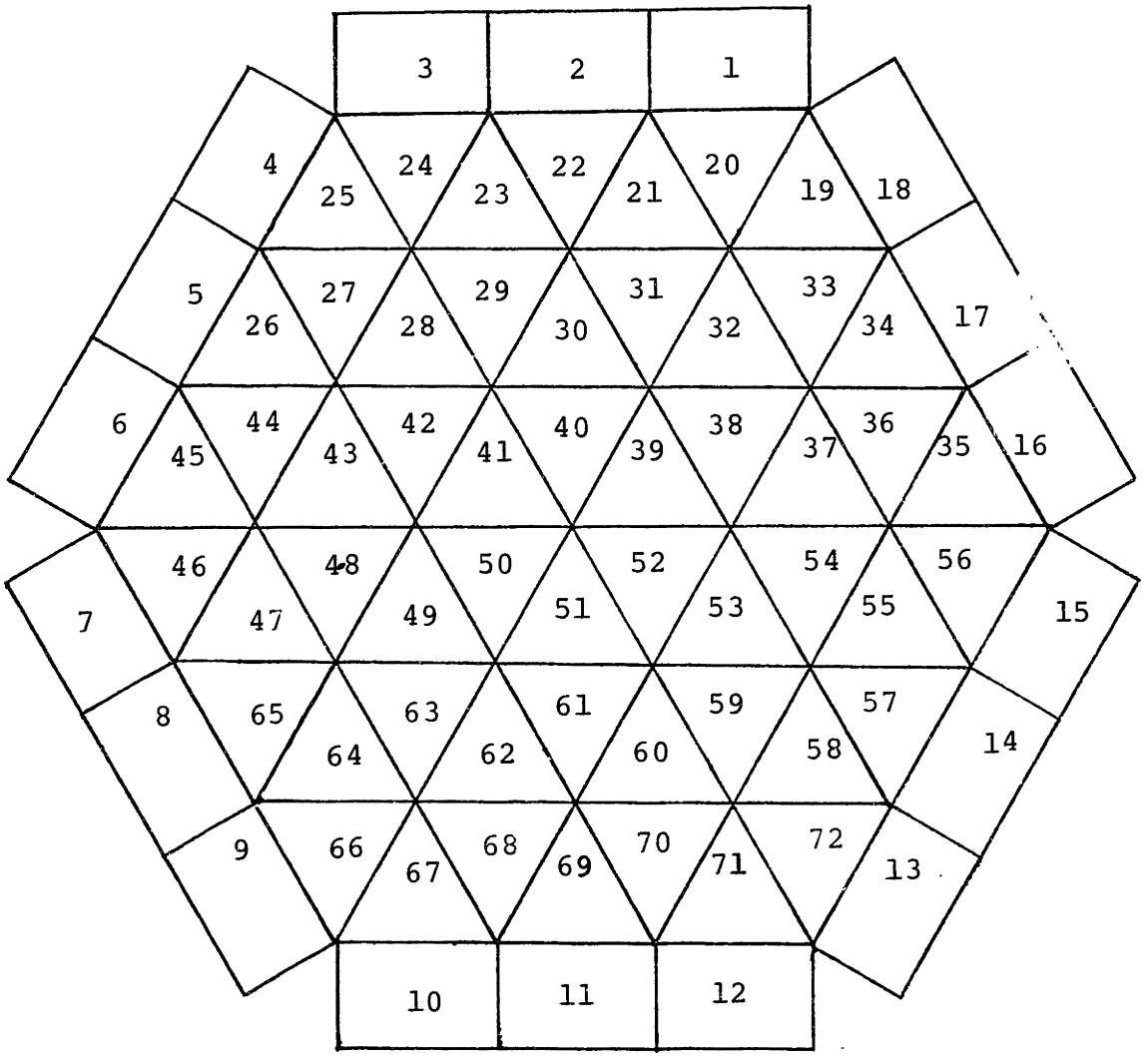

FIGURE 3.1.1 Subchannel Numbering Scheme for Flow Split Experiment

Geometry	Flow Condition
37 Pins	Re = 3086
P/D = 1.15	$\bar{M}_1$ = .275 gpm
H/D = 21.0	Mass Balance Error = -3.9%

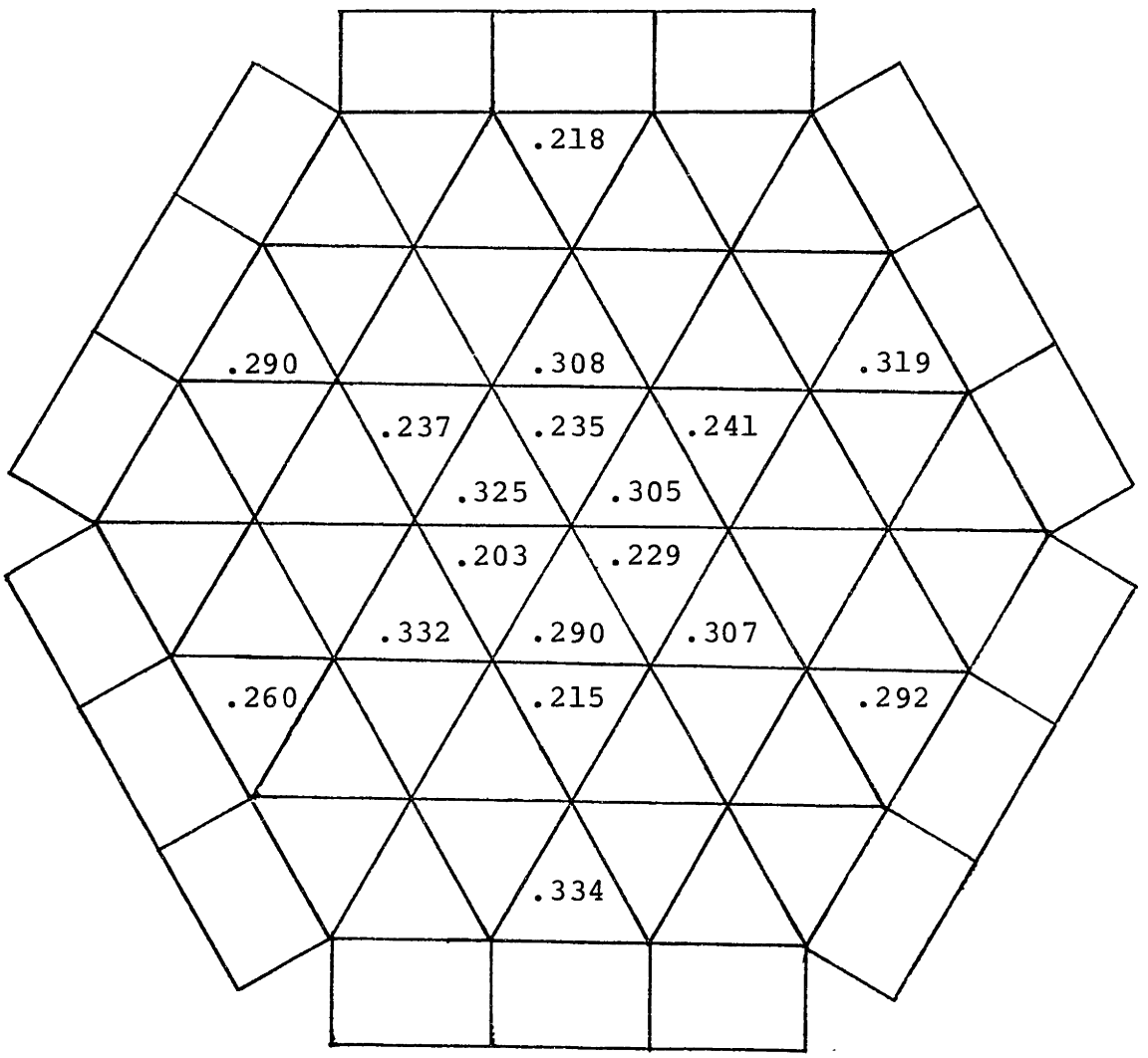

FIGURE 3.1.2 Normalized Cross Flat Traverse Interior Subchannel Flow Map (Re = 3086)

Geometry	Flow Condition
37 Pins	Re = 3822
P/D = 1.15	$\overline{M}_1$ = .330 gpm
H/D = 21.0	Mass Balance Error =-3.6%

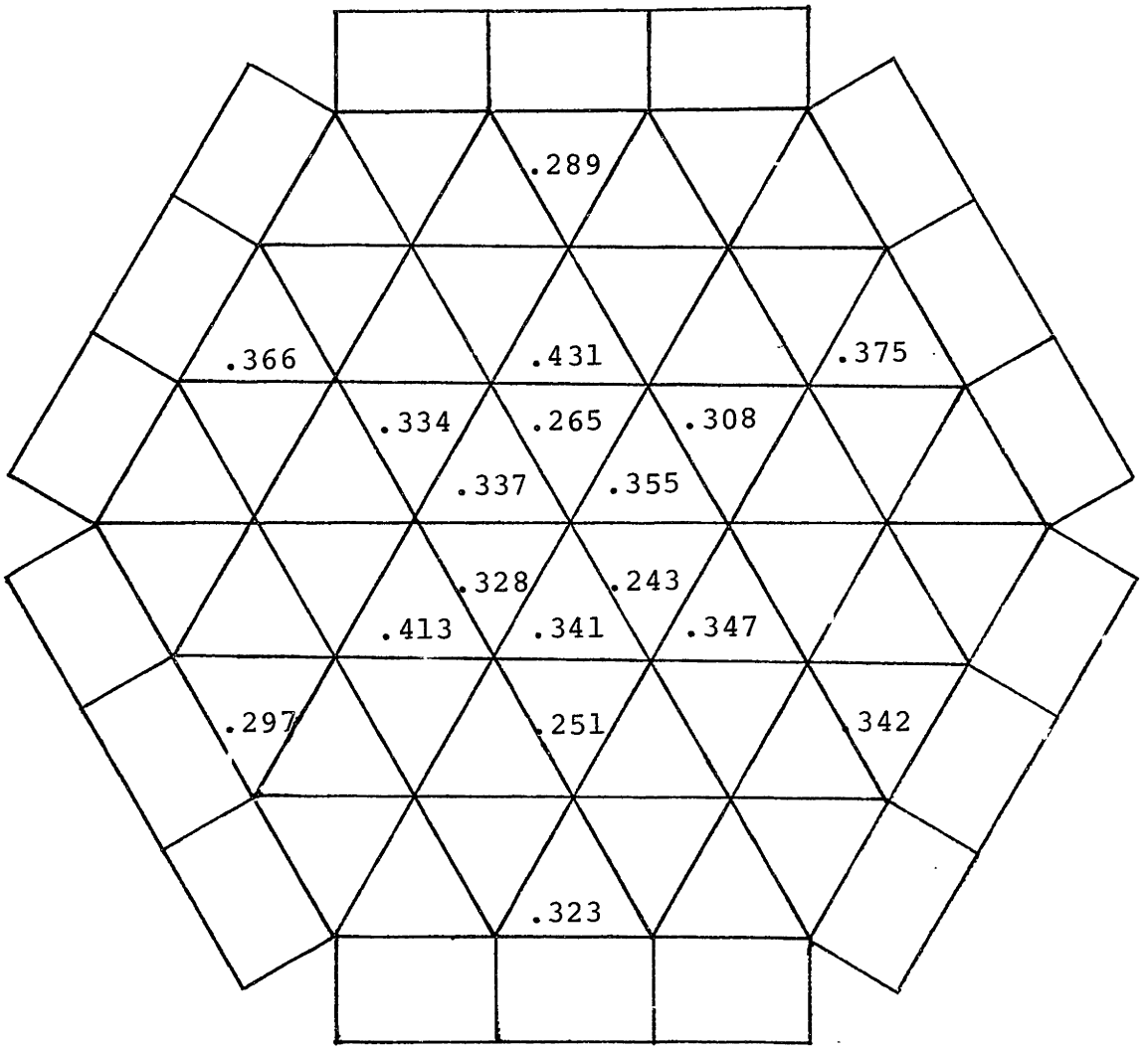

FIGURE 3.1.3 Normalized Cross Flat Traverse Interior Subchannel Flow Map (Re = 3822)

Geometry	Flow Condition
37 Pins	Re = 4503
P/D = 1.15	$\bar{M}_i$ = .394 gpm
H/D = 21.0	Mass Balance Error =-2.7%

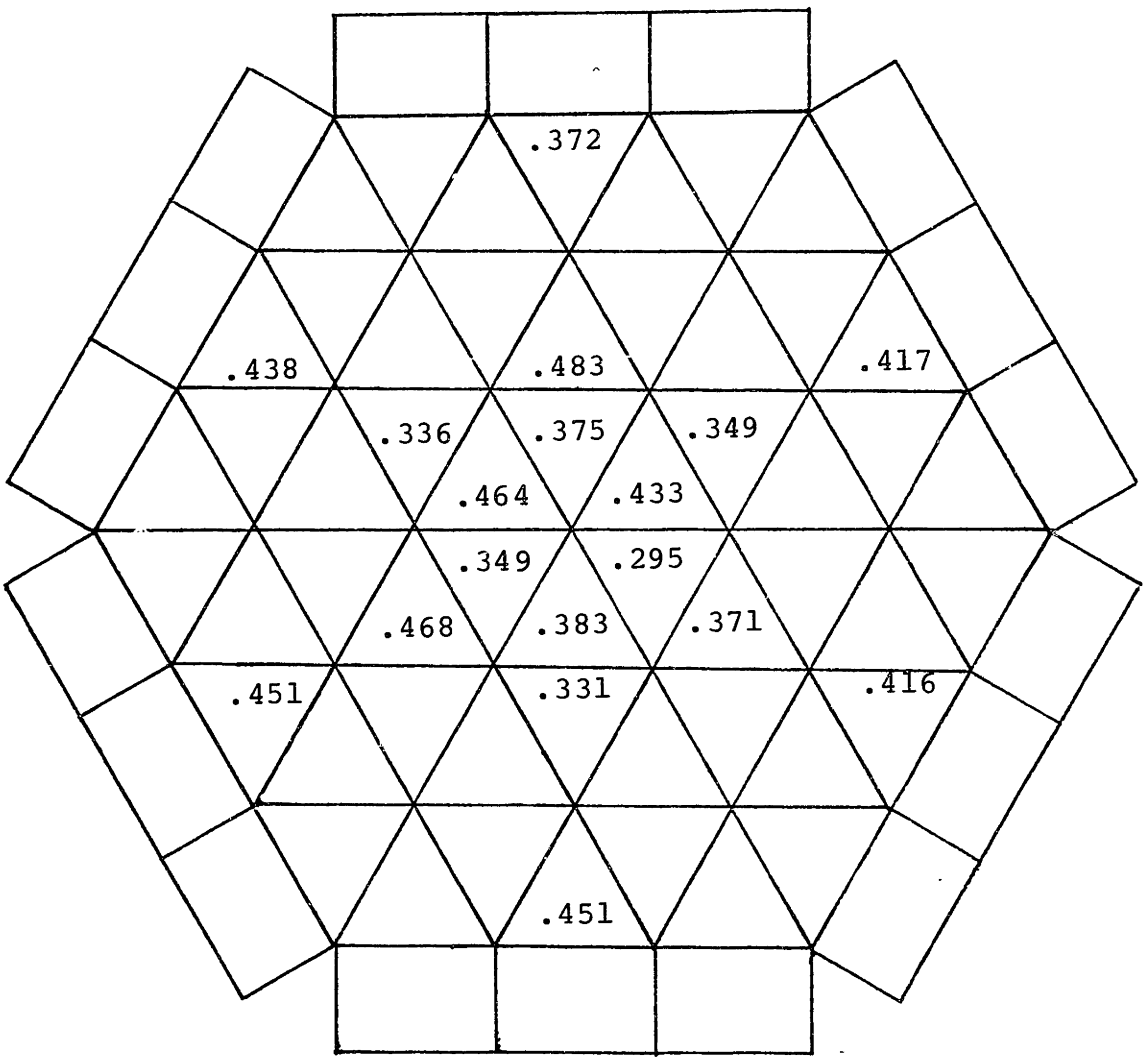

FIGURE 3.1.4 Normalized Cross Flat Traverse Interior Subchannel Flow Map (Re = 4503)

Geometry	Flow Condition
37 Pins	Re = 5263
P/D = 1.15	$\bar{M}_1$ = .513 gpm
H/D = 21.0	Mass Balance Error =-2.1%

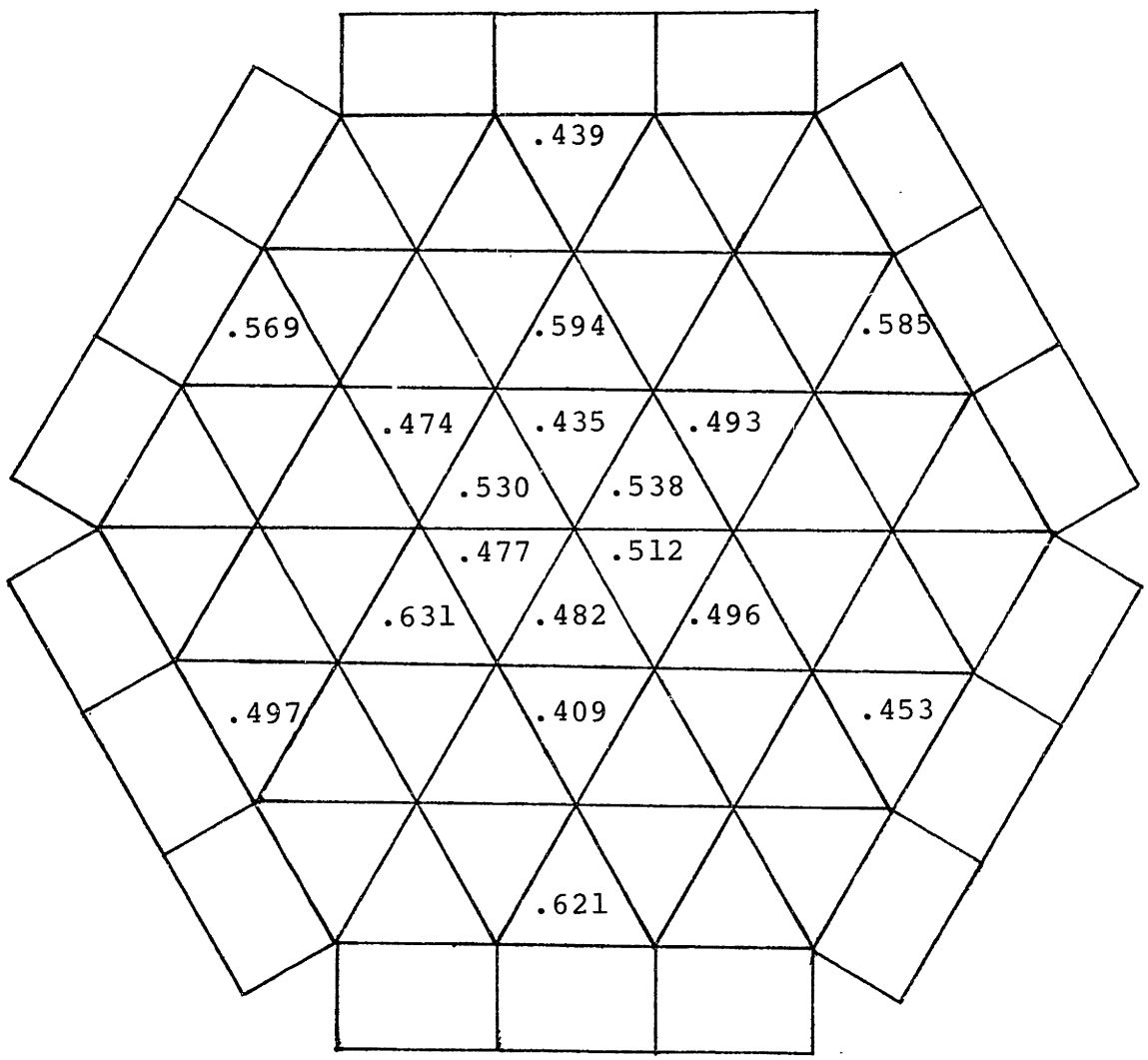

FIGURE 3.1.5 Normalized Cross Flat Traverse Interior Subchannel Flow Map (Re = 5263)

Geometry	Flow Condition
37 Pins	Re = 5279
P/D = 1.15	$\bar{M}_1$ = .464 gpm
H/D = 21.0	Mass Balance Error = -1.4%

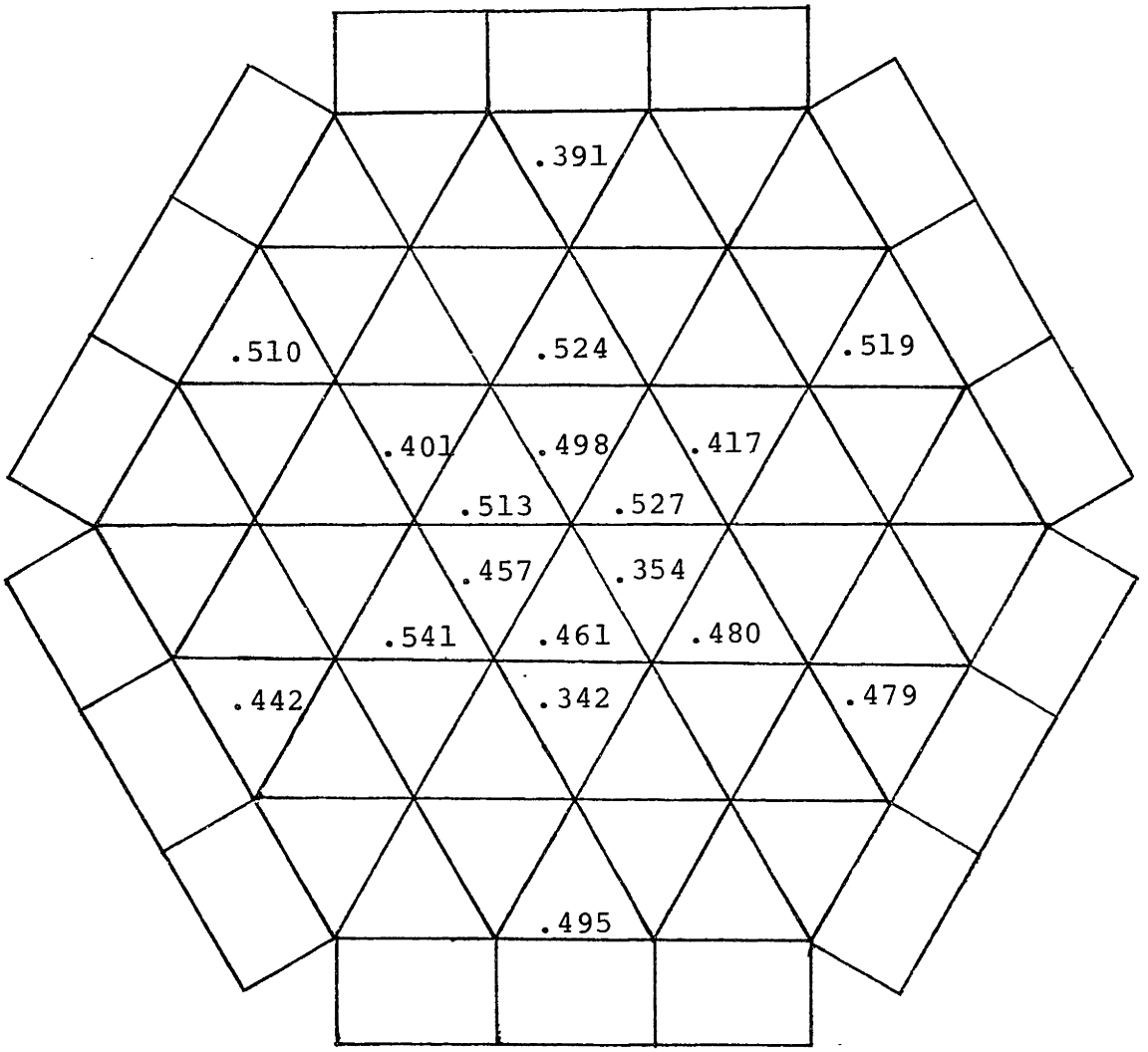

FIGURE 3.1.6 Normalized Cross Flat Traverse Interior Subchannel Flow Map (Re = 5279)

Geometry	Flow Condition
37 pins	Re = 6312
P/D = 1.15	$\bar{M}_1$ = .556 gpm
H/D = 21.0	Mass Balance Error =-3.3%

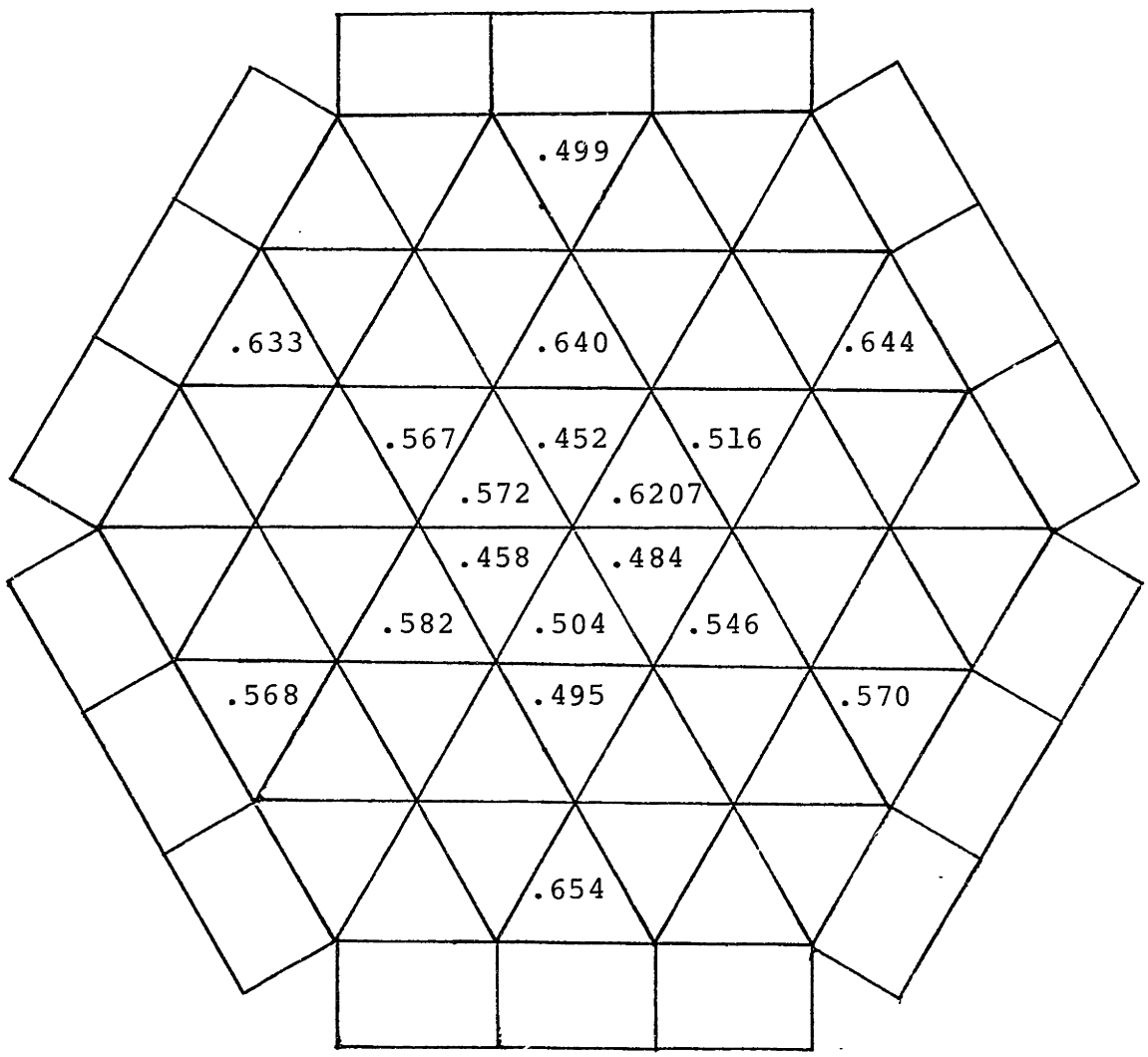

FIGURE 3.1.7 Normalized Cross Flat Traverse Interior Subchannel Flow Map (Re = 6312)

Geometry	Flow Condition
37 Pins	Re = 6315
P/D = 1.15	$\bar{M}_1$ = .598 gpm
H/D = 21.0	Mass Balance Error =-2.5%

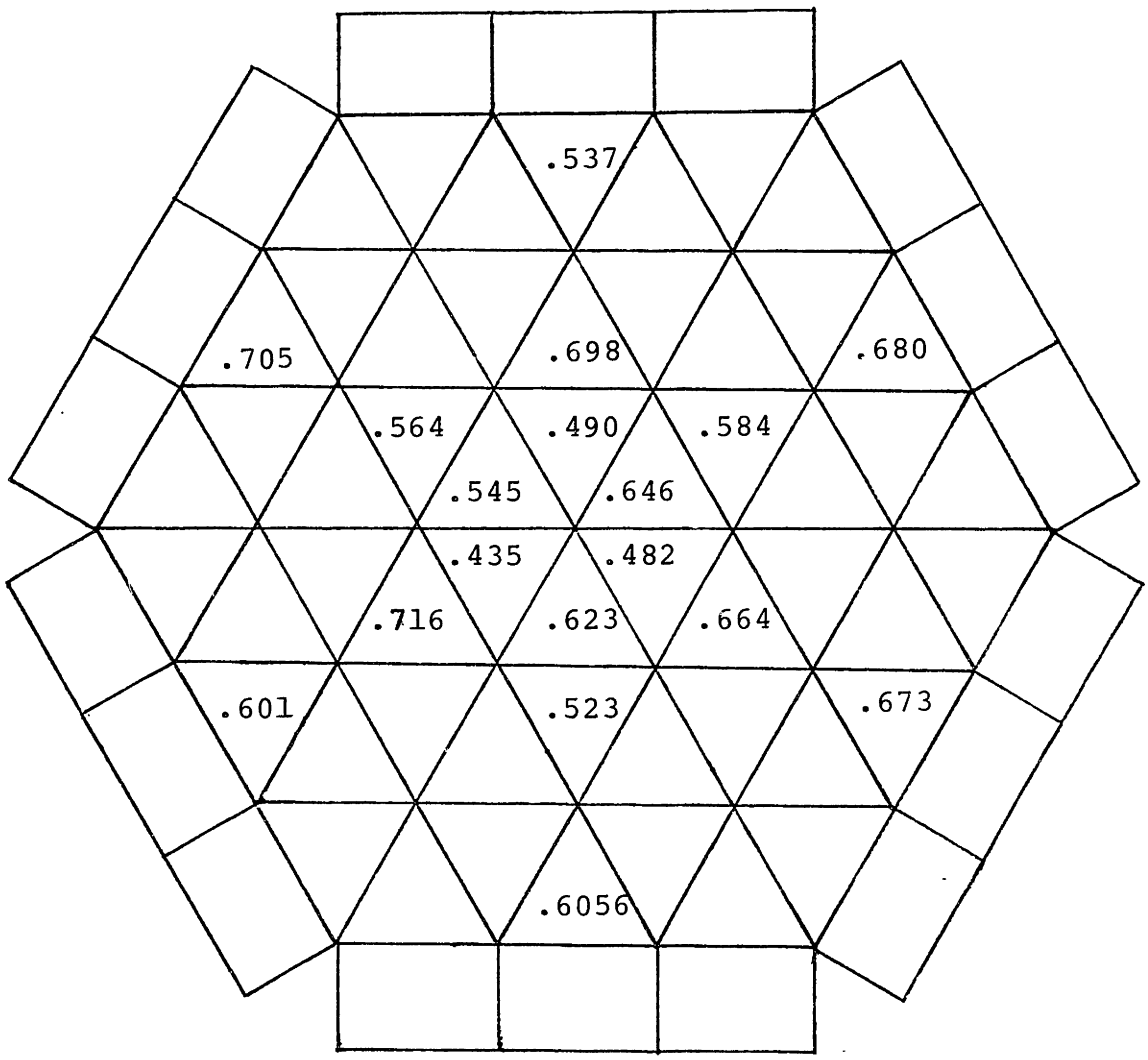

FIGURE 3.1.8 Normalized Cross Flat Traverse Interior Subchannel Flow Map (Re = 6315)

Geometry	Flow Condition
37 Pins	Re = 8518
P/D = 1.15	$\overline{M}_1$ = .776 gpm
H/D = 21.0	Mass Balance Error = 1.6%

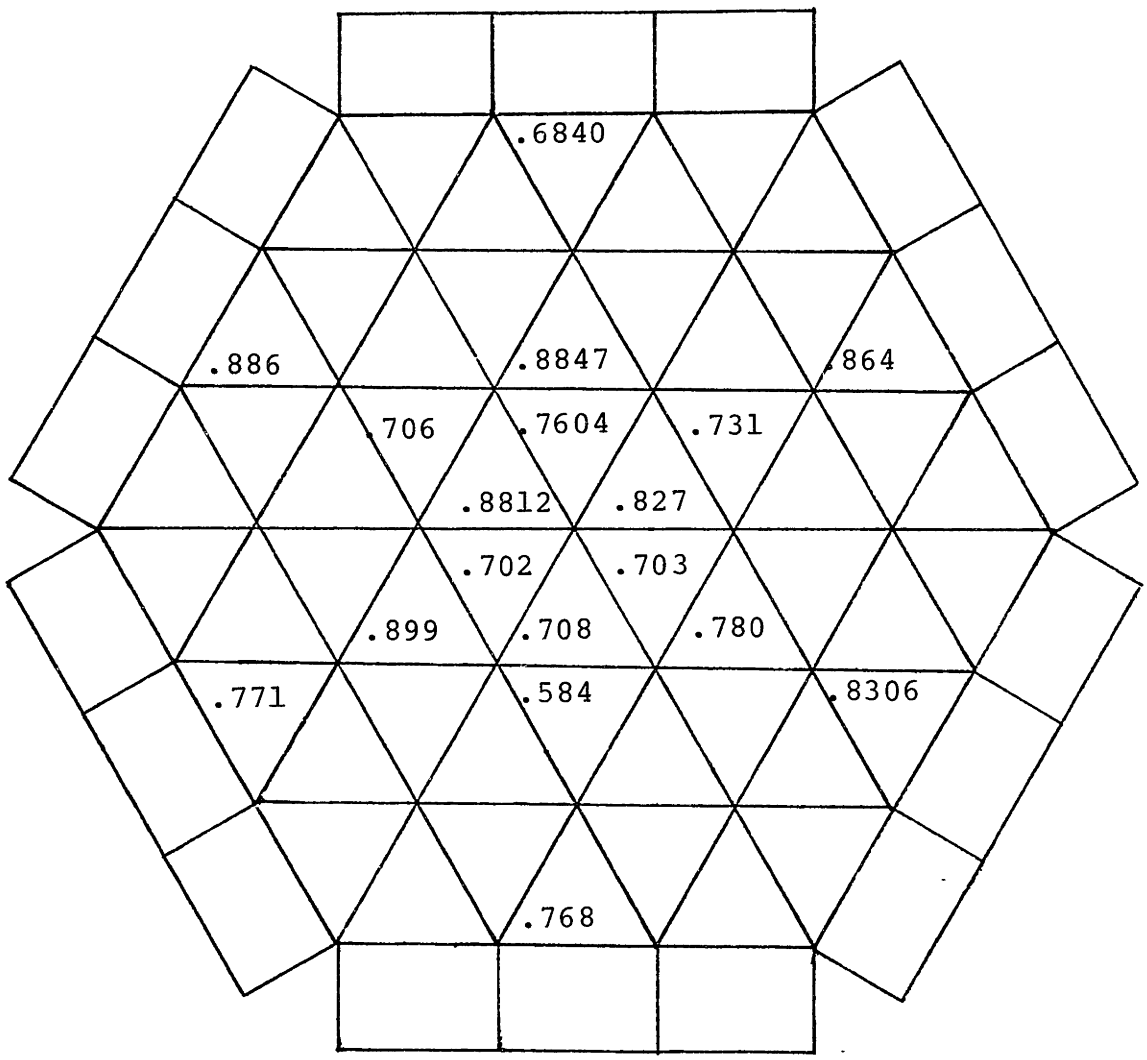

FIGURE 3.1.9 Normalized Cross Flat Traverse Interior Subchannel Flow Map (Re = 8518)

Geometry	Flow Condition
37 Pins	Re = 10772
P/D = 1.15	$\bar{M}_1$ = .994 gpm
H/D = 21.0	Mass Balance Error = 1.96%

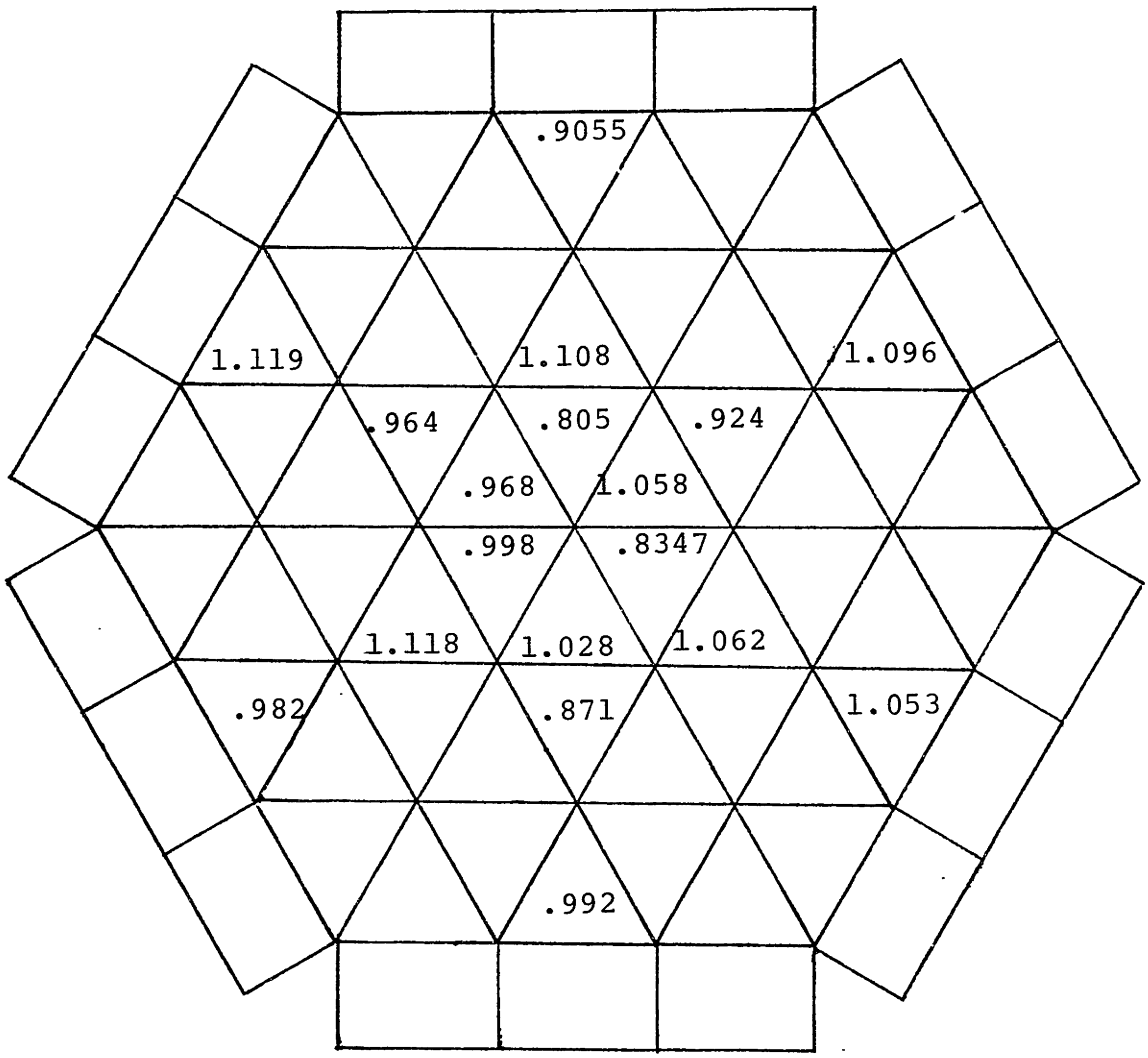

FIGURE 3.1.10 Normalized Cross Flat Traverse Interior Subchannel Flow Map (Re = 10772)

Geometry	Flow Condition
37 Pins	Re = 12280
P/D = 1.15	$\bar{M}_1$ = 1.117 gpm
H/D = 21.0	Mass Balance Error = 3.4%

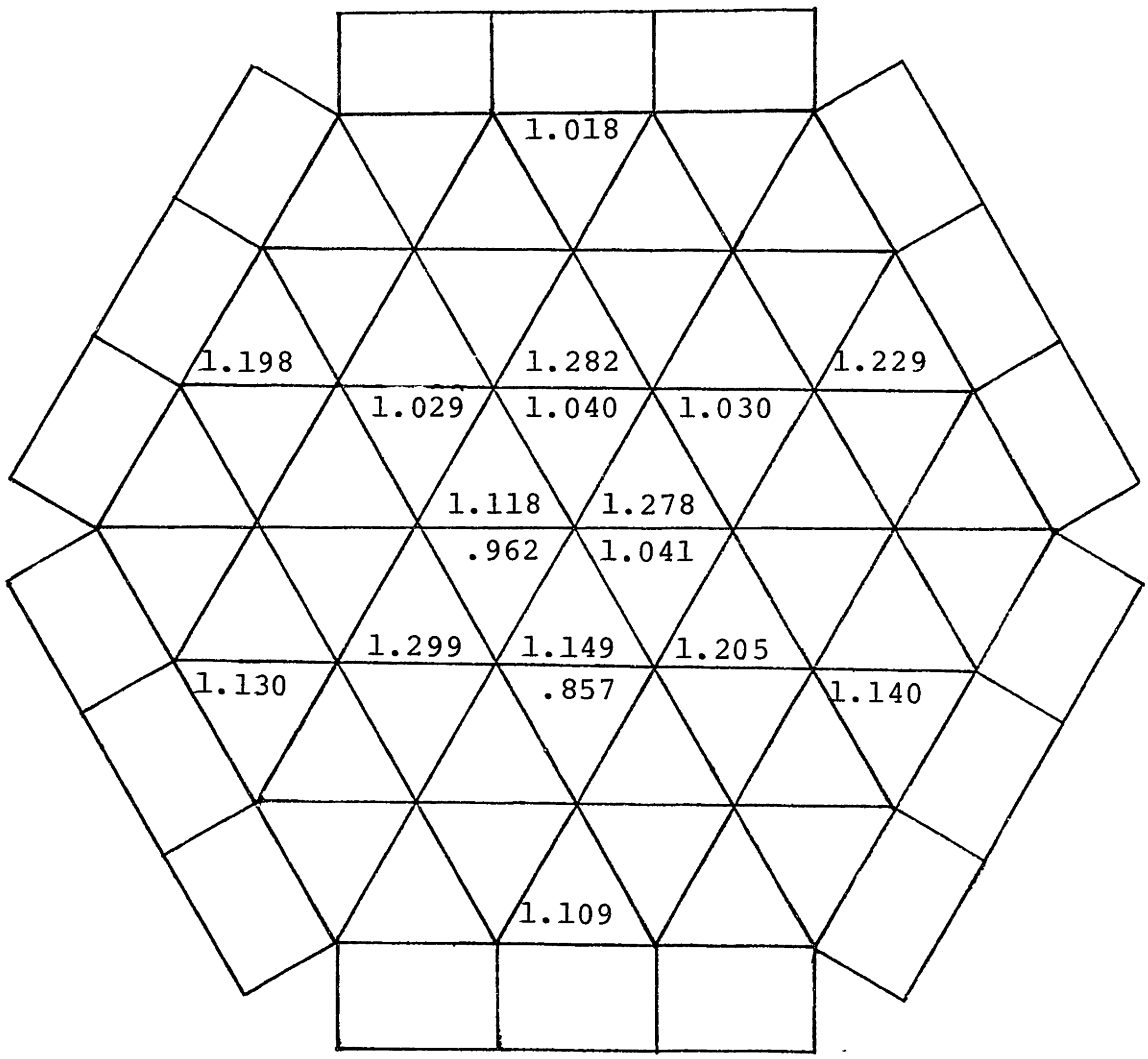

FIGURE 3.1.11 Normalized Cross Flat Traverse Interior Subchannel Flow Map (Re = 12280)

Geometry	Flow Condition
37 Pins	Re = 13974
P/D = 1.15	$\bar{M}_1$ = 1.265 gpm
H/D = 21.0	Mass Balance Error = 1.9%

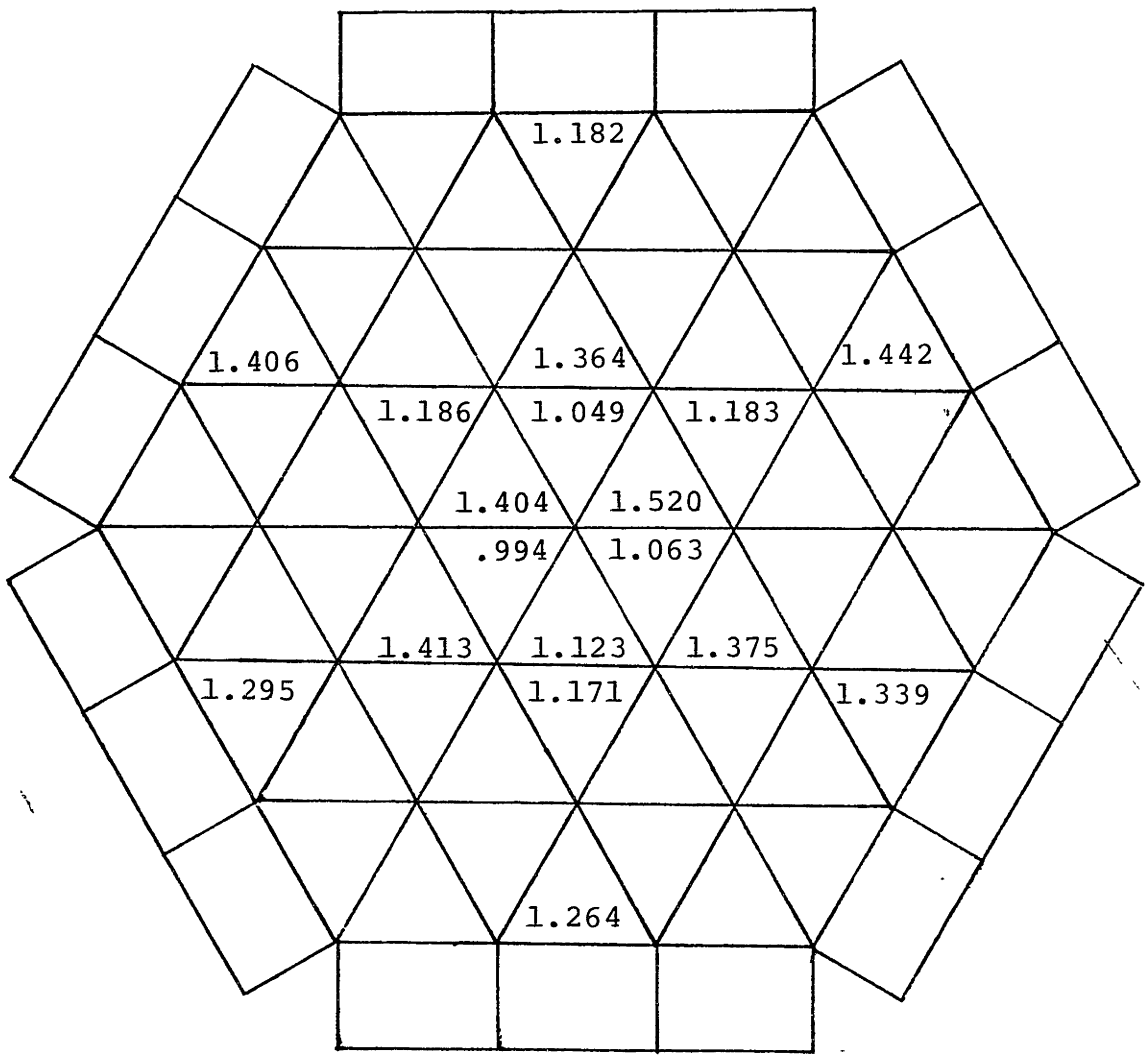

FIGURE 3.1.12 Normalized Cross Flat Traverse Interior Subchannel Flow Map (Re = 13974)

Geometry	Flow Condition
37 Pins	Re = 3235
P/D = 1.15	$\bar{M}_2$ = .586 gpm
H/D = 21.0	Mass Balance Error =-3.6%

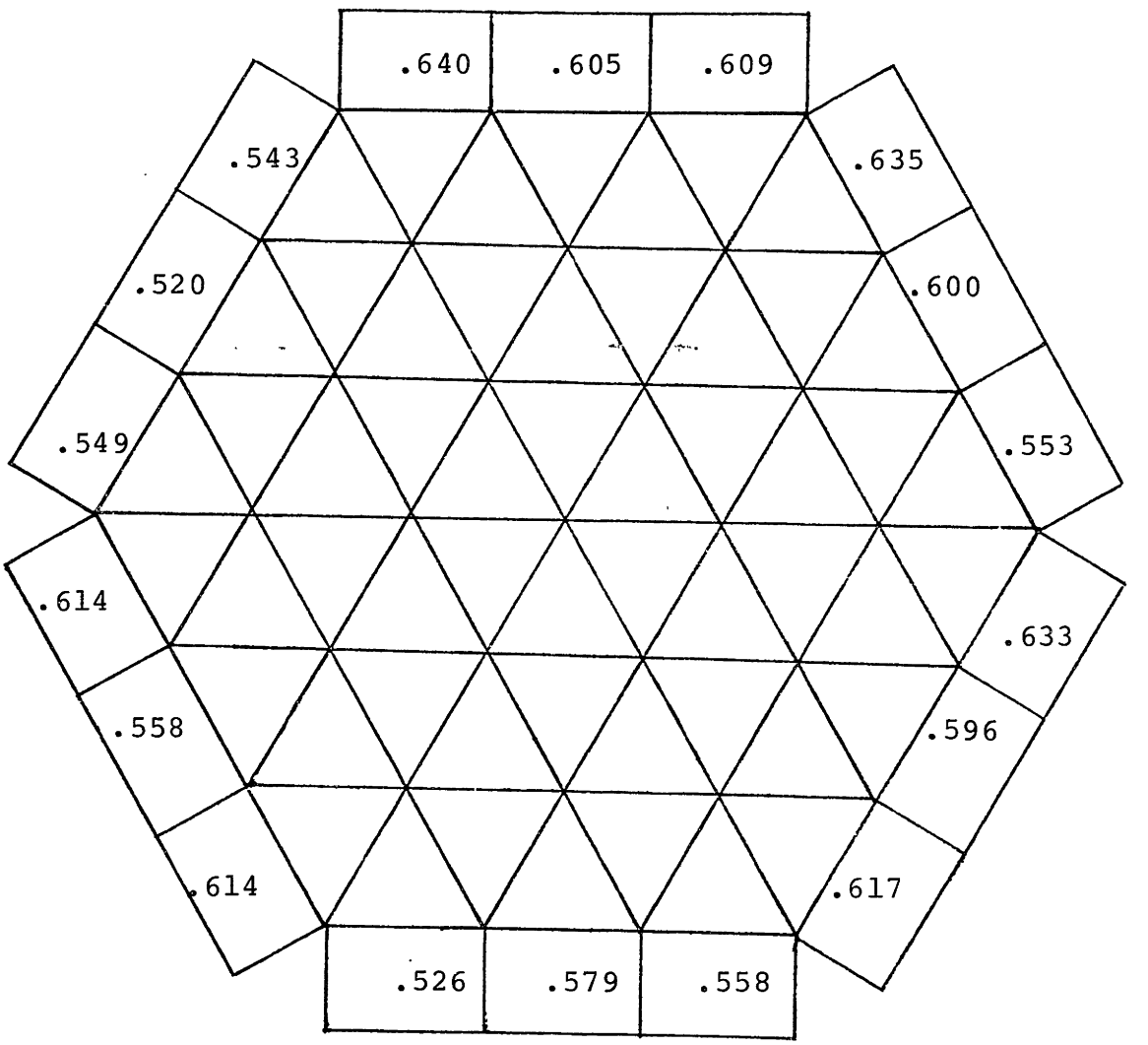

FIGURE 3.1.13 Normalized Edge Subchannel Flow Map (Re = 3235)

Geometry	Flow Condition
37 Pins	Re = 3745
P/D = 1.15	$\overline{M}_2$ = .730 gpm
H/D = 21.9	Mass Balance Error =-3.9%

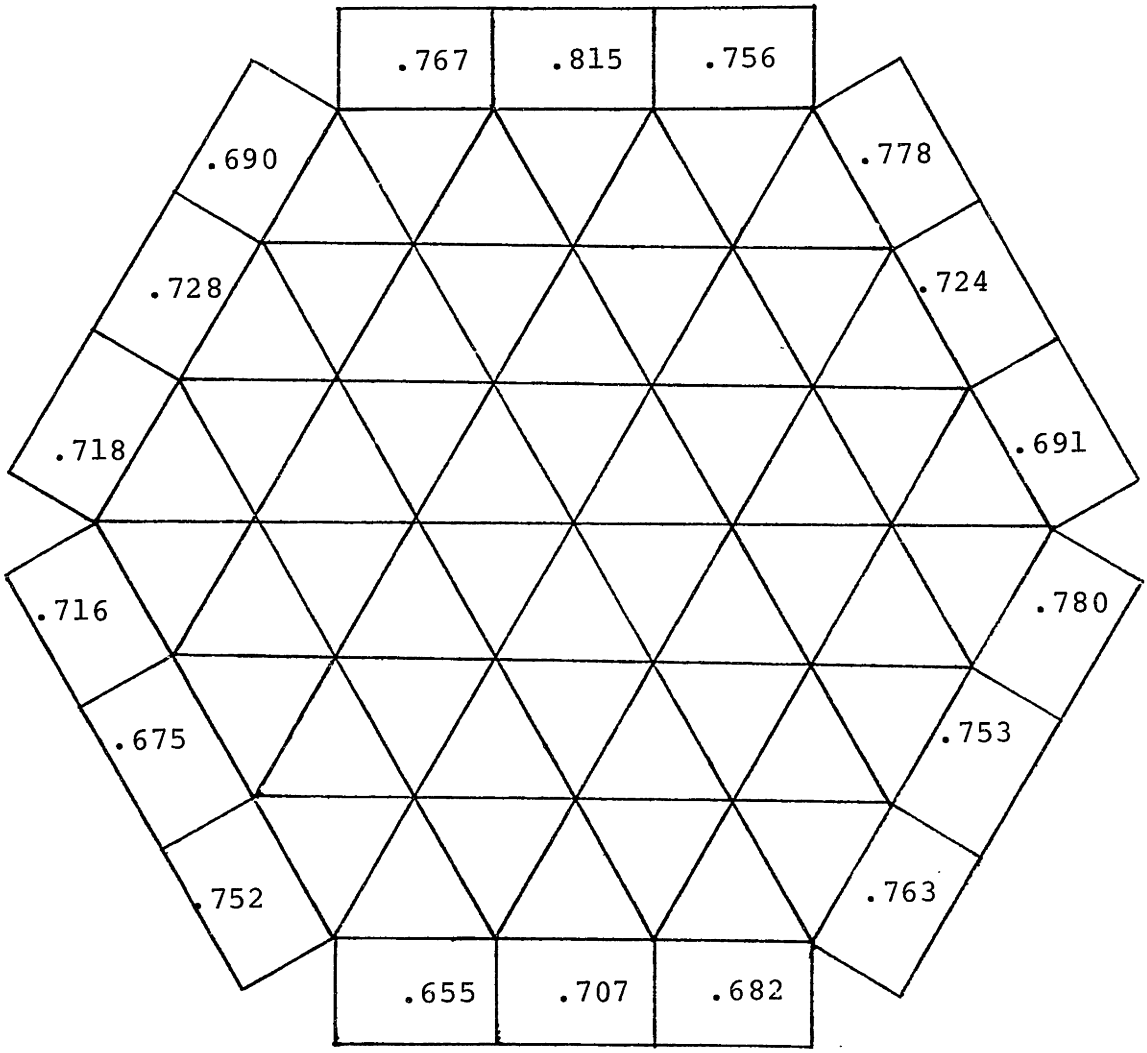

FIGURE 3.1.14 Normalized Edge Subchannel Flow Map (Re = 3745)

Geometry	Flow Condition
37 Pins	Re = 4463
P/D = 1.15	$\overline{M}_2$ = .8450 gpm
H/D = 21.0	Mass Balance Error = - 2.7%

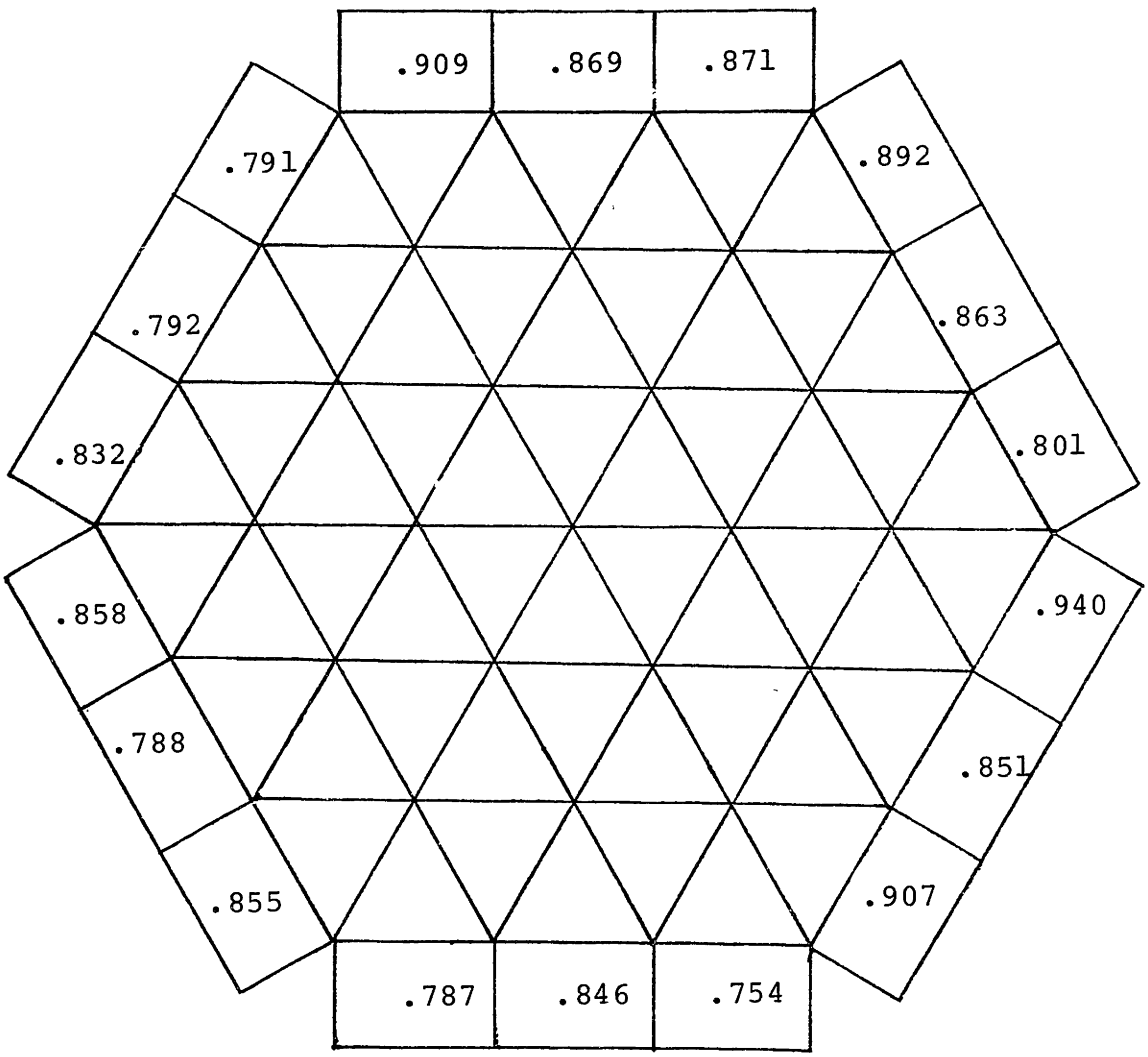

FIGURE 3.1.15 Normalized Edge Subchannel Flow Map (Re = 4463)

Geometry	Flow Condition
37 Pins	Re = 5279
P/D = 1.15	$\bar{M}_2$ = 1.007 gpm
H/D = 21.0	Mass Balance Error =-1.4%

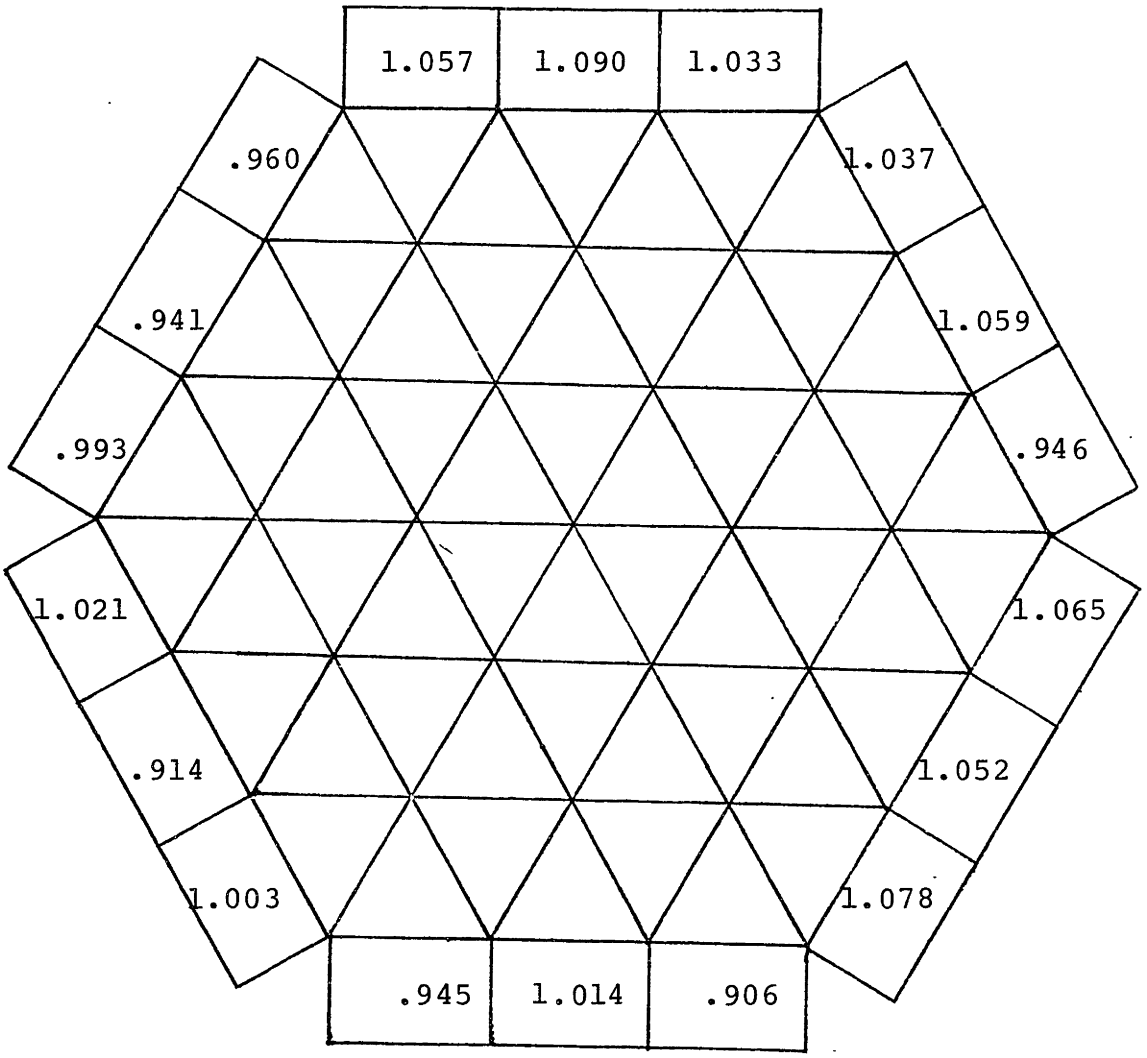

FIGURE 3.1.16 Normalized Edge Subchannel Flow Map (Re = 5279)

Geometry	Flow Condition
37 Pins	Re = 5832
P/D = 1.15	$\bar{M}_2$ = 1.098 gpm
H/D = 21.0	Mass Balance Error =-2.1%

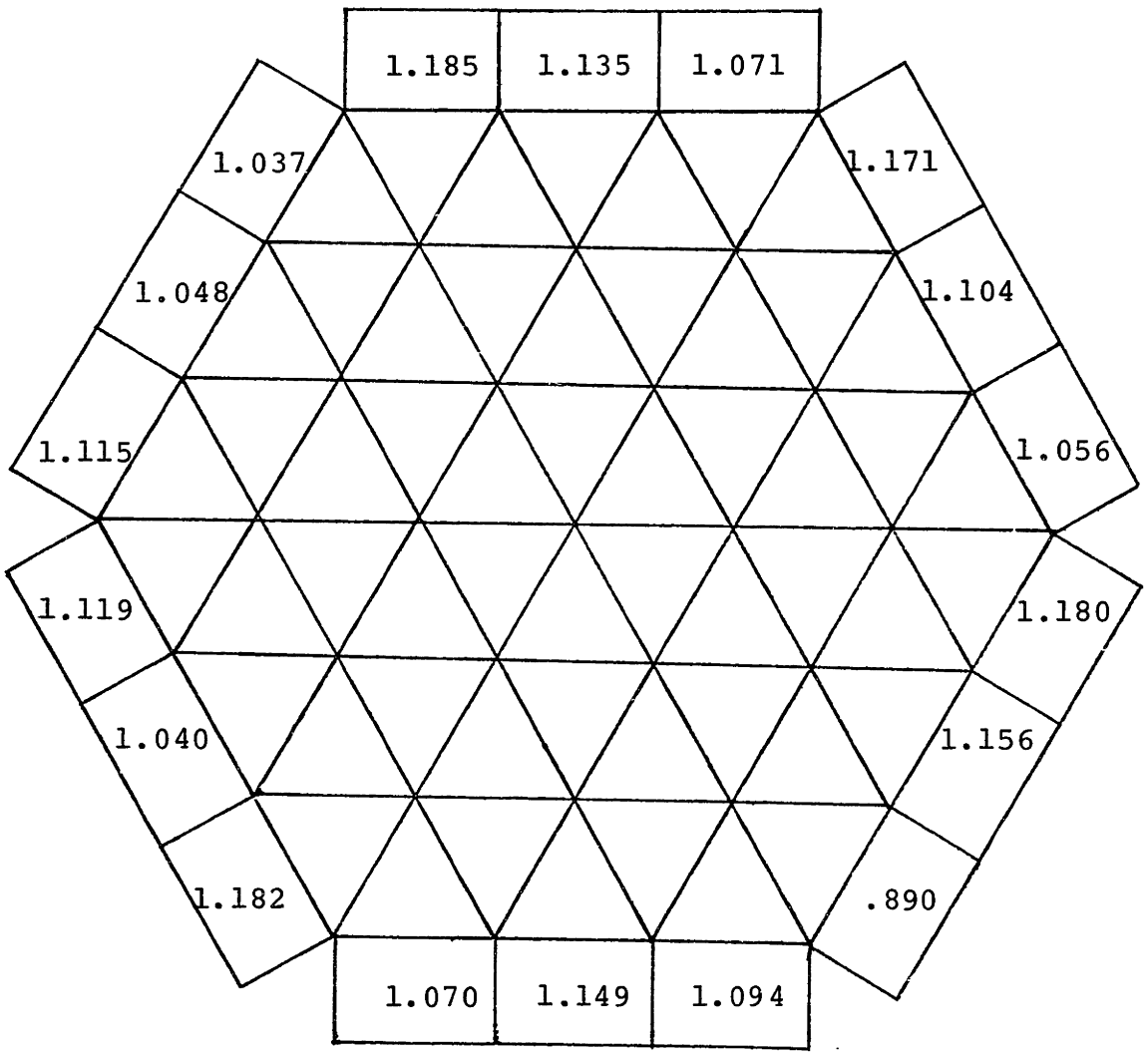

FIGURE 3.1.17 Normalized Edge Subchannel Flow Map (Re = 5832)

Geometry	Flow Condition
37 Pins	Re = 6312
P/D = 1.15	$\bar{M}_2$ = 1.220 gpm
H/D = 21.0	Mass Balance Error = -3.3%

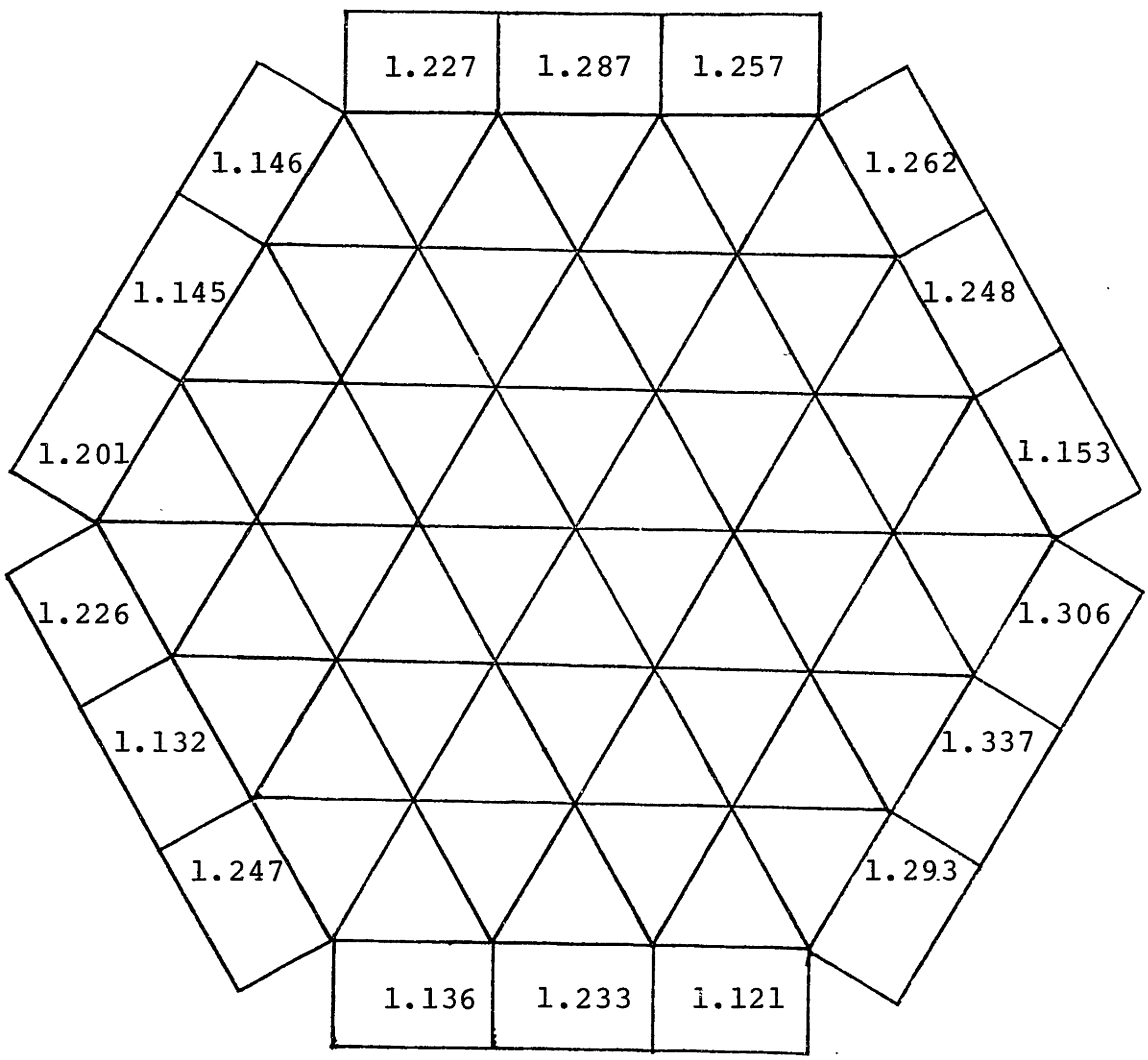

FIGURE 3.1.18 Normalized Edge Subchannel Flow Map (Re = 6312)

Geometry	Flow Condition
37 Pins	Re = 6317
P/D = 1.15	$\overline{M}_2$ = a.332 gpm
H/D = 21.0	Mass Balance Error =-2.5%

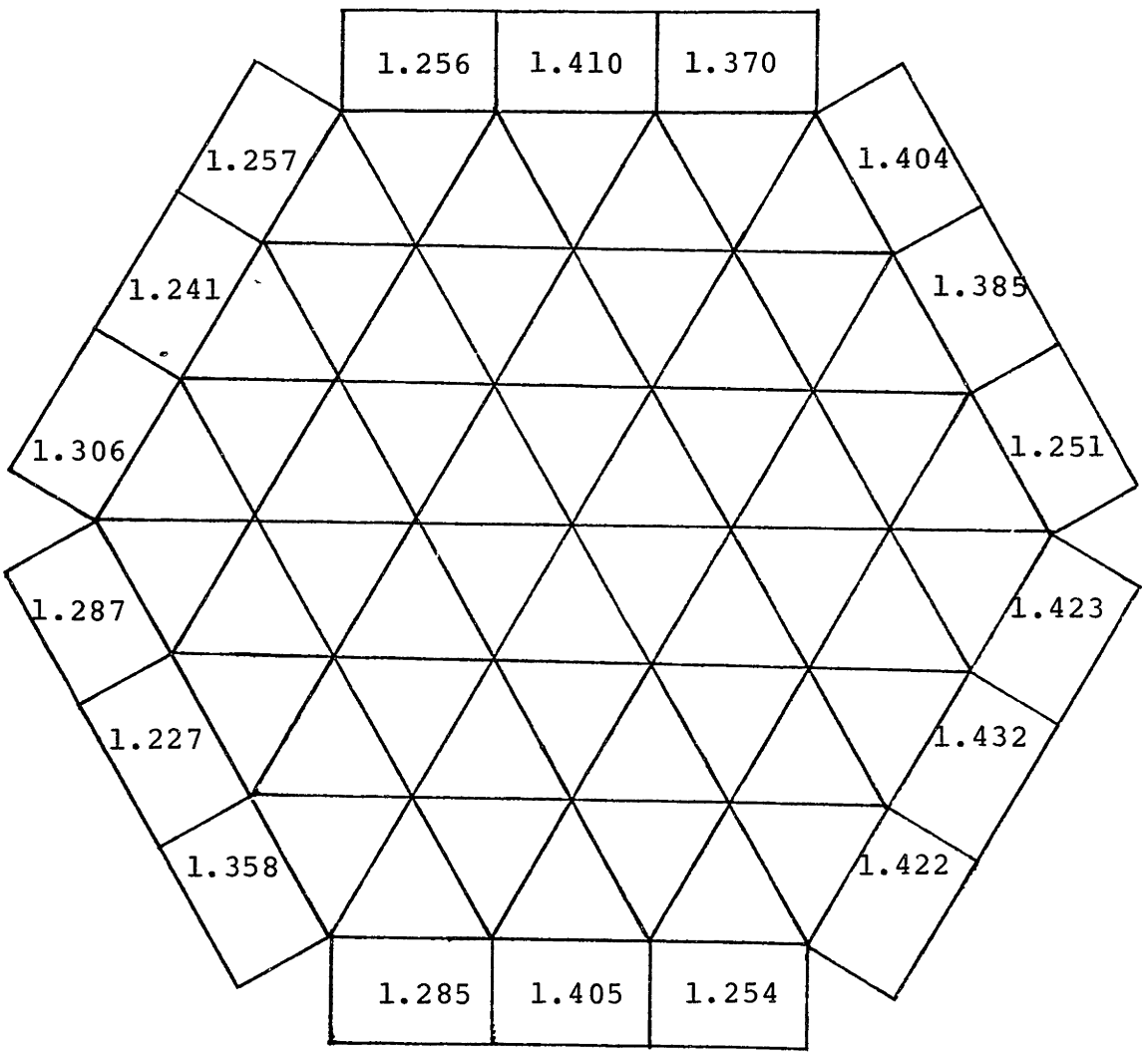

FIGURE 3.1.19 Normalized Edge Subchannel Flow Map (Re = 6317)

Geometry	Flow Condition
37 Pins	Re = 8179
P/D = 1.15	$\overline{M}_2$ = 1.645 gpm
H/D = 21.0	Mass Balance Error = 1.6%

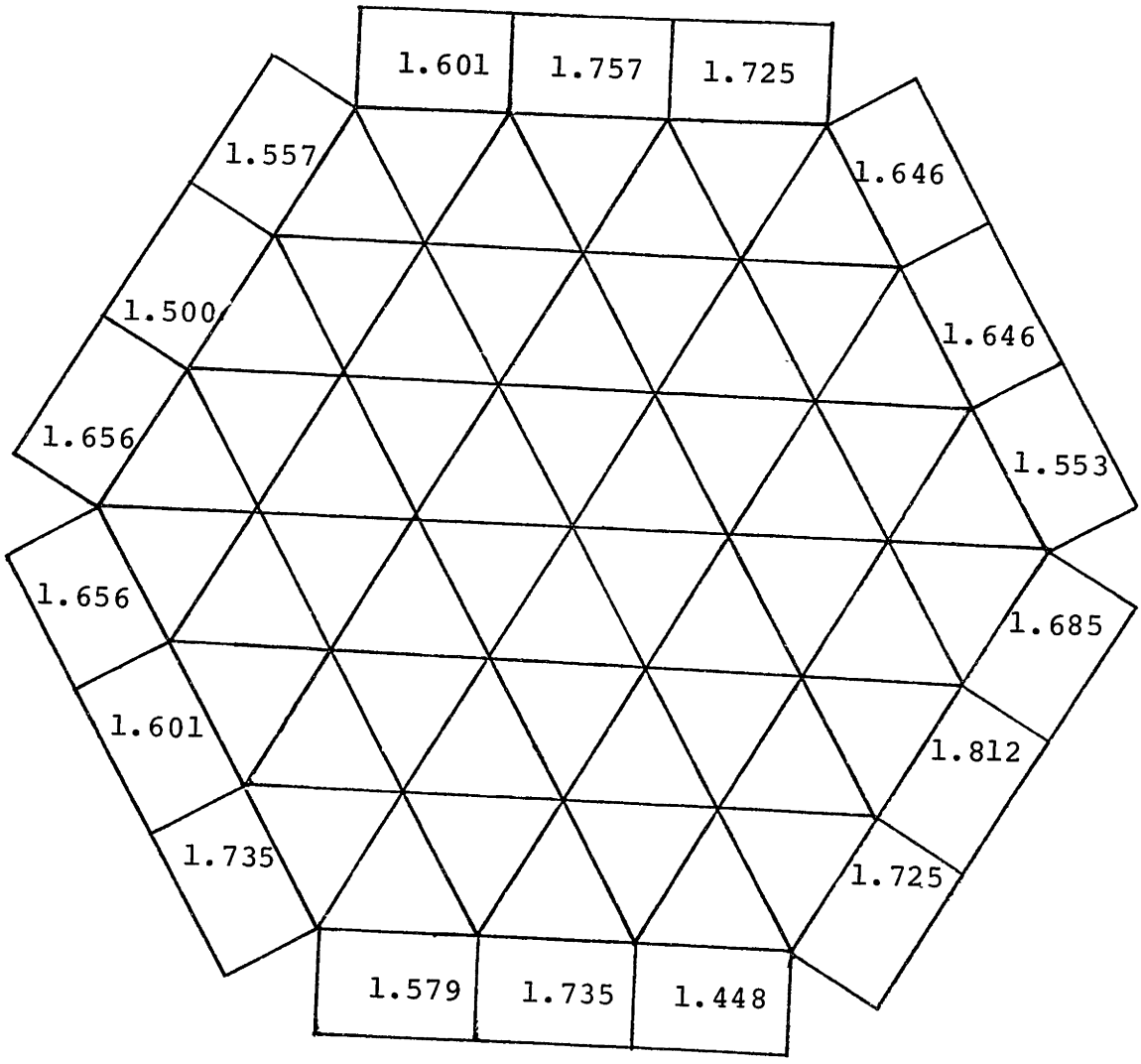

FIGURE 3.1.20 Normalized Edge Subchannel Flow Map (Re = 8179)

Geometry	Flow Condition
37 Pins	Re = 10343
P/D = 1.15	$\bar{M}_2$ = 2.045 gpm
H/D = 21.0	Mass Balance Error = 2.0%

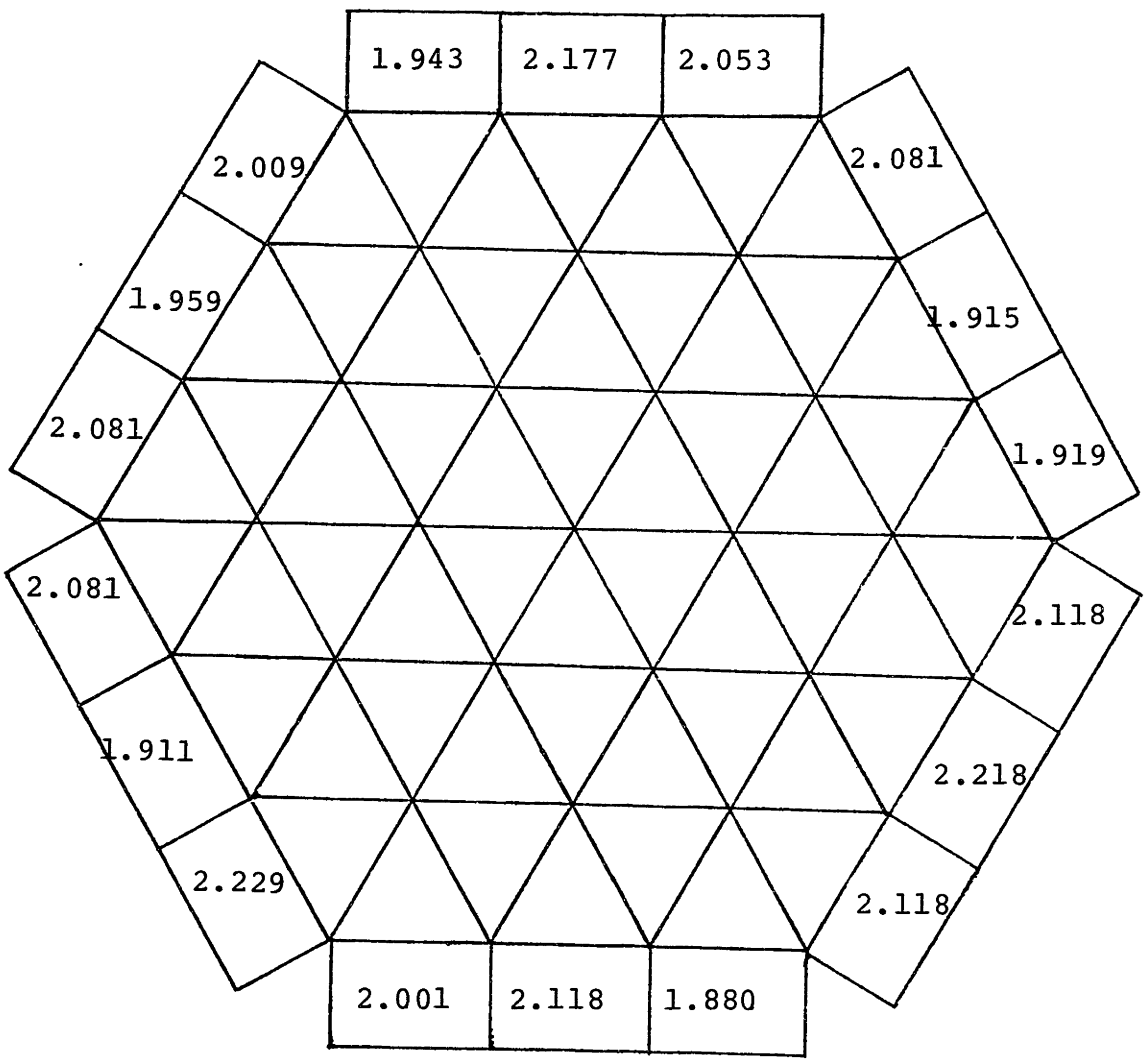

FIGURE 3.1.21 Normalized Edge Subchannel Flow Map (Re = 10343)

Geometry	Flow Condition
37 Pins	Re = 11738
P/D = 1.15	$\overline{M}_2$ = 2.339 gpm
H/D = 21.0	Mass Balance Error = 3.3%

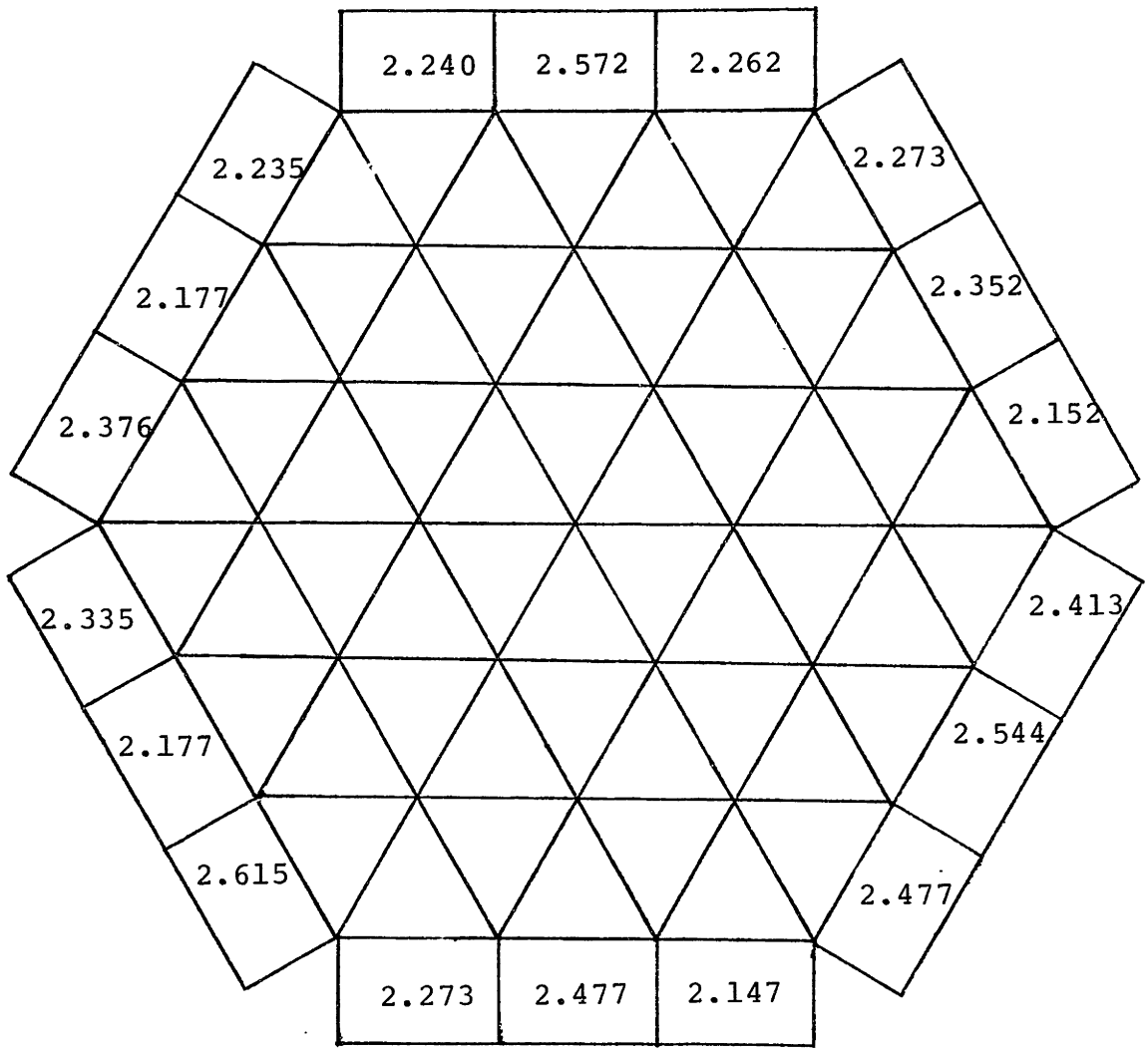

FIGURE 3.1.22 Normalized Edge Subchannel Flow Map (Re = 11738)

Geometry	Flow Condition
37 Pins	Re = 13328
P/D = 1.15	$\overline{M}_2$ = 2.667 gpm
H/D = 21.0	Mass Balance Error = 1.9%

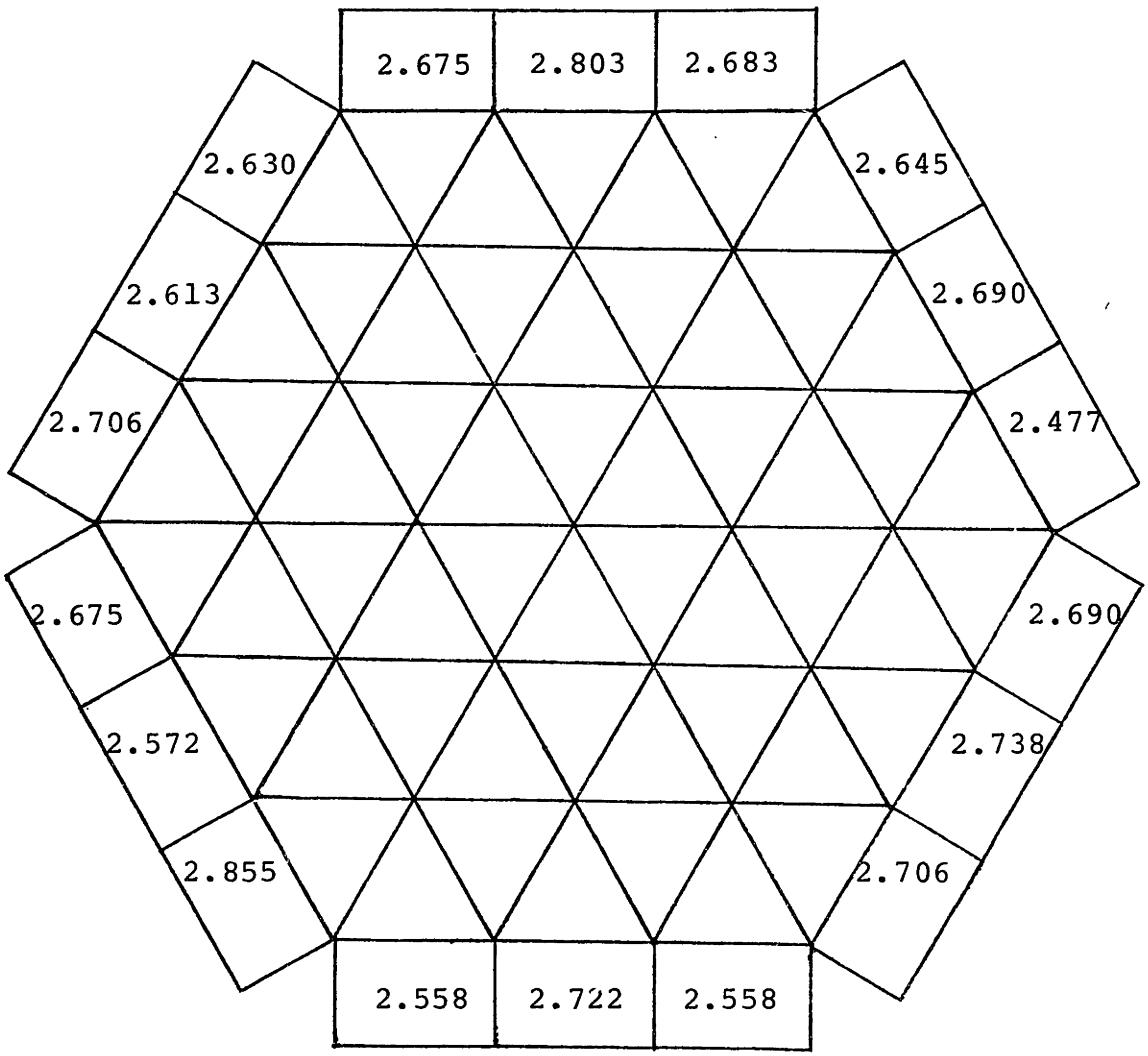

FIGURE 3.1.23 Normalized Edge Subchannel Flow Map (Re = 13328)

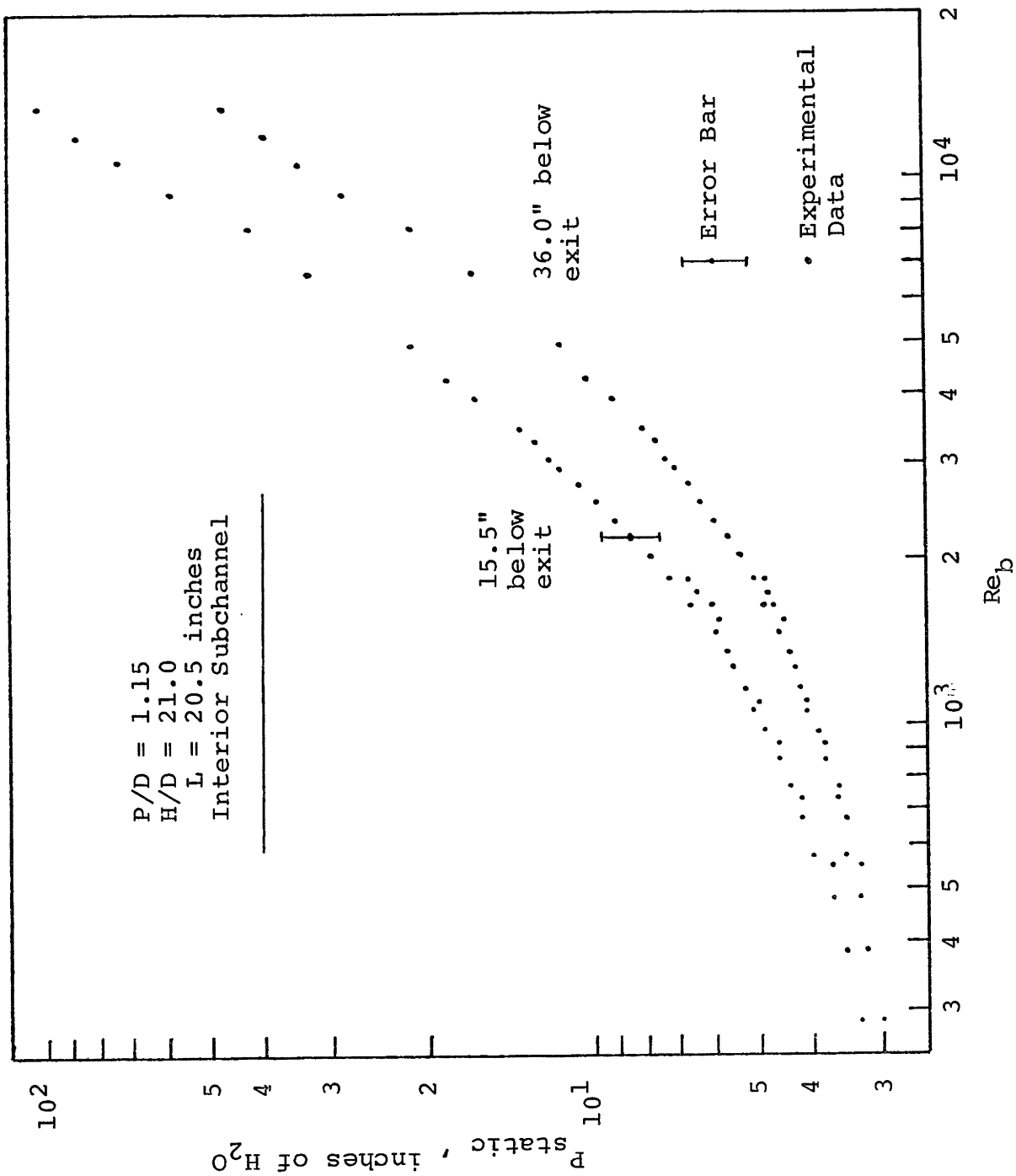

FIGURE 3.2.1 Static Pressure at 15.5" and 36" Below the Exit Plane (Interior Subchannel).

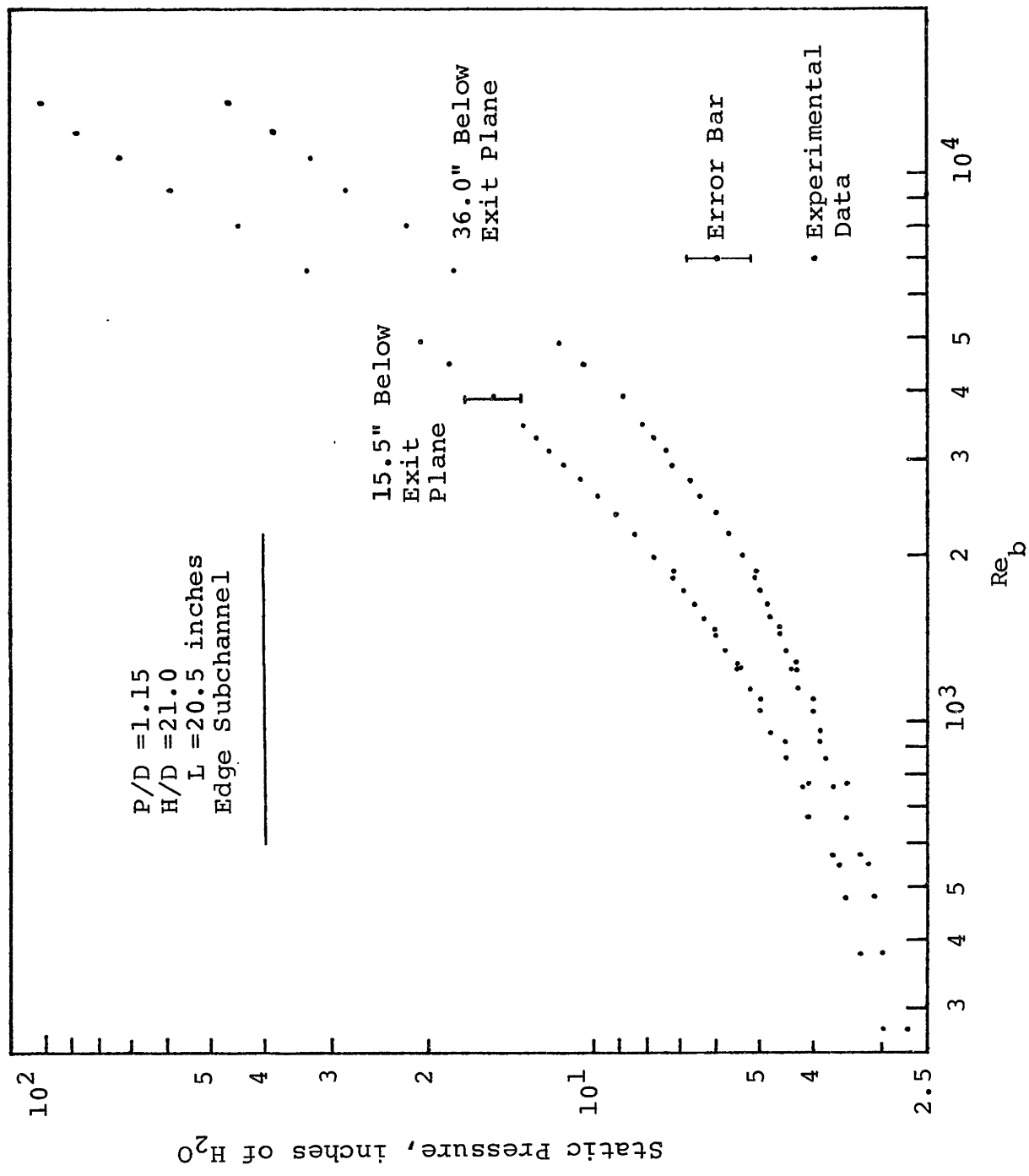

FIGURE 3.2.2 Static Pressure at 15.5" and 36.0" Below the Exit Plane (Edge Subchannel)

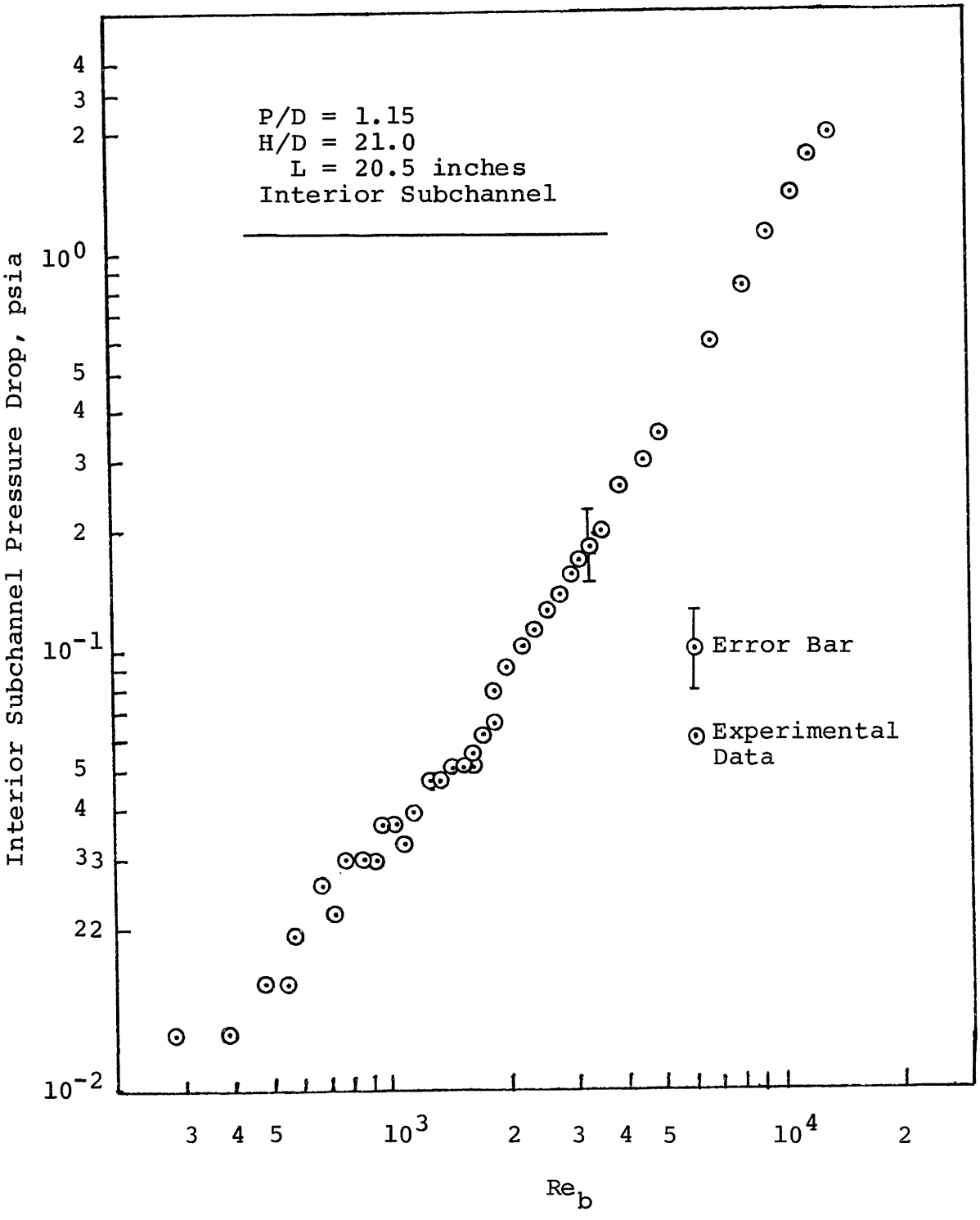

FIGURE 3.2.3 Pressure Drop Data for Interior Subchannel

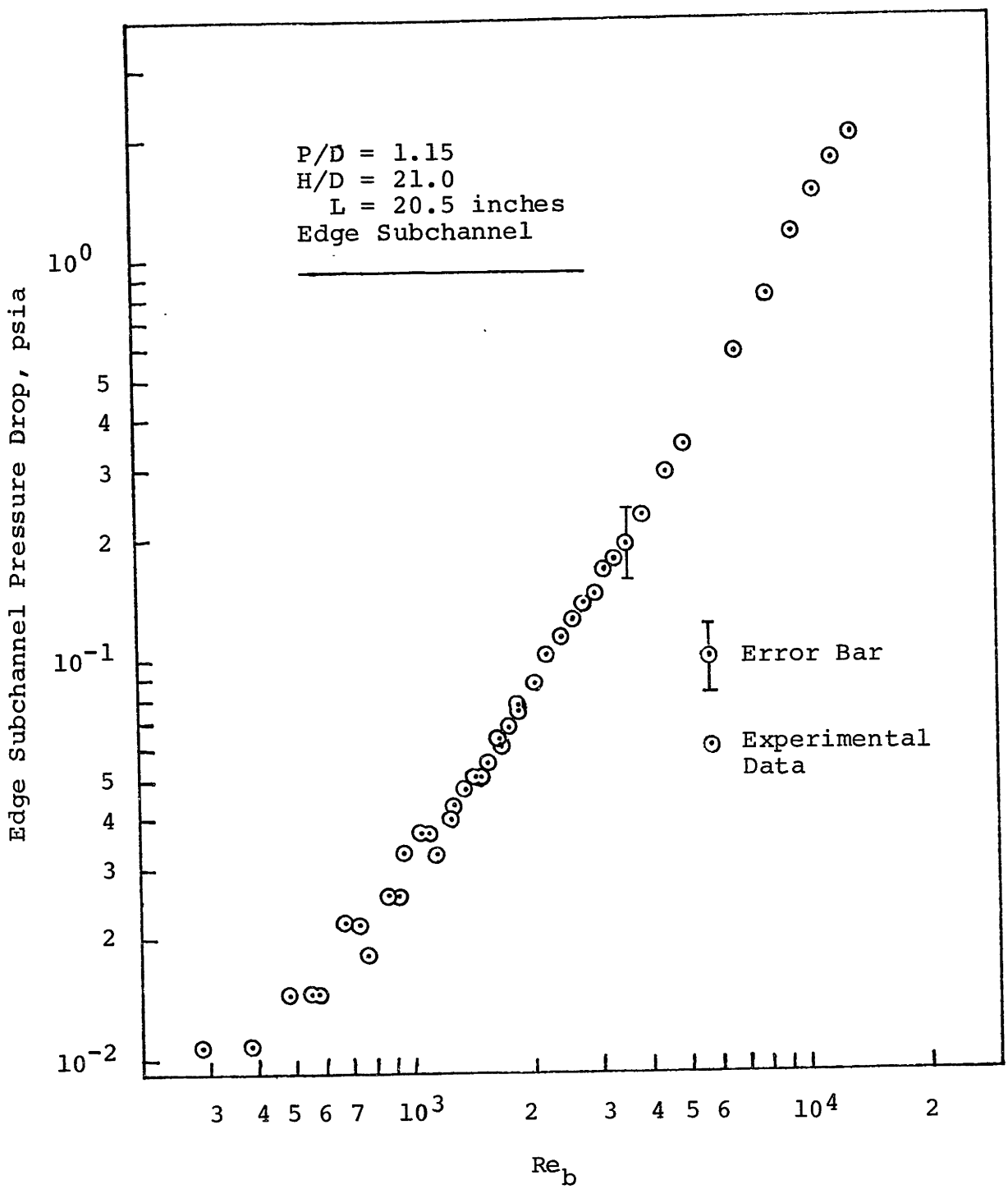

FIGURE 3.2.4 Pressure Drop Data for Edge Subchannel

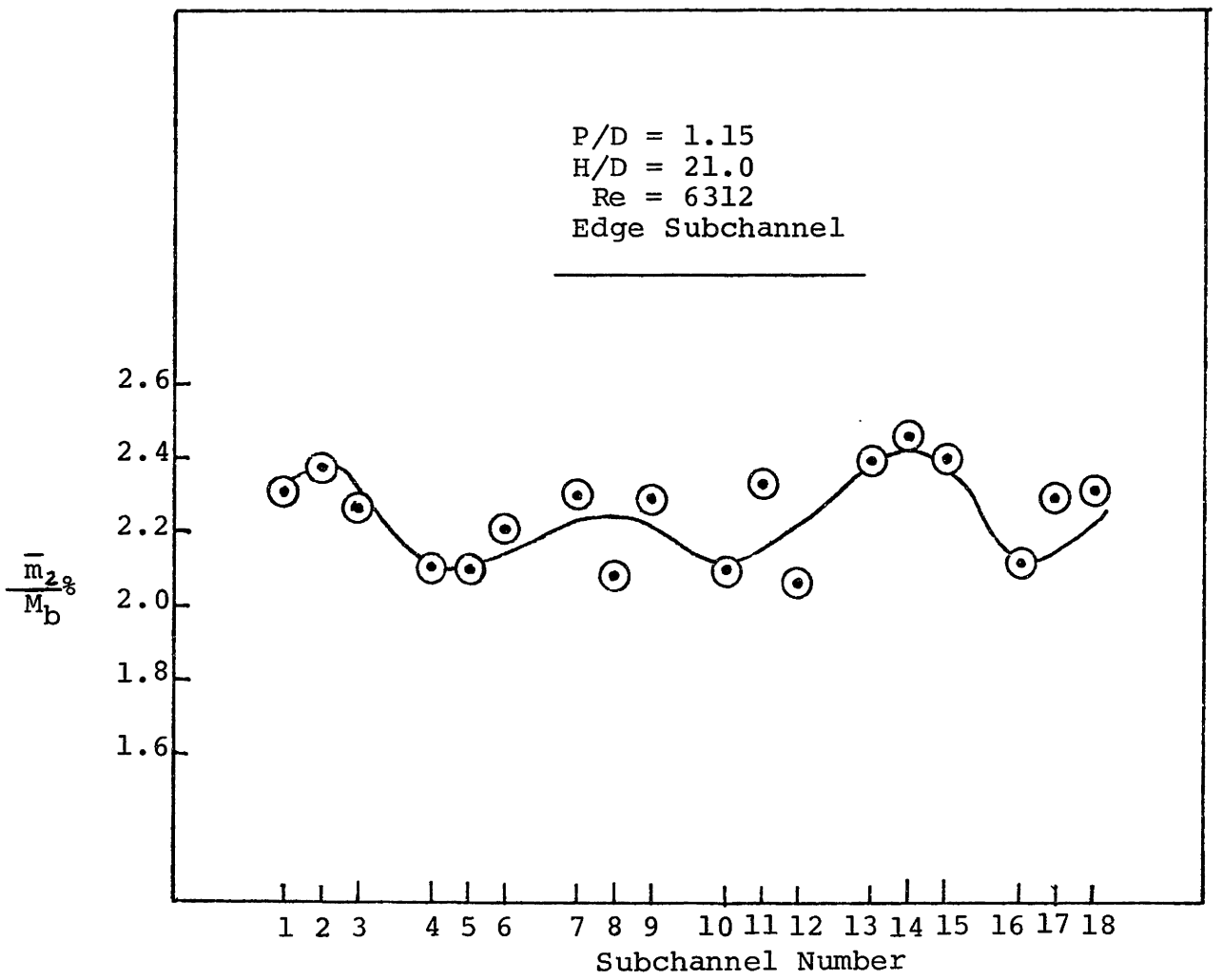

FIGURE 4.1.1 A Typical Normalized Edge Subchannel Flow Rate Pattern

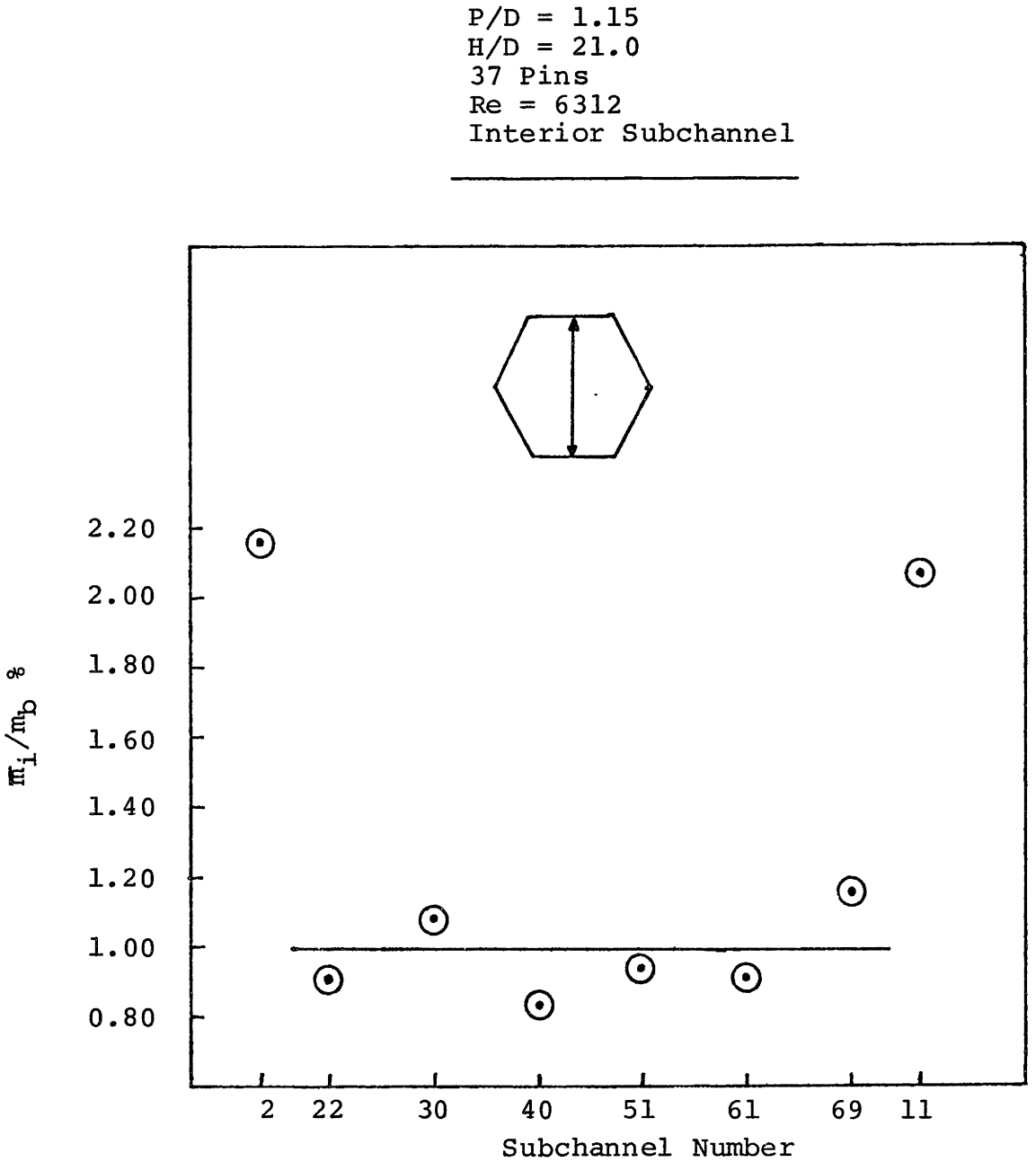

FIGURE 4.1.2 A Typical Cross Flat Traverse Normalized Subchannel Flow Rate Pattern for Interior Subchannel

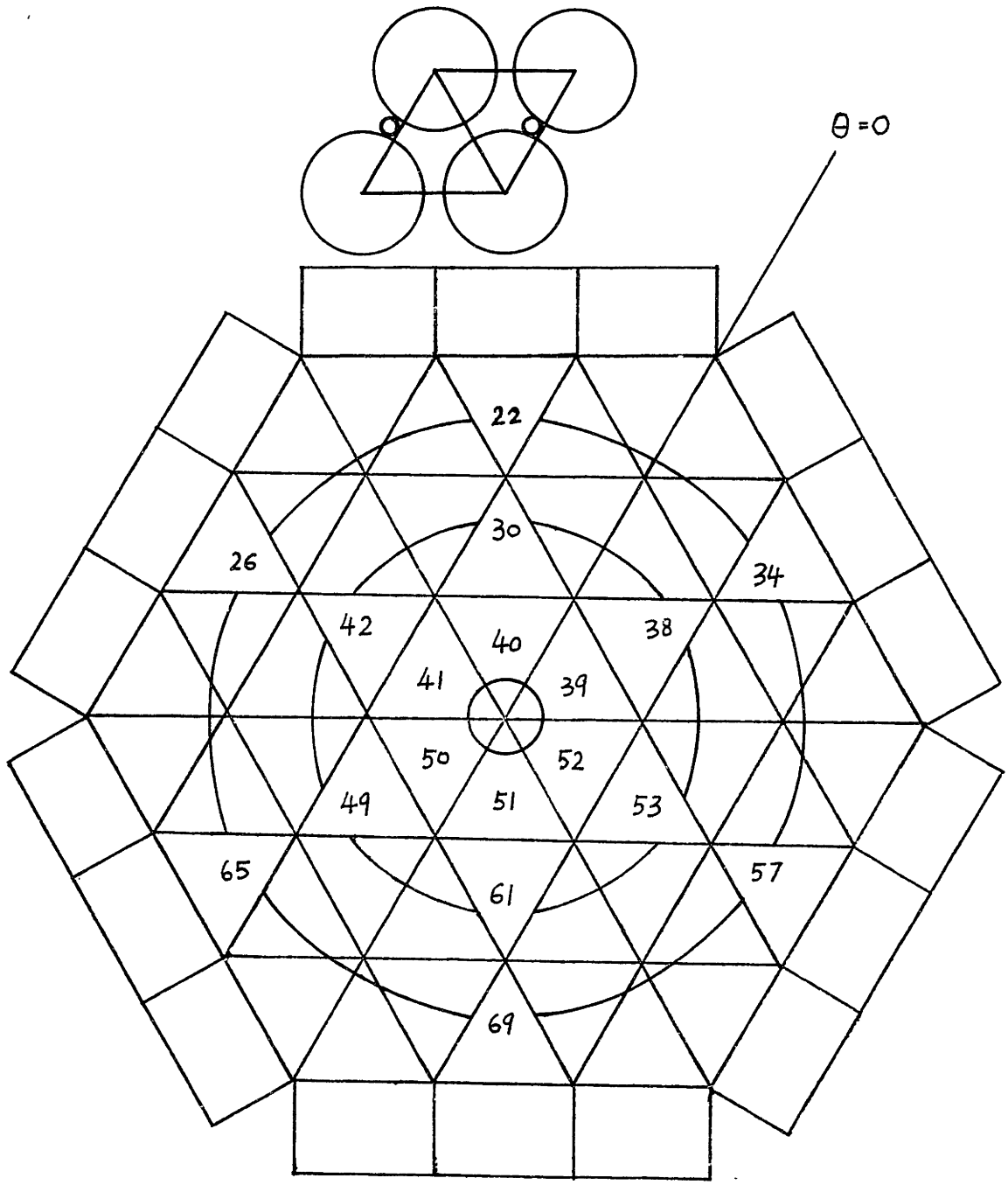

FIGURE 4.1.3 Rings of Interior Subchannels and Wire Positions in Two Different Types of Interior Subchannel

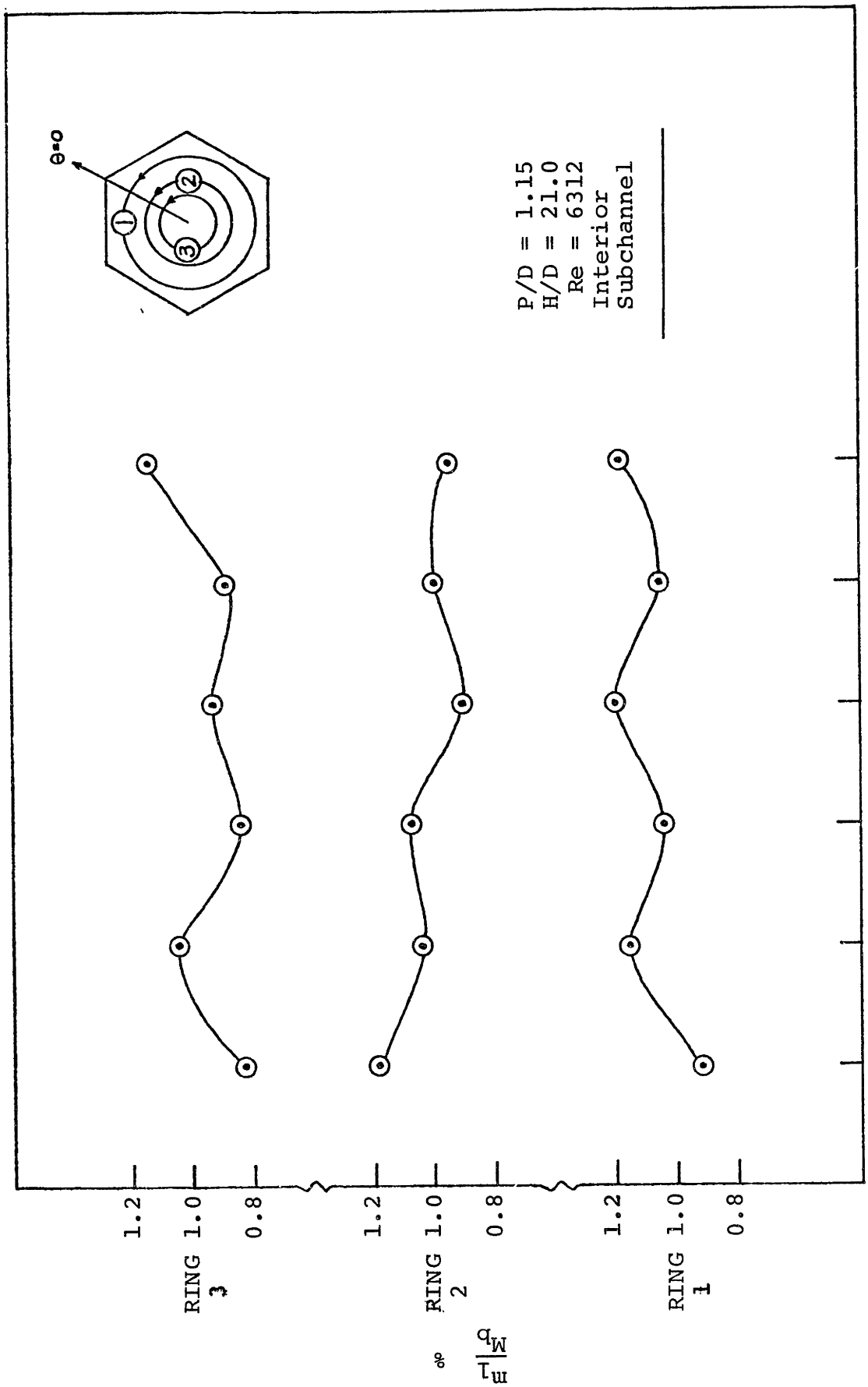

FIGURE 4.1.4 Normalized Interior Subchannel Flow Rate Pattern with respect to the Wire Position

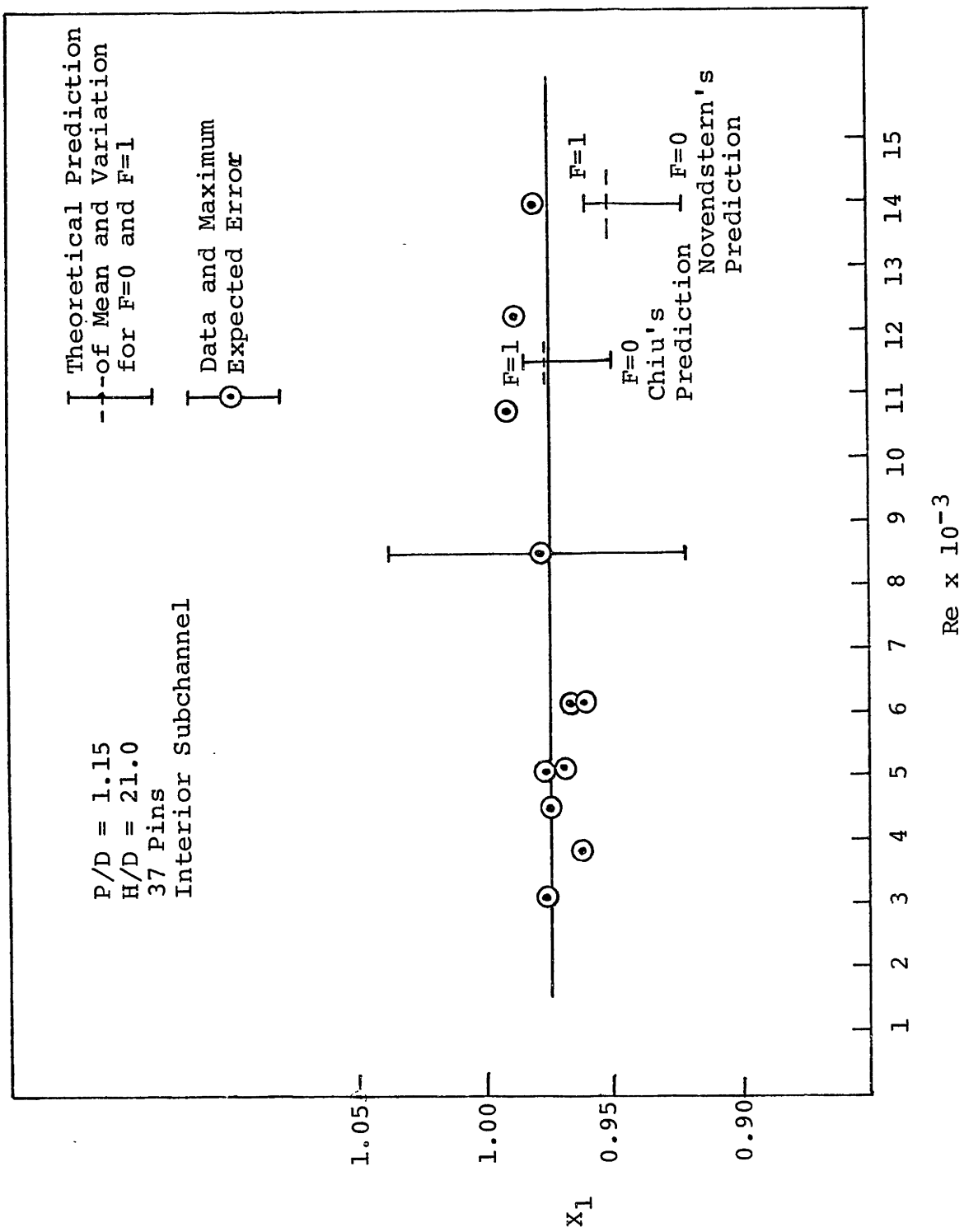

FIGURE 4.2.1 Interior Subchannel Flow Split Parameter X_1 versus Re

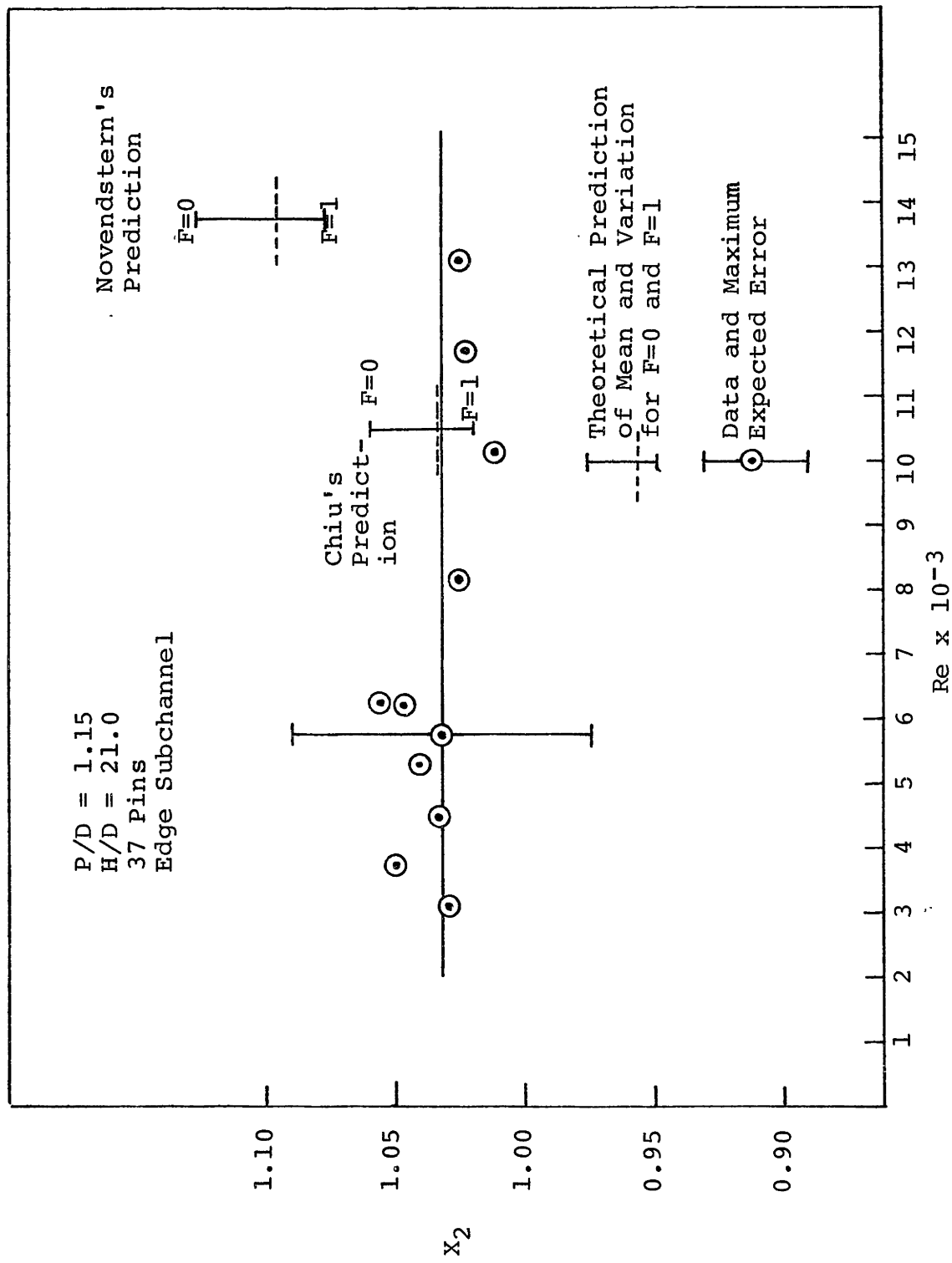

FIGURE 4.2.2 Edge Subchannel Flow Split Parameter X_2 versus Re

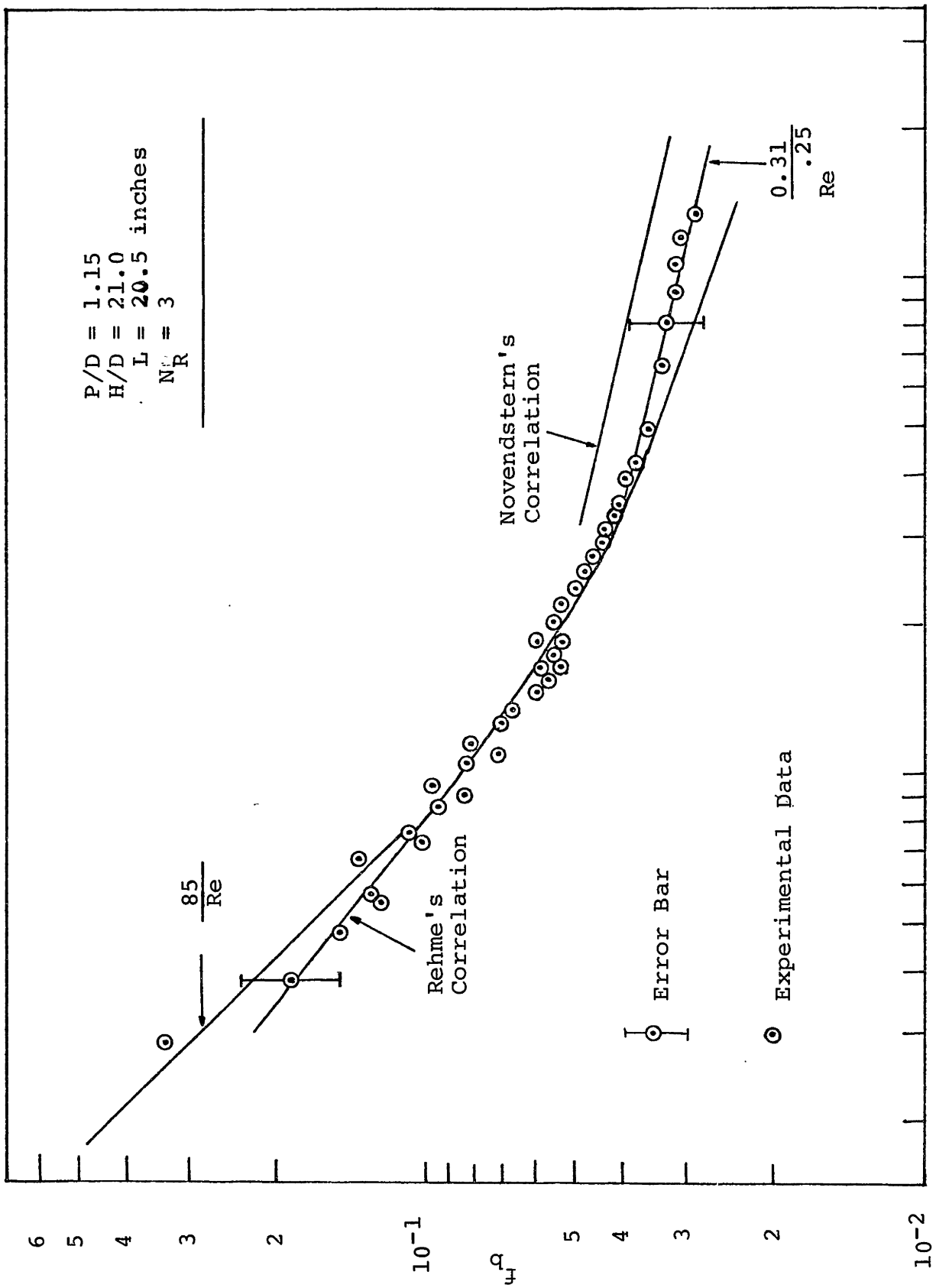

FIGURE 4.3.1 Bundle Average Friction Factor versus Re_b

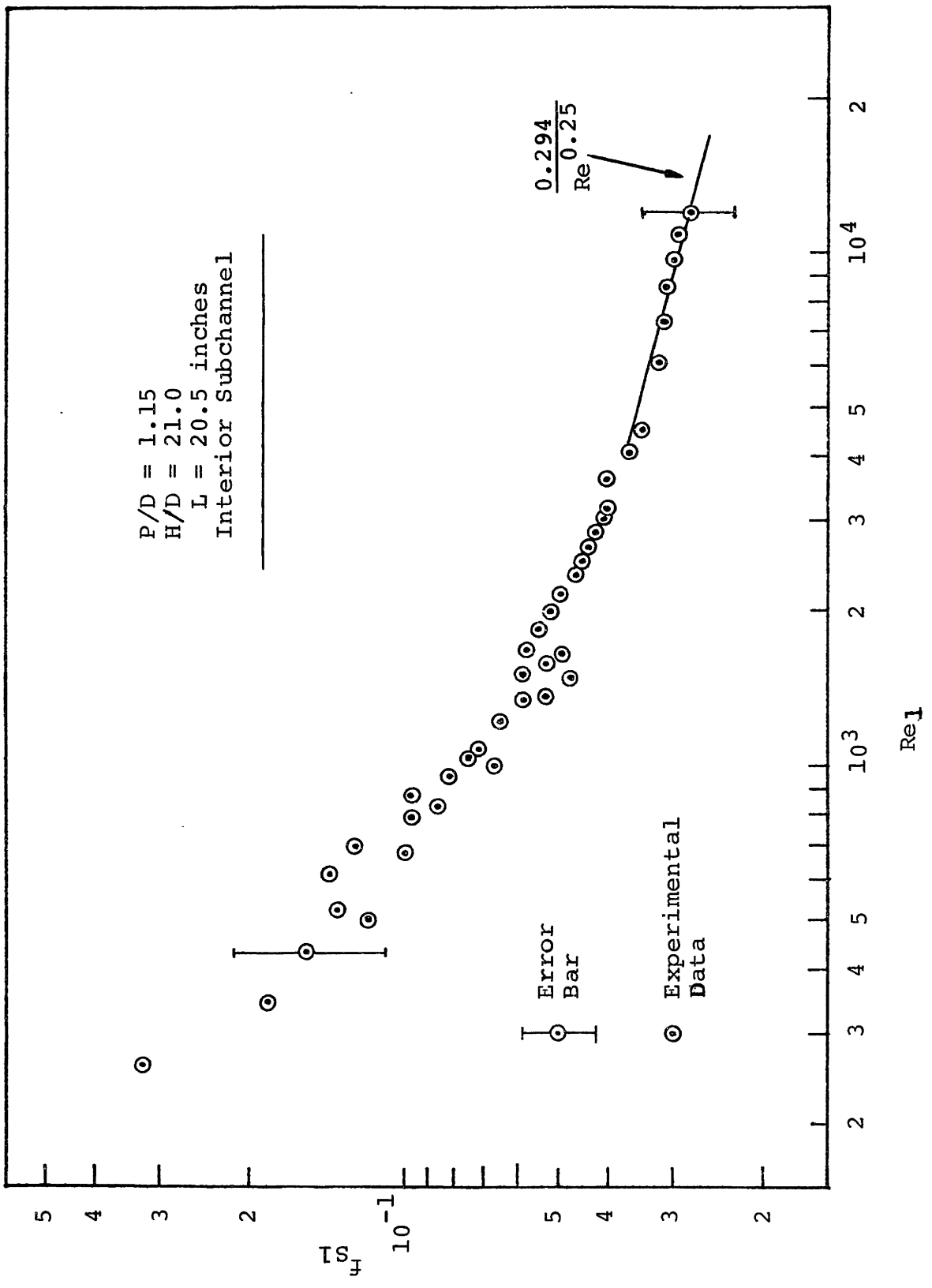

FIGURE 4.3.2 Local Interior Subchannel Friction Factor

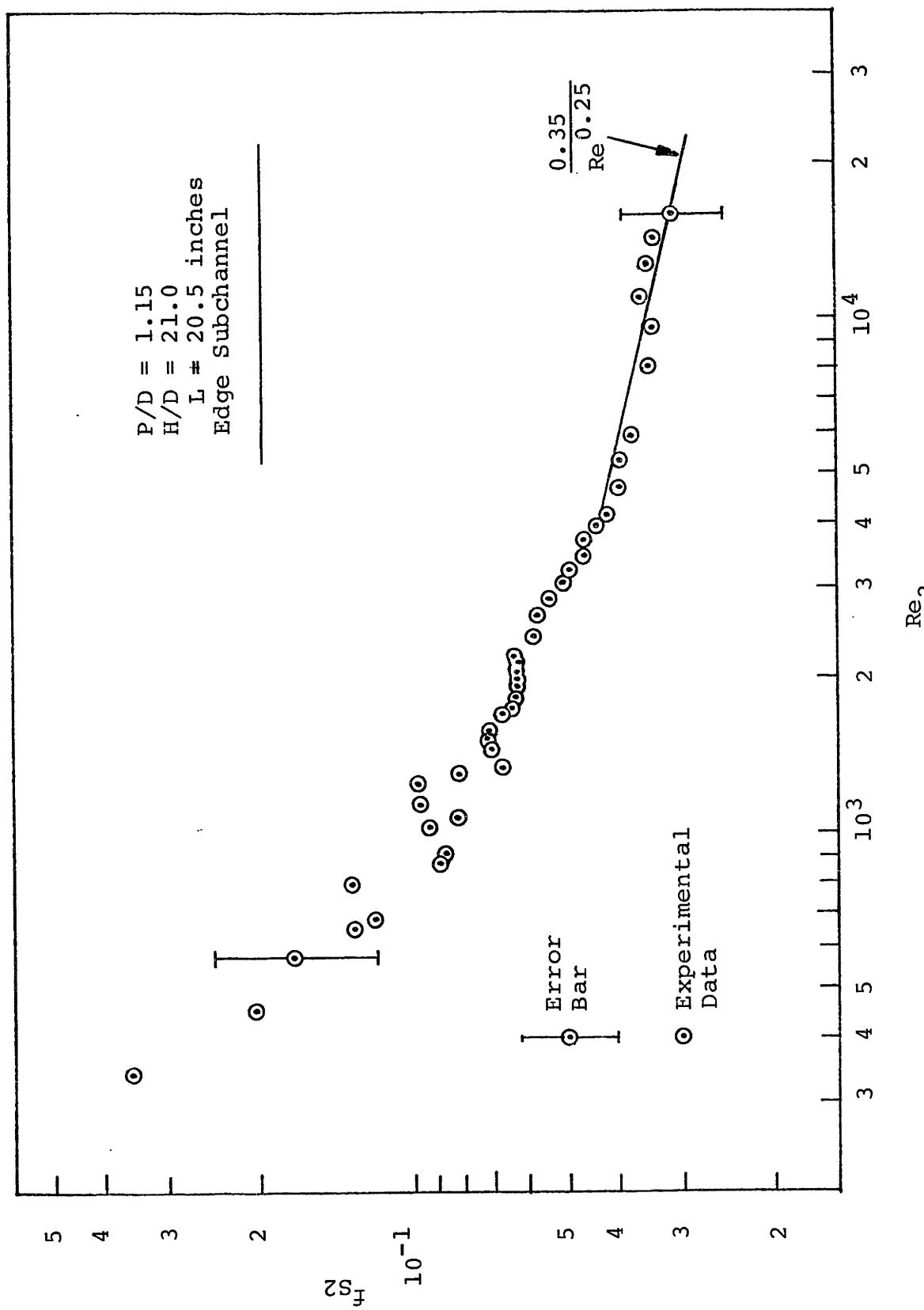

FIGURE 4.3.3 Local Edge Subchannel Friction Factor

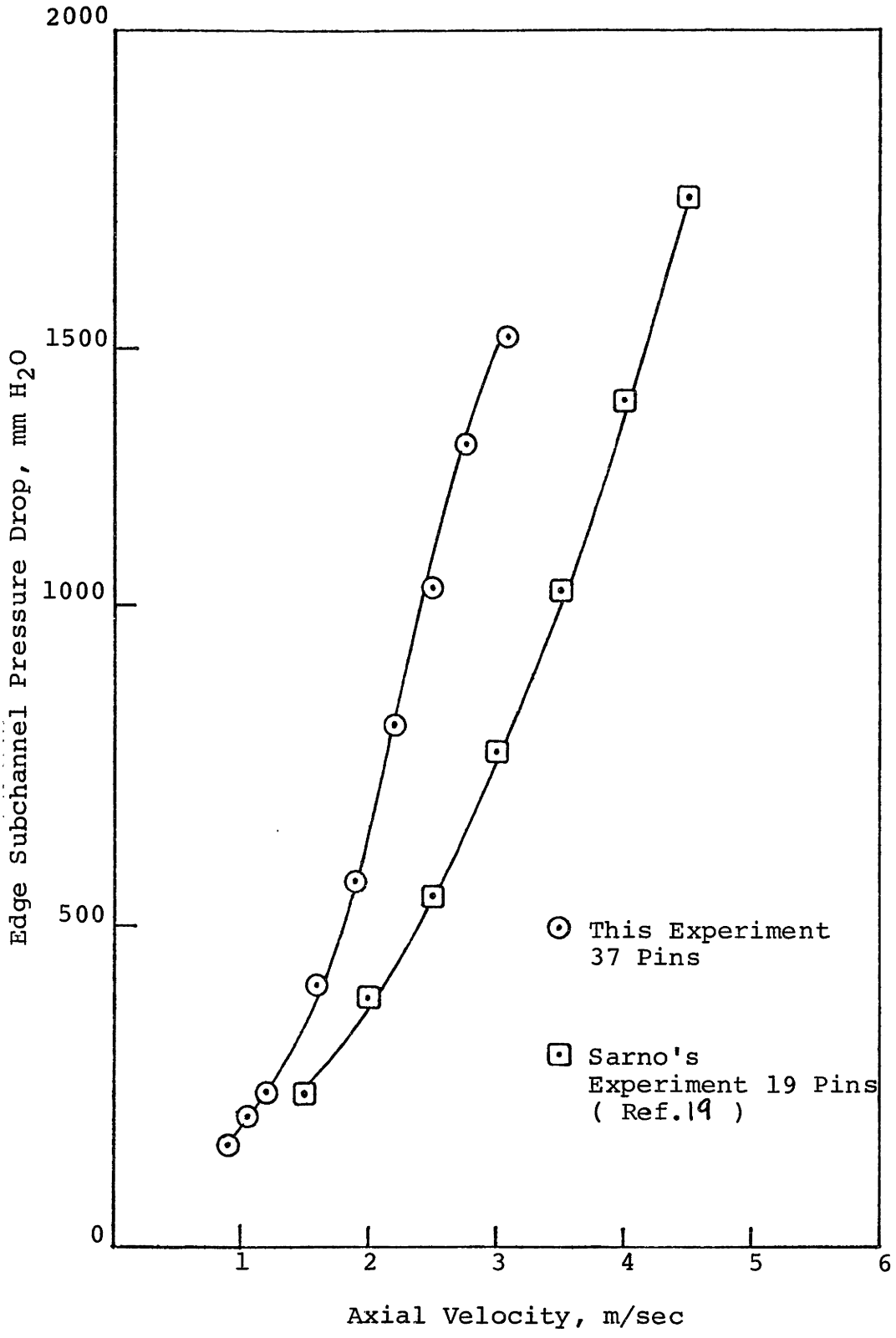

FIGURE 4.3.4 Local Edge Subchannel Friction Factor

APPENDIX A

Ultilization of a Differential Pressure Gauge in Measurement of Flow Rate

The flow meter installed in the bigger flow line is manufactured by Fisher and Porter Company under the model number 10B3565 A. It consists of a variable area flow meter and a squared edge orifice plate. The set up is illustrated in Fig.(A-1). Note that the by-pass range orifice is inside the variable flow meter and it is suspected that some dirt is deposited on it, thus blocking the flow. The blocking the flow. The blockage reduces the pressure and hence the rotometer gives lower main line flow rate that what actually exists.

Anyway, the primary parameter of interest is the pressure drop across the main line orifice plate P_2-P_0. Given the characteristics of the main line pipe diameter and that of the orifice plate, one can calculate the main line flow rate accordingly. The desired parameters are listed as follows:

Main line pipe inside diameter, D_1 = 3 inches

Tap location = Flange, 1 inches from both sides of the orifice plate

Orifice diameter, D_2 = 2.162 inches

According to Ref.(20), the main line flow rate is given as:

$$Q = K A_2 \left(\frac{2 g_c \Delta P}{\rho}\right)^{\frac{1}{2}} \qquad (1)$$

where K = the discharge coefficient which is a function of Reynolds number at the orifice plate and the ratio (β) of the orifice diameter to the pipe inside diameter

A_2 = the orifice area in^2

ΔP = the pressure drop across orifice plate in psi

ρ = density of water in lbm/ft^3 at room temperature

g_c = a constant = $32.17 \frac{lbm\ ft}{lbf\ sec^2}$

Q = the volumetric flow rate in GPM

In Equation (1), ΔP is the input and K is directly dependent on the main line flow rate since β is fixed.

It is given as:

$$K = K_e \frac{1 + A\lambda}{1 + A\lambda_e}$$

where $$A = D_2 \left(830 - 5000\beta + 9000\beta^2 - 4200\beta^3 + \frac{530}{(D_1)^{0.5}}\right)$$

$$K_e = 0.5993 + \frac{.007}{D_1} + \left(0.364 + \frac{.076}{(D_1)^{0.5}}\right)\beta^4 + \left(\frac{65}{D_1^2} + 3\right)(\beta - 0.7)^{5/2}$$

and $$\lambda_e = \frac{15}{10^6 D_2}$$

and = reciprocal of Reynolds number at orifice plate

$$\therefore = \frac{1}{Re} = \frac{\pi \mu D_2}{4 \rho Q}$$

After substitution and conversion, the final equation for flow rate as a function of pressure drop is:

$$Q = \frac{18.700\ (\Delta P)^{0.5} + \left\{\left[18.700\ (\Delta P)^{0.5}\right]^2 + 97.7308(\Delta P)^{0.5}\right\}^{0.5}}{2}$$

where Q in GPM

and ΔP in inches of water

When the correlation value Q is compared to the actual flow rate obtained by using a standard weight tank method in the low flow region, it is found that the error is around ± 2.5% randomly of the actual flow rate.

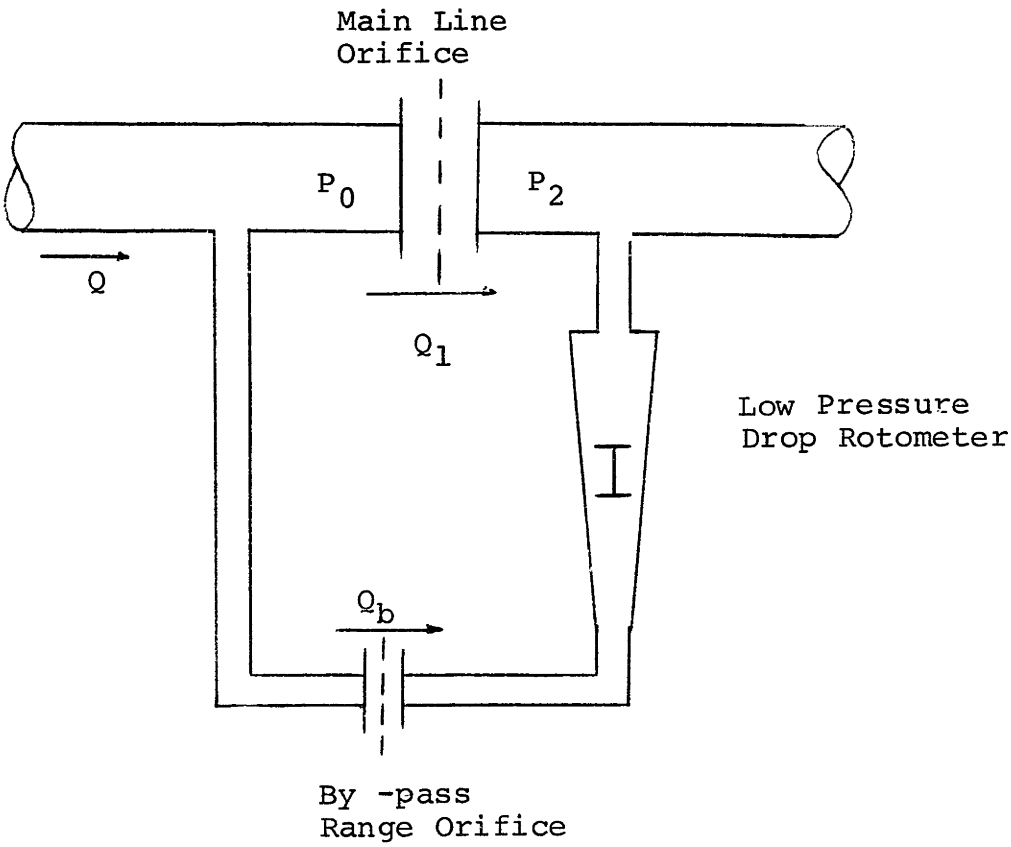

where Q = mainline flow rate
Q_1= flow rate through the mainline orifice
Q_b= flow rate through the by-pass orifice
P_0= pressure upstream of the orifice
P_2= pressure downstream of the orifice

FIGURE A-1 Principle Set-up of the F&P Flowmeter Model no. 10B3565A

APPENDIX B

Wire Wrap Gears Ratio Calculation

The original gears setting of the wire wrap machine is illustrated on Fig.(B-1). A formula for a set of particular gears to get a desired length is derived as follow:

$$\text{Desired Lead Length} = \frac{\text{Distance Which the Shuttle Travelled } (D_s)}{\text{Turns of Rod}}$$

$$\therefore \frac{D_s}{N_d} = H \tag{1}$$

but distance the shuttle travelled = $D_s = N_b L$

$$\therefore H = \frac{N_b L}{N_d} = \frac{N_b}{N_a} \frac{N_a}{N_c} \frac{N_c}{N_d} L \tag{2}$$

but $N_a = N_c$ and $N_a T_a = N_b T_b$ (3)

$\therefore$ Equation (e) becomes

$$H = \frac{T_a}{T_b} \frac{T_d}{T_c} L \tag{4}$$

This is the desired equation to determine the desired lead length by using different combination of gears.

Since the desired lead length is 10.5 inches for this bundle and from Equation (4), we can see that both gear ratios would be very large. Due to limitation of space, large gears cannot be installed on the wire wrap machine. However, by using a intermediate shaft of gears between gear C and gear D, we can have one more multiplying factor to Equation (4). The

intermediate shaft set up is also illustrated in Fig. (B-1).

Since $\frac{N_c}{N_m} = \frac{T_m}{T_c}$ and $\frac{N_n}{N_d} = \frac{T_d}{T_n}$

we have

$$\frac{N_c}{N_d} = \frac{T_m}{T_c} \cdot \frac{T_d}{T_n}$$

$\therefore$ Equation (4) becomes

$$H = \frac{T_a}{T_b} \frac{T_m}{T_n} \frac{T_d}{T_c} L \qquad (5)$$

However, note that the desired turning direction is reversed. This can be corrected by putting a gear between gear N and D. The size of the gear has no effect on Equation (5).

Numerically for this case:

$H = 10.5$

$L = 0.1$ inch/turn

From Equation (5) we have:

$$105 = \frac{T_a}{T_b} \frac{T_m}{T_n} \frac{T_d}{T_c} \qquad (6)$$

With careful search and trial and error with Equation (6) the following gears are used:

T_a = 120 teeth

T_b = 15 teeth

$T_m = T_d$ = 80 teeth

$T_n = T_c$ = 22 teeth

The resulting H is 0.75% from the desired lead length.

Nomenclature

N = number of turns of a gear

T = teeth of a gear

L = inch/turn of the lead screw which drives the shuttle

H = lead length

D_s = distance the shuttle travels

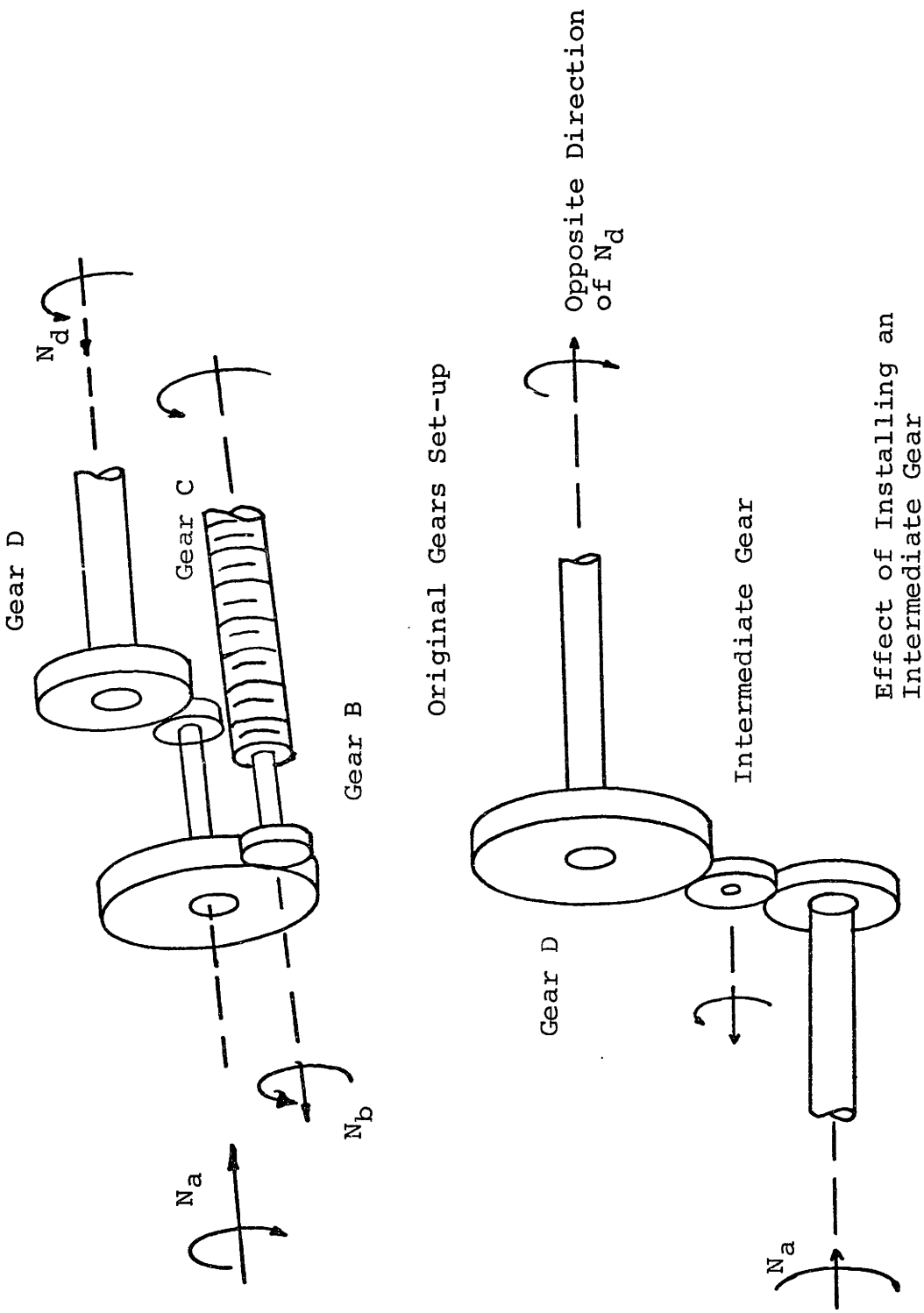

FIGURE C-1 Gear Set-up for the Wire Wrap Machine

APPENDIX C

Lists of Data

Lists of Data from

Flow Split Experiment

Measured Bundle Flow Rate = 27.7 (gpm)

Water Temperature = 28.1°C

Re = 3086

Subchannel Type = Interior

Subchannel Number	Amount of Fluid Collected (ml)	Time (sec)	Flow Rate (gpm)
22	941	68.3	0.2184
26	934	51.0	0.2903
30	935	48.2	0.3075
34	939	46.6	0.3194
38	921	60.6	0.2409
39	928	48.2	0.3052
40	929	62.6	0.2352
41	922	45.0	0.3248
42	950	63.6	0.2368
49	951	45.4	0.3321
50	950	74.1	0.2032
51	940	51.4	0.2899
52	946	65.4	0.2293
53	949	49.0	0.3070
57	942	51.2	0.2917
61	931	68.7	0.2148
65	933	56.8	0.2604
69	927	43.8	0.3355

Average Flow Rate = 0.2750 gpm

Measured Bundle Flow Rate = 33.65 gpm

Water Temperature = 28.8°C

Re = 3822

Subchannel Type = Interior

Subchannel Number	Amount of Fluid Collected (ml)	Time (sec)	Flow Rate (gpm)
22	940	51.6	0.2888
26	936	40.6	0.3655
30	941	34.6	0.4311
34	923	39.0	0.3752
38	948	48.8	0.3079
39	918	41.0	0.3549
40	954	57.0	0.2653
41	930	43.8	0.3366
42	932	44.2	0.3343
49	942	36.2	0.4125
50	930	45.0	0.3276
51	951	44.2	0.3411
52	860	56.0	0.2434
53	941	43.0	0.3469
57	940	43.6	0.3419
61	901	57.0	0.2506
65	921	49.2	0.2967
69	939	47.6	0.3232

Average Flow Rate = 0.3302 gpm

Measured Bundle Flow Rate = 39.25 gpm

Water Temperature = 28.8°C

Re = 4503

Subchannel Type = Interior

Subchannel Number	Amount of Fluid Collected (ml)	Time (sec)	Flow Rate (gpm)
22	937	39.9	0.3723
26	928	33.6	0.4379
30	933	30.6	0.4833
34	931	35.4	0.4169
38	941	42.8	0.3485
39	920	33.7	0.4328
40	936	39.6	0.3747
41	942	32.2	0.4637
42	940	44.4	0.3356
49	932	31.6	0.4675
50	919	41.8	0.3485
51	933	38.6	0.3832
52	920	49.4	0.2952
53	940	40.2	0.3707
57	931	35.5	0.4157
61	918	44.0	0.3307
65	930	40.6	0.3631
69	945	33.2	0.4512

Average Flow Rate = 0.3940 gpm

Measured Bundle Flow Rate = 50.75 gpm

Water Temperature = 23.8°C

Re = 5263

Subchannel Type = Interior

Subchannel Number	Amount of Fluid Collected (ml)	Time (sec)	Flow Rate (gpm)
22	969	35.0	0.4389
26	977	27.2	0.5694
30	976	25.9	0.5974
34	970	26.3	0.5847
38	932	30.0	0.4925
39	978	28.8	0.5383
40	968	35.3	0.4347
41	950	28.4	0.5303
42	959	32.1	0.4736
49	955	24.0	0.6308
50	975	32.4	0.4770
51	960	31.6	0.4816
52	943	29.2	0.5119
53	951	30.4	0.4959
57	954	33.4	0.4528
61	946	36.7	0.4086
65	965	30.8	0.4967
69	963	24.6	0.6205

Average Flow Rate = 0.5131 gpm

Measured Bundle Flow Rate = 45.85 gpm

Water Temperature = 28.4°C

Re = 5279

Subchannel Type = Interior

Subchannel Number	Amount of Fluid Collected (ml)	Time (sec)	Flow Rate (gpm)
22	938	38.0	0.3913
26	945	29.4	0.5095
30	932	28.2	0.5239
34	953	29.1	0.5191
38	920	35.0	0.4167
39	931	28.0	0.5271
40	937	29.8	0.4984
41	939	29.0	0.5133
42	921	36.4	0.4011
49	935	27.4	0.5409
50	940	32.6	0.4571
51	924	31.8	0.4606
52	931	41.7	0.3539
53	941	31.1	0.4796
57	925	30.6	0.4792
61	922	42.8	0.3415
65	926	33.2	0.4421
69	949	30.4	0.4949

Average Flow Rate = 0.4639 gpm

Measured Bundle Flow Rate = 56.27 gpm

Water Temperature = 28.4 ^{o}C

Re = 6312

Subchannel Type = Interior

Subchannel Number	Amount of Fluid Collected (ml)	Time (sec)	Flow Rate (gpm)
22	970	30.8	0.4992
26	963	24.1	0.6334
30	2018	50.0	0.6398
34	946	23.3	0.6436
38	943	29.0	0.5155
39	971	24.8	0.6207
40	952	33.4	0.4518
41	952	26.4	0.5716
42	930	26.0	0.5670
49	962	26.2	0.5820
50	942	32.6	0.4581
51	941	29.6	0.5039
52	958	31.4	0.4836
53	944	27.4	0.5461
57	963	26.8	0.5696
61	949	30.4	0.4949
65	961	26.8	0.5684
69	945	22.9	0.6542

Average Flow Rate = 0.5558 gpm

Measured Bundle Flow Rate = 60.42 gpm

Water Temperature = 24.4°C

Re = 6315

Subchannel Type = Interior

Subchannel Number	Amount of Fluid Collected (ml)	Time (sec)	Flow Rate (gpm)
22	1998	59.0	0.5368
26	2002	45.0	0.7052
30	1999	45.4	0.6980
34	2003	46.7	0.6799
38	2005	54.4	0.5843
39	1997	49.0	0.6461
40	993	32.1	0.4901
41	2002	58.5	0.5453
42	2000	56.2	0.5641
49	1986	44.0	0.7155
50	965	35.2	0.4346
51	1996	50.8	0.6228
52	2005	66.0	0.4816
53	2009	48.0	0.6635
57	1996	47.0	0.6732
61	1999	60.6	0.5229
65	2000	52.8	0.6005
69	2002	52.4	0.6056

Average Flow Rate = 0.5983 gpm

Measured Bundle Flow Rate = 73.71 gpm

Water Temperature = 27.2°C

Re = 8518

Subchannel Type = Interior

Subchannel Number	Amount of Fluid Collected (ml)	Time (sec)	Flow Rate (gpm)
22	2002	46.4	0.6840
26	2023	36.2	0.8859
30	1998	35.8	0.8847
34	1995	36.6	0.8641
38	1988	43.1	0.7312
39	1998	38.3	0.8270
40	1986	41.4	0.7604
41	1990	35.8	0.8812
42	1987	44.6	0.7062
49	1991	35.1	0.8992
50	1985	44.8	0.7024
51	2009	45.0	0.7077
52	1987	44.8	0.7031
53	1987	40.4	0.7804
57	1991	38.0	0.8306
61	1990	54.0	0.5842
65	1995	41.0	0.7713
69	2005	41.4	0.7677

Average Flow Rate = 0.7762 gpm

Measured Bundle Flow Rate = 92.90 gpm

Water Temperature = 27.2 °C

Re = 10772

Subchannel Type = Interior

Subchannel Number	Amount of Fluid Collected (ml)	Time (sec)	Flow RAte (gpm)
22	2005	35.1	0.9055
26	1990	28.2	1.1186
30	2026	29.0	1.1075
34	2005	29.0	1.0960
38	1990	34.2	0.9224
39	2015	30.2	1.0577
40	1990	39.2	0.8047
41	2015	33.0	0.9679
42	2006	33.0	0.9636
49	2010	28.5	1.1180
50	2014	32.0	0.9977
51	1998	30.8	1.0283
52	2001	38.0	0.8347
53	2010	30.0	1.0621
57	1993	30.0	1.0531
61	2001	36.4	0.8714
65	1995	32.2	0.9821
69	2003	32.0	0.9922

Average Flow Rate = 0.9935 gpm

Measured Bundle Flow Rate = 119.57 gpm

Water Temperature = 27.6 ^{o}C

Re = 13974

Subchannel Type = Interior

Subchannel Number	Amount of Fluid Collected (ml)	Time (sec)	Flow Rate (gpm)
22	2014	27.0	1.1824
26	2004	22.6	1.4056
30	2022	23.5	1.3640
34	2010	22.1	1.4417
38	2000	26.8	1.1830
39	2014	21.0	1.5203
40	1998	30.2	1.0488
41	2020	22.8	1.4044
42	2005	26.8	1.1859
49	2005	22.5	1.4126
50	2018	32.2	0.9935
51	2005	28.3	1.1231
52	2018	30.1	1.0628
53	1995	23.0	1.3750
57	2011	23.8	1.3394
61	2009	27.2	1.1708
65	1993	24.4	1.2948
69	2009	25.2	1.2639

Average Flow Rate = 1.2651 gpm

Measured Bundle Flow Rate = 103.72 gpm

Water Temperature = 27.5°C

Re = 12280

Subchannel Type = Interior

Subchannel Number	Amount of Fluid Collected (ml)	Time (sec)	Flow Rate (gpm)
22	2009	31.3	1.0175
26	2010	26.6	1.1978
30	2005	24.8	1.2816
34	2000	25.8	1.2288
38	2001	30.8	1.0299
39	2015	25.0	1.2777
40	2008	30.6	1.0402
41	2010	28.5	1.1180
42	1999	30.8	1.0288
49	2000	24.4	1.2993
50	1991	32.8	0.9622
51	2000	27.6	1.1487
52	1997	30.4	1.0413
53	1992	26.2	1.2052
57	1999	27.8	1.1399
61	1990	36.8	0.8572
65	2010	28.2	1.1299
69	2000	28.6	1.1085

Average Flow Rate = 1.1174 gpm

Measured Bundle Flow Rate = 119.57 gpm

Water Temperature = 25.4°C

Re = 13328

Subchannel Type = Edge

Subchannel Number	Amount of Fluid Collected (lbm)	Time (sec)	Flow Rate (gpm)
1	13.0	34.9	2.6827
2	13.0	33.4	2.8032
3	13.0	35.0	2.6751
4	13.0	35.6	2.6300
5	13.0	35.8	2.6153
6	13.0	34.6	2.7060
7	13.0	35.0	2.6751
8	13.0	36.4	2.5722
9	13.0	32.8	2.8545
10	13.0	36.6	2.5581
11	13.0	34.4	2.7217
12	13.0	36.6	2.5581
13	13.0	34.6	2.7060
14	13.0	34.2	2.7376
15	13.0	34.8	2.6904
16	13.0	37.8	2.4769
17	13.0	34.8	2.6904
18	13.0	35.4	2.6448

Average Flow Rate = 2.6666 gpm

Measured Bundle Flow Rate = 103.72 gpm

Water Temperature = 25.4° C

Re = 11738

Subchannel Type = Edge

Subchannel Number	Amount of Fluid Collected (lbm)	Time (sec)	Flow Rate (gpm)
1	13.0	41.4	2.2615
2	13.0	36.4	2.5722
3	13.0	41.8	2.2399
4	13.0	41.9	2.2345
5	13.0	43.0	2.1774
6	13.0	39.4	2.3763
7	13.0	40.1	2.3348
8	13.0	43.0	2.1774
9	13.0	35.8	2.6153
10	13.0	41.2	2.2725
11	13.0	37.8	2.4769
12	13.0	43.6	2.1474
13	13.0	37.8	2.4769
14	13.0	36.8	2.5442
15	13.0	38.8	2.4131
16	13.0	43.5	2.1524
17	13.0	39.8	2.3524
18	13.0	41.2	2.2725

Average Flow Rate = 2.3388 gpm

Measured Bundle Flow Rate = 92.90 gpm

Water Temperature = 25.3°C

Re = 10343

Subchannel Type = Edge

Subchannel Number	Amount of Fluid Collected (lbm)	Time (sec)	Flow Rate (gpm)
1	13.0	45.6	2.0532
2	13.0	43.0	2.1774
3	13.0	48.2	1.9425
4	13.0	46.6	2.0092
5	13.0	47.8	1.9588
6	13.0	45.0	2.0806
7	13.0	45.0	2.0806
8	13.0	49.0	1.9107
9	13.0	42.0	2.2292
10	13.0	46.8	2.0006
11	13.0	44.2	2.1182
12	13.0	49.8	1.8801
13	13.0	44.2	2.1182
14	13.0	42.2	2.2187
15	13.0	44.2	2.1182
16	13.0	48.8	1.9186
17	13.0	48.9	1.9146
18	13.0	45.0	2.0806

Average Flow Rate = 2.0450 gpm

Measured Bundle Flow Rate = 73.17 gpm

Water Temperature = 25.3°C

Re = 8179

Subchannel Type = Edge

Subchannel Number	Amount of Fluid Collected (lbm)	Time (sec)	Flow Rate (gpm)
1	8.0	33.4	1.7250
2	8.0	32.8	1.7566
3	8.0	36.0	1.6005
4	8.0	37.0	1.5572
5	8.0	38.4	1.5004
6	8.0	34.8	1.6556
7	8.0	34.8	1.6556
8	8.0	36.0	1.6005
9	8.0	33.2	1.7354
10	8.0	36.5	1.5785
11	8.0	33.2	1.7354
12	8.0	39.8	1.4477
13	8.0	33.4	1.7250
14	8.0	31.8	1.8118
15	8.0	34.2	1.6847
16	8.0	37.1	1.5530
17	8.0	35.0	1.6462
18	8.0	35.0	1.6462

Average Flow Rate = 1.6453 gpm

Measured Bundle Flow Rate = 60.42 gpm

Water Temperature = 24.4°C

Re = 6315

Subchannel Type = Edge

Subchannel Number	Amount of Fluid Collected (ml)	Time (sec)	Flow rate (gpm)
1	2005	23.2	1.3700
2	2010	22.6	1.4099
3	2012	25.4	1.2557
4	1998	25.2	1.2568
5	2004	25.6	1.2409
6	2010	24.4	1.3058
7	2013	24.8	1.2867
8	1997	25.8	1.2270
9	2021	23.6	1.3575
10	2002	24.7	1.2849
11	2021	22.8	1.4051
12	2010	25.4	1.2544
13	2009	22.4	1.4217
14	2005	22.2	1.4317
15	2002	22.3	1.4231
16	2004	25.4	1.2507
17	2009	23.0	1.3846
18	2019	22.8	1.4037

Average Flow Rate = 1.3317 gpm

Measured Bundle Flow Rate = 56.27 gpm

Water Temperature = 28.4°C

Re = 6312

Subchannel Type = Edge

Subchannel Number	Amount of Fluid Collected (ml)	Time (sec)	Flow Rate (gpm)
1	2030	25.6	1.2570
2	1997	24.6	1.2869
3	2012	26.0	1.2267
4	2010	27.8	1.1461
5	2000	27.7	1.1446
6	2000	26.4	1.2009
7	2010	26.0	1.2255
8	2014	28.2	1.1321
9	1998	25.4	1.2469
10	2007	28.0	1.1363
11	2007	25.8	1.2331
12	2009	28.4	1.1214
13	2006	24.6	1.2927
14	2008	23.8	1.3374
15	2019	24.5	1.3063
16	2007	27.6	1.1527
17	2016	25.6	1.2483
18	2014	25.3	1.2619

Average Flow Rate = 1.2198 gpm

Measured Bundle Flow Rate = 45.85 gpm

Water Temperature = 28.4 ^{o}C

Re = 5270

Subchannel Type = Edge

Subchannel Number	Amount of Fluid Collected (ml)	Time (sec)	Flow Rate (gpm)
1	1994	30.6	1.0330
2	2007	29.2	1.0896
3	2000	30.0	1.0568
4	1998	33.0	0.9598
5	2006	33.8	0.9408
6	2004	32.0	0.9927
7	1996	31.0	1.0207
8	1995	34.6	0.9140
9	2000	31.6	1.0033
10	1991	33.4	0.9450
11	1995	31.2	1.0136
12	2001	35.0	0.9063
13	2000	29.4	1.0784
14	2017	30.4	1.0518
15	2015	30.0	1.0647
16	1999	33.5	0.9459
17	2005	30.0	1.0594
18	2002	31.6	1.0371

Average Flow Rate = 1.0065 gpm

Measured Bundle Flow Rate = 50.75 gpm

Water Temperature = 28.6 ^{o}C

Re =5832

Subchannel Type = Edge

Subchannel Number	Amount of Fluid Collected (ml)	Time (sec)	Flow Rate (gpm)
1	2013	29.8	1.0708
2	1990	27.8	1.1347
3	2004	26.8	1.1854
4	2014	30.8	1.0366
5	1996	30.2	1.0477
6	2012	28.6	1.1152
7	1977	28.0	1.1193
8	2008	30.6	1.0402
9	2014	27.0	1.1824
10	1997	29.6	1.0695
11	2007	27.7	1.1486
12	2001	29.0	1.0938
13	2005	37.0	0.8590
14	2011	27.6	1.1550
15	1995	26.8	1.1800
16	1985	29.8	1.0559
17	2020	29.0	1.1042
18	1995	27.0	1.1713

Average Flow Rate = 1.0983 gpm

Measured Bundle Flow Rate = 39.25 gpm

Water Temperature = 28.4 ^{o}C

Re = 4463

Subchannel Type = Edge

Subchannel Number	Amount of Fluid Collected (ml)	Time (sec)	Flow Rate (gpm)
1	2000	36.4	0.8710
2	2000	36.5	0.8686
3	2006	35.0	0.9085
4	1997	40.0	0.7914
5	1998	40.0	0.7918
6	2005	38.2	0.8320
7	2003	37.0	0.8582
8	1997	40.2	0.7875
9	1996	37.0	0.8552
10	1995	40.2	0.7867
11	2006	37.6	0.8457
12	2012	42.3	0.7540
13	1990	34.8	0.9065
14	1999	37.3	0.8496
15	2016	34.0	0.9399
16	2000	39.6	0.8006
17	2004	36.8	0.8632
18	2008	35.4	0.8992

Average Flow Rate = 0.8450

Measured Bundle Flow Rate = 27.70 gpm

Water Temperature = 28.4 ^{o}C

Re = 3235

Subchannel Type = Edge

Subchannel Number	Amount of Fluid Collected (ml)	Time (sec)	Flow Rate (gpm)
1	960	25.0	0.6087
2	2007	52.6	0.6048
3	1995	49.4	0.6402
4	1992	58.4	0.5426
5	2009	61.2	0.5204
6	1996	57.6	0.5493
7	1999	51.6	0.6141
8	2015	57.2	0.5584
9	2000	51.6	0.6144
10	1999	60.2	0.5264
11	2006	54.9	0.5792
12	2015	57.2	0.5584
13	2002	51.4	0.6174
14	1999	53.2	0.5956
15	2004	50.2	0.6328
16	1997	57.2	0.5534
17	2002	53.0	0.5988
18	2002	50.0	0.6347

Average Flow Rate = 0.5861 gpm

Measured Bundle Flow Rate = 33.65 gpm

Water Temperature = 27.9°C

Re = 3745

Subchannel Type = Edge

Subchannel Number	Amount of Fluid Collected (ml)	Time (sec)	Flow Rate (gpm)
1	2002	42.0	0.7556
2	2005	39.0	0.8150
3	2005	42.0	0.7567
4	2003	46.0	0.6903
5	2003	43.6	0.7282
6	2003	44.2	0.7184
7	2000	44.3	0.7157
8	2000	47.0	0.6746
9	2020	42.6	0.7517
10	1999	48.4	0.6547
11	2008	45.0	0.7074
12	2004	46.6	0.6817
13	2002	41.6	0.7629
14	2005	42.2	0.7532
15	2002	40.7	0.7797
16	2012	46.2	0.6908
17	2009	44.0	0.7238
18	2002	40.8	0.7778

Average Flow Rate = 0.7229 gpm

Lists of Data from

Pressure Drop Experiment

Static Pressure Data (Interior Subchannel)

GPM	Re_b	P_{static} "H_2O (36.0")	P_{static} "H_2O (15.5")
2.90	287	3.3	3.0
3.86	382	3.5	3.2
4.83	478	3.7	3.3
5.79	573	4.0	3.5
6.76	669	4.2	3.5
7.72	764	4.4	3.3
8.69	860	4.6	3.8
9.65	955	4.9	3.9
10.62	1051	5.1	4.1
11.58	1146	5.3	4.2
13.51	1338	5.7	4.4
15.44	1529	5.9	4.5
16.41	1624	6.1	4.7
17.37	1720	6.5	4.8
18.34	1816	6.7	4.9

Static Pressure Data (Interior Subchannel)

GPM	Re_b	P_{static} "H_2O (36.0")	P_{static} "H_2O (15.5")
5.55	549	3.7	3.3
7.40	733	4.2	3.6
9.25	916	4.6	3.8
11.10	1099	5.0	4.1
12.95	1282	5.6	4.3
14.80	1465	6.0	4.6
16.65	1648	6.7	4.9
18.50	1832	7.3	5.1
20.35	2015	7.9	5.4
22.20	2198	8.5	5.7
24.05	2381	9.1	6.0
25.90	2564	9.8	6.4
27.75	2747	10.5	6.7
29.60	2930	11.3	7.1
31.45	3114	12.0	7.4
33.30	3297	12.7	7.7
35.15	3480	13.6	8.1

Static Pressure Data (Interior Subchannel)

GPM	Re_b	P_{static} "H_2O (36.0")	P_{static} "H_2O (15.5")
40.0	3960	16.3	9.2
45.0	4455	18.4	10.2
50.0	4950	21.1	11.5
68.19	6750	33.0	16.6
81.5	8070	44.1	21.3
94.6	9370	58.7	28.3
108.56	10700	72.5	34.0
121.04	12000	87.0	39.5
135.70	13400	101.0	47.0

Static Pressure Data (Edge Subchannel)

GPM	Re_b	P_{static} "H_2O (36.0")	P_{static} "H_2O (15.5")
2.90	287	3.0	2.7
3.86	382	3.3	3.0
4.83	478	3.5	3.1
5.79	573	3.7	3.3
6.76	669	4.1	3.5
7.72	764	4.2	3.7
8.69	860	4.5	3.8
9.65	955	4.8	3.9
10.62	1051	5.0	4.0
11.58	1146	5.2	4.3
12.55	1242	5.5	4.4
13.51	1338	5.8	4.5
14.48	1433	6.0	4.6
15.44	1529	6.3	4.8
16.41	1624	6.6	4.9
17.37	1720	6.9	5.0
18.34	1816	7.2	5.1

Static Pressure Data (Edge Subchannel)

GPM	Re_b	P_{static} "H_2O (36.0")	P_{static} "H_2O (15.5")
5.55	549	3.6	3.2
7.40	733	4.1	3.5
9.25	916	4.5	3.8
11.10	1099	5.0	4.0
12.95	1282	5.5	4.3
14.80	1465	6.0	4.6
16.65	1648	6.6	4.9
18.50	1832	7.2	5.1
20.35	2015	7.8	5.4
22.20	2198	8.5	5.7
24.05	2381	9.1	6.0
25.90	2564	9.8	6.4
27.75	2747	10.5	6.7
29.60	2930	11.2	7.2
31.45	3114	12.0	7.4
33.30	3297	12.7	7.8
35.15	3480	13.5	8.2

Static Pressure Data (Edge Subchannel)

GPM	Re_b	P_{static} "H_2O (36.0")	P_{static} "H_2O (15.5")
40.0	3960	15.2	8.9
45.0	4455	18.4	10.4
50.0	4950	20.9	11.6
68.19	6750	33.1	17.0
81.5	8070	44.4	22.0
94.6	9370	59.5	27.3
108.56	10700	73.5	32.9
121.04	12000	88.0	39.6
135.70	13400	102.0	46.0

Subchannel Pressure Drop Data (Interior Subchannel)

GPM	Re_1	ΔP_1 (Psia)	f_1*
2.90	261	0.0108	0.324
3.86	347	0.0108	0.184
4.83	434	0.0144	0.156
5.79	520	0.0180	0.136
6.76	608	0.0253	0.140
7.72	694	0.0289	0.123
8.69	781	0.0289	0.097
9.65	867	0.0361	0.0980
10.62	954	0.0361	0.0812
11.58	1041	0.0397	0.0750
13.51	1215	0.0469	0.0650
15.44	1388	0.0505	0.0536
16.41	1475	0.0505	0.0475
17.37	1562	0.0613	0.0514
18.34	1649	0.0650	0.0489

* The friction factors in these tables are calculated according to Equation (4.3.5)

Subchannel Pressure Drop Data (Interior Subchannel)

GPM	Re_1	ΔP_1 (Psia)	f_1
5.55	499	0.0144	0.118
7.40	666	0.0217	0.100
9.25	831	0.0289	0.0856
11.10	998	0.0325	0.0668
12.95	1164	0.0469	0.0708
14.80	1330	0.0505	0.0584
16.65	1497	0.0650	0.0593
18.50	1664	0.0794	0.0578
20.35	1830	0.0902	0.0551
22.20	1996	0.101	0.0519
24.05	2162	0.112	0.0490
25.90	2328	0.123	0.0461
27.75	2494	0.137	0.0451
29.60	2664	0.152	0.0440
31.45	2828	0.166	0.0425
33.30	2994	0.180	0.0411
35.15	3160	0.198	0.0406

Subchannel Pressure Drop Data (Interior Subchannel)

GPM	Re_1	ΔP_1 (Psia)	f_1
40.0	3596	0.256	0.0405
45.0	4046	0.296	0.0370
50.0	4495	0.343	0.0347
68.19	6130	0.592	0.0322
81.50	7328	0.823	0.0314
94.60	8509	1.10	0.0311
108.56	9717	1.39	0.0301
121.04	10897	1.71	0.0295
135.70	12169	1.95	0.0269

Subchannel Pressure Drop Data (Edge Subchannel)

GPM	Re_2	ΔP_2 (Psia)	f_2
2.90	341	0.0108	0.357
3.86	454	0.0108	0.201
4.83	568	0.0144	0.171
5.79	681	0.0144	0.119
6.76	795	0.0217	0.132
7.72	908	0.0180	0.0848
8.69	1022	0.0253	0.0930
9.65	1135	0.0325	0.0969
10.62	1249	0.0361	0.0889
11.58	1362	0.0325	0.0673
12.55	1476	0.0397	0.0700
13.51	1590	0.0469	0.0712
14.48	1703	0.0505	0.0669
15.44	1817	0.0541	0.0629
16.41	1930	0.0613	0.0632
17.37	2044	0.0686	0.0631
18.34	2158	0.0758	0.0625

Subchannel Pressure Drop Data (Edge Subchannel)

GPM	Re_2	ΔP_2 (Psia)	f_2
5.55	652	0.0144	0.130
7.40	871	0.0217	0.0884
9.25	1088	0.0253	0.0821
11.10	1306	0.0361	0.0813
12.95	1523	0.0433	0.0717
14.80	1741	0.0505	0.0640
16.65	1958	0.0613	0.0614
18.50	2177	0.0758	0.0614
20.35	2394	0.0866	0.0580
22.20	2612	0.101	0.0568
24.05	2829	0.112	0.0537
25.90	3047	0.123	0.0509
27.75	3264	0.137	0.0494
29.60	3481	0.144	0.0456
31.45	3700	0.166	0.0466
33.30	3917	0.177	0.0443
35.15	4135	0.191	0.0429

Subchannel Pressure Drop Data (Edge Subchannel)

GPM	Re_2	ΔP_2 (Psia)	f_2
40.0	4705	0.227	0.0394
45.0	5293	0.289	0.0396
50.0	5882	0.336	0.0373
68.19	8020	0.581	0.0347
81.50	9589	0.808	0.0337
94.60	11133	1.16	0.0359
108.56	12713	1.47	0.0349
121.04	14258	1.78	0.0336
135.70	15922	2.02	0.0306

APPENDIX D

Experience Learnt in Taking Correct Flow Split Measurement

During the course of the flow split experiment, experience was gained in taking correct flow split results. Incorrect flow split measurements are due to improper set up of the equipment. These experiences are disscused into the following paragraphs.

Before running any flow split experiments, the flow collector has to be checked thoroughly for leaks on the pitot tubes and connections between the pitot tubes and the rubber tubes. It is desirable to use RTV 116 as a sealant. RTV 116 is a self leveling sealant and therefore it penetrates any gaps that exist. It also has clear color so that leaks can be checked visually. Moreover, all welded joints should be carefully checked from time to time for cracks. A crack in the outside pitot tube will result in a relative higher static pressure than the inside and hence less flow from the subchannel will be collected.

In setting up the test section, a rubber gasket is placed between the end plate and the wall of the test section. A hole is cut to fit the exit plane of the test section. This hole has to be cut to a larger size than the exit plane area to allow for the expansion of the gasket when end plates on both ends of the test section are tightened. To be more precise, the rubber gasket is flush with the end plate. Excessive gasket material will obstruct the seating of the collector on the top surfaces

of the pins, thereby causing an incorrect subchannel flow rate to be measured.

In placing the collector on top of the subchannel, no contraint on pulling the collector should exit. In some subchannels, the collector could not be seated tight on the subchannel. Therefore any pulling plus the upward force exert by the flow could displace the collector out of the exit plane of the subchannel, resulting in an incorrect measured subchannel flow rate.

From the experience gained, displacement of the collector from the exit plane of the subchannel would result in a larger and inconsistent measured flow rate from the subchannel.

REFERENCES

(1) E. Khan, W.M.Rohsenow, A. Sonin and N. Todreas, "A Porous Body Model for Predicting Temperature Distributions in Wire Wrapped Fuel and Blanket Assemblies of a LMFBR," COO-2245-16TR, MIT, March,1975.

(2) E. Khan, W.M. Rohsenow, A. Sonin and N. Todreas, "Input Parameters to the ENERGY Code," COO-2245-17TR, MIT, May, 1975.

(3) E. Khan, W. Rohsenow, A. Sonin and N. Todreas, "Manual for ENERGY Codes I, II, III," COO-2245-18TR, MIT, May, 1975.

(4) E. Khan, W.M. Rohsenow, A. Sonin and N. Todreas, "Manual for ENERGY Codes I, II, III Computer Programs," COO-2245-18TR Revision 1, MIT, July, 1976.

(5) B. Chen and N. Todreas, "Prediction of Coolant Temperature Field in a Breeder Reactor Including Interassembly Heat Transfer," COO-2245-20TR, MIT, May, 1975.

(6) C. Chiu, W.M. Rohsenow and N. Todreas, "Turbulent Sweeping Flow Mixing Model for Wire Wrapped LMFBR Assemblies," COO-2245-55TR, MIT, April, 1978.

(7) E. Khan, W.M. Rohsenow, A. Sonin, S.F. Wang and N. Todreas, "Input Parameters to Codes Which Analyze LMFBR Wire Wrapped Bundles," COO-2245-17TR Revision 1, MIT, May, 1978.

(8) C. Chiu, W.M. Rohsenow and N. Todreas, "Flow Split Measurements in LMFBR Blanket Assemblies," COO-2245-41TR, MIT, April, 1978.

(9) E. Novendstern, "Turbulent Flow Pressure Drop Model for Fuel Rod Assemblies, Utilizing a Helical Wire-Wrap Spacer System," Nuclear Engineering and Design, Vol. 22, No. 1, August, 1972.

(10) C. Chiu, W.M. Rohsenow and N. Todreas, "A Turbulent Flow Split Model for Wire Wrapped LMFBR Assemblies," COO-2245-56TR, MIT, May, 1978.

(11) C. Chiu, W.M. Rohsenow and N. Todreas, " A Turbulent Flow Split Model and Supporting Experiments for Wire Wrapped Core Assemblies," COO-2245-56TR Revision 1, MIT, January, 1979.

(12) C.H. Oosterman, "An Experimental Investigation of Coolant Mixing in a Wire Wrapped LMFBR Blanket Subassembly," M.S. Thesis, Department of Nuclear Engineering, MIT, June, 1975.

(13) B.J. Bosy, "Fabrication Details for Wire Wrapped Fuel Assembly Component," COO-2245-27TR, MIT, November, 1975.

(14) H. Khan, C. Chiu and N. Todreas, "Laboratory Manual for Salt Mixing Test in Rod Bundles," To be issued as Topical Report COO-2245-62TR, Department of Nuclear Engineering, MIT.

(15) A.S. Hanson and N. Todreas, "Fluid Mixing Studies in an Hexagonal 61-Pin, Wire-Wrapped Rod Bundles," COO-2245-51TR, MIT, August,1977.

(16) S. Glazer, C. Chiu and N. Todreas, "Collection and Evaluation of Salt Mixing Data with the Real Time Data Acquisition System," COO-2245-36TR, MIT, April, 1977.

(17) C. Chiu, J. Hawley, W.M. Rohsenow and N. Todreas, "Pressure Drop Measurement in LMFBR Wire Wrapped Blanket Assemblies," COO-2245-42TR, MIT, July, 1977.

(18) K. Rehme, "Prssure Drop Correlations for Fuel Element Spacers," Nuclear Technology, Vol. 17, (15-21), January, 1973.

(19) A. Sarno, P. Gori and G. Andalo, "Local Pressure and Velocity Measurement in a Water 19-Rod Bundle Using a Wire Wrap Spacer System," A Paper for IWCFR-Specialist's Meeting on "Thermodynamics of FBR Fuel Subassemblies Under Nominal and Non-nominal Operating Conditions, Karlsruhe, February, 1979.

(20) Stearns, "Flow Measurement with Orifice Meter," Published by Van Nostrand Inc., 1954.